A LABORATORY PERMEAMETER STUDY OF GEOTEXTILE-SOIL RETENTION IN CYCLIC FLOW

by

ATITEP SRIKONGSRI

B.Eng. King Mongkut University of Technology Thonburi, 1996
M.Eng. Asian Institute of Technology, 1999

A THESIS SUBMITTED IN PARTIAL FULFILLMENT OF
THE REQUIREMENTS FOR THE DEGREE OF

DOCTOR OF PHILOSOPHY

in

The Faculty of Graduate Studies

(Civil Engineering)

THE UNIVERSITY OF BRITISH COLUMBIA

(Vancouver)

May 2010

ABSTRACT

In the absence of an extensive body of laboratory and field data, empirical criteria for soil retention in dynamic or cyclic flow are not yet well-defined with reference to a margin of safety. A performance-based approach is taken in this study: the method of investigation involves laboratory tests on a total of seven geotextiles (needle-punched nonwoven and woven materials) and a total of four uniformly-graded soils (non-plastic fine sand and coarse silt). Filtration compatibility in unidirectional and cyclic flow reversal is evaluated using two rigid-wall permeameters: a small bench-mounted device, and a large floor-mounted device. Analysis of the results addresses the effects of specimen size (small and large), sidewall friction and stress distribution, and examines the influence of filter ratio (AOS/D_n), hydraulic gradient (i) and confining stress (σ□) over a range of cyclic flow reversal times or wave period (T).

A novel analytical framework is proposed from the permeameter test results, to unify AOS/D_n and a hydromechanical index that accounts for the combined effect of hydraulic gradient and confining stress. The framework provides a distinction between the benign actions of mass loss through the geotextile by washout, in contrast to the more problematic action of piping. A filter ratio AOS/D_{85} appears better-suited to interpretation of the data than AOS/D_{50}. The framework is used to examine the margin of safety inherent in current design guidance. Independent verification of the framework through comparison with other laboratory studies, and a consideration of field observations reported by others, leads to a recommendation that $AOS/D_{85} \leq 1$ to address undue conservatism in design guidance.

TABLE OF CONTENTS

LIST OF TABLES

LIST OF FIGURES

LIST OF SYMBOLS

AOS	Apparent opening size of geotextile (m)
c	Side-wall interface cohesion (kPa)
C_u	Coefficient of uniformity which is equal to D_{60}/D_{10} (dimensionless)
CYC	Cyclic flow
D	Diameter of the test specimen (m)
D_n	Indicative particle size of the base soil at *n* % passing by weight (m)
DPT	Differential pressure transducer
f	Coefficient of sidewall friction (dimensionless)
G_s	specific gravity of soil (dimensionless)
G_r	Specific gravity of rock (dimensionless)
GR_x	Gradient Ratio of *x* mm thick of soil-geoetxtile composite (dimensionless)
H_s	Significant wave height or design value of wave height (m)
H_{xy}	Head loss across the ports x and y (m)
i_{av}	Average hydraulic gradient across the test specimen (dimensionless)
K_0	Coefficient of lateral pressure at- rest (dimensionless)
k_g	Permeability of the geotextile (m/s)
k_s	Permeability of the base soil (m/s)
LVDT	Linear variable differential transformer
m_{av}	Average mass loss (g/m^2/100 cycles)

m_p	Mass loss per unit area (g/m^2)
OCR	Over consolidation ratio (dimensionless)
O_F	Filtration opening size of geotextile (m)
O_x	Pore opening size of geotextile, at which x% of pores are finer (m)
P_{max}	Maximum water pressure in the filter layer of rip-rap (kPa)
p_i	Hydrodynamic mean effective stress at the soil-geotextile interface (kPa)
$p_{i(0)}$	Hydrostatic mean effective stress at the soil-geotextile interface or initial confining stress (kPa)
S	Seepage pressure (kPa)
UNI	Unidirectional flow
W_{50}	Weight of median rock size (N)
w_r	Density of rock mass (kg/m^3)
Z	Length of the test specimen (m)
$\Delta\sigma'_v$	Stress difference in hydrodynamic condition (kPa)
$\Delta\sigma'_{v(0)}$	Stress difference in hydrostatic condition (kPa)
δ	Soil-wall interface friction angle (degree)
γ'	Submerged unit weight of soil (kN/m^3)
γ_w	Unit weight of water (kN/m^3)
φ	Internal friction angle (degree)
σ'_{vb}	Hydrodynamic effective vertical stress at the base of the test specimen (kPa)

$\sigma'_{vb(0)}$	Hydrostatic effective vertical stress at the base of the test specimen (kPa)
σ'_{vm}	Average effective vertical stress in hydrodynamic condition (kPa)
$\sigma'_{vm(0)}$	Average effective vertical stress in hydrostatic condition (kPa)
σ'_{vt}	Effective vertical stress applied on top of the test specimen (kPa)
τ_{av}	Average side-wall friction resistance (kPa)
θ	Slope of the rip-rap (degree)

ACKNOWLEDGEMENTS

I wish to thank and express my sincere gratitude to my research supervisor, Dr. Jonathan Fannin, for his continued guidance and kind support throughout the course of this study. I also wish to thank the members of my supervisory committee, Dr. John Howie and Dr. Frank Ko, for their input and constructive comments on the manuscript. I am deeply grateful for funding in support of this research, which was provided by the Natural Sciences and Engineering Research Council (NSERC) of Canada and also Ten Cate Geosynthetics with assistance from Mr. Chris Lawson.

I would like to thank the Civil Engineering Workshop staff (Bill Leung and Harald Shremp) and also the Electronics Workshop staff (Scott Jackson). My thanks are extended to all of the graduate students in the geotechnical laboratory for their support and valuable discussions.

DEDICATION

To my parents, who have been a constant source of love, support and encouragement to me.

CO-AUTHORSHIP STATEMENT

The content of this thesis comprises four proposed manuscripts (chapters 2, 3, 4 and 5, respectively). For the first manuscript (chapter 2), I was responsible for novel revisions to data reduction and analysis, based on some of the laboratory tests performed by Ms. R. Hawley and reported in her MASc thesis in 2001. In recognition of her data collection, and my complementary revisions of the data analysis, she is included as a co-author. For the remaining manuscripts (chapters 3 to 5), I performed all the laboratory tests myself, including all data reduction and analysis. Preparation of all four manuscripts, including the contents, figures and tables, has been solely my responsibility. Dr. R. J. Fannin reviewed all the manuscripts, gave feedback on technical content, assisted with the formulation of my ideas and made suggestions for clarity of presentation. Accordingly, Dr. Fannin is a co-author on all four manuscripts.

1 Introduction

The term “filtration”, as used with reference to civil engineering works, describes the restriction of particle migration from a soil (the “base” soil) into or through an adjacent medium (the “filter” material) as a consequence of groundwater seepage. The filtration process itself is predicated on the development, over time, of a stable interface between the base soil and the filter material. In construction practice, there is a considerable body of experience with the use of granular soils as a filter material and, in comparison, a growing body of experience with the use of geotextiles as a filter material. The primary objective of the filter is to protect against soil erosion in applications where groundwater flow has the potential to cause a seepage-induced movement of particles while, at the same time, providing for adequate discharge capacity and therefore an unimpeded drainage of the soil to be protected. Accordingly, properly designed filters are integral to the performance of construction works, both with respect to the economic concerns governing serviceability and also for safety concerns governing stability at the ultimate limit state.

1.1 Geotextile filters

The manufacturing process yields several constructions or styles of geotextile, two of which, a nonwoven and a woven fabric, are typically used in filtration applications.

The styles are inherently different. A nonwoven geotextile comprises a layer of many randomly-oriented polymer strands that are bonded to obtain a planar fabric. The individual strands are usually a short fibre or a continuous filament, generally made of polypropylene and occasionally of polyester or polyethylene. The common methods of bonding are either physical entanglement of the strands, yielding a needle-punched nonwoven geotextile, or thermal fusing of contact points between the strands during a calendaring operation, which produces a heat-bonded nonwoven geotextile. In contrast, a woven geotextile is made from individual polymer strands that are aligned and orthogonally interlaced on a weaving loom, again yielding a planar fabric. The strand itself is usually a slit film, a monofilament, or a multifilament yarn. A fibrillated strand is one that has been intentionally split along portions of its length, as a part of the manufacturing process, to condition its properties.

In contrast to a nonwoven geotextile, which has a wide range of pore opening sizes, a woven geotextile tends to have a narrower range of relatively larger openings. A characteristic opening size of the fabric is generally established through indirect means, by placement of a test gradation of either soil or glass ballotini on a specimen of the geotextile, and subsequent determination of the grain size distribution curve of the fraction of that gradation which passes through the fabric under a prescribed disturbance. The disturbing action typically involves either dry shaking or hydrodynamic flushing. A characteristic opening size, for example O_{95} (μm), is taken to be the equivalent size of the fraction passing, in this case D_{95}, with the implicit

understanding that 95% of the pore openings are less than or equal to this value (Fischer 1994; Fischer et al. 1996; Bhatia et al., 1996).

Filtration compatibility is predicated on the geotextile satisfying a requirement for soil retention. Incompatibility may take the form of unacceptable piping or clogging. Piping refers to a particle migration through the geotextile, while clogging is a result of entrapment of particles on or within the geotextile. With reference to the permeability of the soil that is retained, piping yields a zone of relatively high permeability adjacent to the geotextile while, in contrast, clogging generates a zone of relatively low permeability. Compatibility may therefore be evaluated by placing soil and geotextile in a permeameter, imposing a prescribed seepage regime, and monitoring any change in the permeability of the soil-geotextile interface relative to that of the undisturbed soil. Interpretation of the results involves comparison of observed change against a threshold value of acceptable filtration compatibility.

1.2 Soil-geotextile filtration mechanism

Filtration compatibility requires there be no unacceptable erosion as a consequence of soil loss through the geotextile while, at the same time, providing for unimpeded flow of water seeping from that soil into the drainage aggregate. The expectation, as with granular filters, is that retention of coarser particles in the soil then promotes

development of a stable interface or 'bridging zone' in a thin zone of soil adjacent to geotextile (Lawson, 1982). Given this expectation, the design approach is predicated on matching a characteristic pore size opening of the geotextile (for example, O_{95}) to a characteristic particle size of the soil (for example, D_{85b} or D_{50b} and D_{15b}) yielding:

$$C_1 \times D_{85b} > O_{95} > C_2 \times D_{15b} \quad (1)$$

$$C_3 \times D_{50b} > O_{95} \quad (2)$$

where C_1, C_2 and C_c are constants that depend on soil type and shape of the grain size distribution curve (Leuttich et al. 1992 and Holtz et al. 1997). The approach is very similar to that adopted in granular filters, where C_1 addresses soil retention and C_2 addresses clogging (Ogink, 1975; Schober and Teindl, 1979; Giroud 1982; Christopher and Holtz, 1985; Gourc and Faure, 1990; Lafleur et al. 1992; Palmeira and Fannin, 2002). With respect to the cross-plane permeability, filtration compatibility is contingent on the geotextile having a capacity for discharge flow significantly greater than that of the soil against which it is placed. The expectation, as for granular filters, is that if each successive layer in the direction of seepage flow exhibits a greater permeability, there is no potential to impede discharge flow through those layers.

Geotextiles exhibit a relatively wide range of volumetric flow rate per unit area across the plane of the fabric, with discharge capacity again being largely determined by the

manufacturing process. To characterize discharge capacity, the geotextile is mounted in a permeameter and subject to flow under the influence of either a constant differential head or a falling head. A calculation is typically made of the normal permeability k_n (cm/s), which may also be reported as a value of permittivity ψ (s^{-1}) if divided by the thickness of the fabric. In routine applications, the design approach is commonly based on matching an index value of cross-plane permeability for the geotextile (k_n) to the permeability of the soil (k_s). Where concern exists for entrapment of fine particles against and/or within the geotextile, which may result in blinding and/or clogging of the fabric (Koerner and Ko 1982; Lafleur et al. 1989), the ASTM Gradient-Ratio test (D5101) was developed as a performance-oriented test for evaluation of soil-geotextile compatibility (Calhoun 1972; Haliburton and Wood, 1982; Fannin et al., 1994; Fannin et al. 1996). In steady unidirectional flow, filtration compatibility is evaluated based on empirical acceptance criteria. No such performance-oriented criteria exist for cyclic, reversing or pulsating flow applications where flow regimes are not easily reproduced in a simple test device, and interpretation of the onset of retention incompatibility is generally found more complex than unidirectional flow (Giroud, 1996; Mlynarek, 2000; Fannin, 2007). Moreover, the absence of a standardized test method for cyclic flow, and very limited well-documented laboratory and field data, leave considerable uncertainty in design practice. Consequently, and perhaps with good reason, current design guidance adopts a conservative approach. The research of this thesis seeks to address that conservatism.

Onset of retention incompatibility in cyclic flow reversal is governed by several factors, including: (i) soil properties, (ii) geotextile properties (iii) effective stress at the soil-geotextile interface, (iv) hydraulic gradient across the soil-geotextile interface, and (v) period of flow reversal (as noted in several studies, including de Graauw et al., 1983; Cazzuffi et al., 1999; Chew et al., 2000; Hameiri, 2000; Hawley, 2001; Chen et al. 2008). The first and second factors represent a geometric constraint or capacity, termed "filter ratio", that describes the ratio of characteristic filter opening size to indicative particle size of base soil (O_F/D_n). Collectively, the third and fourth factors represent a hydromechanical demand on the pore size openings of the filter. At a certain period of flow reversal, it is postulated the relation between hydromechanical demand and geometric constraint determines the onset of retention incompatibility in a geotextile filter.

1.3 Objectives and scope of the study

Fine sand, sand with some silt and sandy silt are commonly found in estuarine and coastal environments where reversing flow conditions prevail: they represent a challenging base soil for selection and use of geotextile products as a filter in erosion-control structures. The typical wave environment comprises a relatively fast reversing flow (e.g. wind-generated or gravity waves for which a wave period is typically in the

range 1 s $\leq$ T $\leq$ 10 s), and a slower reversing flow resulting from energy conversion processes acting on gravity waves that filters out the higher frequency (e.g. infragravity waves for which a wave period is typically in the range 50 s $\leq$ T $\leq$ 350 s), as described by Munk (1949). In the absence of an extensive body of laboratory and field experience, current design guidance takes an understandably conservative approach. For example, a criterion advocated by Canadian Foundation Engineering Manual for applications of cyclic flow (O_{95} or AOS $\leq 0.5D_{85}$, adopted from Holtz et al. 1997) yields a maximum value of 0.05 mm for the characteristic opening size of the fabric for a fine sand having D_{85} of 0.1 mm. Note that AOS is an Apparent Opening Size of a geotextile, according to ASTM D 4751: the O_{95} size obtained by dry sieving. This AOS or O_{95} value is much smaller than the typical range of opening size available in geotextile products, and thereby eliminates the options of using a geotextile in some situations where it may offer significant cost saving. Moreover, a smaller opening size tends to reduce the cross-plane permeability of the geotextile, which may have adverse consequences for filtration performance. As a result, selection of a suitable geotextile for cyclic flow applications is made with considerably less understanding than for unidirectional flow. Well-known criteria such as Holtz et al. (1997), and also Luettich et al. (1992) and Pilarczyk (2000), are wholly developed from a body of practical experience and judgment that is based on very limited field data. None of the design criteria for cyclic flow have been developed from systematic laboratory studies, and a consideration of hydromechanical analysis. Furthermore, they for soil retention have not yet been well-defined, and demonstrated valid with reference to a margin of safety.

The research of this thesis seeks to introduce a science-based explanation, based on a consideration of the five factors outlined above that are believed to govern retention incompatibility, and thereby enhance confidence in engineering practice.

More specifically, the study has two main objectives. First, to develop a hydromechanics-based framework that accounts for the influence both of hydromechanical demand and geometric constraint on onset of retention incompatibility in cyclic flow. Second, to characterize the margin of safety between current design guidance, based on the work of Luettich et al. (1992), Holtz et al. (1997) and Pilarczyk (2000), if appropriate, to make recommendations for modifications to design guidance that address undue conservatism in current practice.

The research takes a performance-based approach to the study of geotextile filtration compatibility. The method of investigation involves laboratory tests on a total of seven geotextiles (needle-punched nonwoven and woven materials) and a total of four uniformly-graded soils (non-plastic fine sands and coarse silt). Given the grain size distribution of the soils, and opening size of the geotextiles, the variety of soil-geotextile combinations yielded a range in filter ratio of $0.7 \leq AOS/D_{85} \leq 3.7$ (greater than the design guidance, $AOS \leq 0.5D_{85}$). Filtration compatibility is evaluated using two rigid-wall permeameters, a small bench-mounted device and a large floor-mounted device. The small permeameter is a modified version of the ASTM Gradient Ratio permeameter, and the large device was commissioned to examine seepage-induced

instability in the core of earth dams and was also modified for the purposes of the current study. Analysis of the results addresses the influence of filter ratio (AOS/D_{85}), hydraulic gradient (i) and confining stress (σ□) over a range of cyclic flow reversal times or wave period (T). However, an explicit correlation of retention capability between nonwoven and woven geotextiles to account the influence of various fabric structures is not inclusive.

The intended contribution of the research is to build confidence in implementing a simple geometric constraint, based on an empirical filter ratio AOS/D_n, through a unified plot against a measure of the hydromechanical demand that is quantified by normalized seepage pressure ($S/p_{i(0)}$). The demand parameter is a ratio of seepage pressure (S) to initial mean effective stress at the soil-geotextile interface ($p_{i(0)}$). The novel conceptual framework provides a science-based explanation for onset of soil piping through a geotextile filter and, furthermore, a means to identify the margin of safety inherent in current empirical design criteria. The conceptual framework is developed from testing in the small and large permeameters, and verified independently with reference to laboratory test data and a field study reported in the literature.

1.4 Thesis organization

This manuscript-based thesis consists of six chapters, which are briefly outlined as follows:

- Chapter 1 provides an introduction to the phenomenon of retention incompatibility in soil-geotextile filtration, and insight into the nature of conservatism in current design practice, as background context for the objectives and scope of study.

- Chapter 2 presents an analysis and interpretation of data from a recently-completed study of soil-geotextile compatibility using the small permeameter, reviews selected design criterion for cyclic flow, addresses uncertainty in margins of safety; the findings identify the role and likely contribution of a systematic mechanics-based study to improving design practice.

- Chapter 3 describes experimental data from the small and the large permeameter test device, with emphasis on matters of scale effect in the test equipment, test methodology and influence of the test device itself on the soil-geotextile interface, in order to ensure the appropriateness of using the small permeameter for a systematic study of variables governing cyclic flow. Additionally, the comparison of data leads to recommendations for the main experimental program.

- Chapter 4 presents the findings of the main experimental program. The utility of an empirical filter ratio, expressed as AOS/D_{50} and AOS/D_{85}, is evaluated. The potential for a relation between filter ratio and normalized seepage pressure ($S/p_{i(0)}$) to explain the onset of retention incompatibility in cyclic flow is explored, leading to a conceptual hydromechanical framework for interpretation of the test data. The framework is then used to consider the margin of safety inherent in current design guidance.

- Chapter 5 provides an independent verification of the proposed framework, through a comparison with other laboratory studies and a consideration of field observations reported by others. Verification of the concept leads to a recommendation to address undue conservatism, by means of a revision to current design guidance.

- Chapter 6 concludes the study. Findings of the experimental study are summarized, together with accompanying theoretical provisions for their analysis and interpretation. Given the nature of the experimental work, and its contribution, recommendations are then provided for future research.

1.5 References

ASTM D 4751, *Standard Test Method for Determining Apparent Opening Size of a Geotextile*. American Society for Testing and Materials, West Conshohocken, PA, USA.

ASTM D 5101, *Standard Test Method for Measuring the Soil-Geotextile System Clogging Potential by the Gradient Ratio*. American Society for Testing and Materials, West Conshohocken, PA, USA.

Bathia, S. K., Smith, J. L. and Christopher, B. R. (1996). Characterization and pore-size distribution: part III: comparison of methods and application to design", *Geosynthetics International*, **3**, No. 3, 301-328.

Calhoun, C.C., Jr. (1972). Development of design criteria and acceptance specifications for plastic filter cloths. *Technical Report S-72-7*, US Army Engineer Waterways Experiment Station, Vicksburg, Mississippi, USA, 82 p.

Canadian Geotechnical Society (2006). *Canadian Foundation Engineering Manual*. 4th edition, BiTech Publishers Ltd.

Cazzuffi, D. A., Mazzucato, A., Moraci, N., & Tondello, M. (1999). A new test apparatus for the study of geotextiles behaviour as filters in unsteady flow conditions: relevance and use. *Geotextiles and Geomembranes* **17**, No. 5-6, 313 - 329.

Chen, R.-H., Ho, C.-C. & Hsu, C.-Y. (2008). The effect of fine soil content on the filtration characteristics of geotextile under cyclic flows. *Geosynthetics International*, **15**, No. 2, 95–106.

Christopher, B.R., and Holtz, R.D. (1985). Geotextile engineering manual, *Report No. FHWA-TS-86/203*, Federal Highway Administration, D.C., USA.

de Graauw, A., van der Meulen, T. & van der Does de Bye, M. (1983). Design criteria for granular filters. *Publication no. 278*, Delft hydraulics laboratory, Delft, The Netherlands.

Fannin, R.J. (2007). Chapter 6: The use of geosynthetics as filters. *Geosynthetics in Civil Engineering*. Woodhead Publishing, Cambridge, UK, 295p.

Fannin, R. J., Vaid, Y. P., Palmeira, E. M. & Shi, Y. (1996). A modified gradient ratio device. *Recent Developments in Geotextile Filters and Prefabricated Drainage Geocomposites*, ASTM STP 1281, Philadelphia, PA, USA, 100 – 112.

Fannin, R. J., Vaid, Y. P. and Shi, Y. (1994). Filtration behaviour of nonwoven geotextiles. *Canadian Geotechnical Journal*, **31**, No. 4, 555 – 563.

Fischer, G. R. (1994). The influence of fabric pore structure on the behavior of geotextile filters. PhD Thesis, University of Washington, Washington, USA, 502 p.

Fischer, G. R., Holtz, R. D., and Christopher, B.R. (1996). Evaluating geotextile pore structure. *Recent Developments in Geotextile Filters and Prefabricated Drainage Geocomposites*, ASTM STP 1281, Philadelphia, PA, USA, 100 – 112.

Giroud, J.P. (1982). Filter criteria for geotextiles, *Proceedings of the 2nd International Conference on Geotextiles*, Las Vegas, NV, Industrial Fabrics Association International, St. Paul, MN, USA, Vol. 1, pp. 103-108.

Giroud, J. P. (1996). Granular filters and geotextile filters, *Proceedings of Geofilters'96 Conference*, Montreal, Quebec, Canada, pp 565-680.

Gourc, J. P. and Faure, Y. H. (1990). Filter criteria for geotextiles. *Proceedings of the 4th International Conference on Geotextiles*, Hague, the Netherlands, Vol. 4, pp. 949–971.

Haliburton, T.A. and Wood,. P.D. (1982). Evaluation of U.S. Army Corps of Engineers Gradient Ratio test for geotextile performance. *Proceedings of the 2nd International Conference on Geotextiles*, Las Vegas, NV, Industrial Fabrics Association International, St. Paul, MN, USA, pp. 97-101

Hameiri, A. (2000). Soil geotextile filtration behavior under dynamic conditions of vibration and cyclic flow. PhD Thesis, University of British Columbia, BC, Canada, 270p.

Hawley, R. (2001). Filtration performance of geotextiles in cyclic flow conditions. MASc Thesis, University of British Columbia, BC, Canada, 141p.

Holtz, R.D, Christopher, B.R., and Berg, R.R. (1997). *Geosynthetic Engineering*. BiTech Publishers, Richmond, BC, Canada, 452 p.

Koerner, R. M. and Ko, F. K. (1982). Laboratory studies on long-term drainage capability of geotextiles. *Proceedings of the 2nd International Conference on Geotextiles*, Las Vegas, NV, Industrial Fabrics Association International, St. Paul, MN, USA, pp. 91 – 95.

Lafleur J., Mlynarek J., and Rollin A. L. (1989). Filtration of broadly graded cohesionless soils. *Journal of Geotechnical Engineering*, ASCE, **115**, No. 12, pp. 1747-1768.

Lafleur J., Mlynarek J., and Rollin A. L. (1992). Filter criteria for well graded cohesionless soils. *Filters in Geotechnical and Hydraulic Engineering*, Balkema, Rotterdam, The Netherlands, pp. 97 – 106.

Lawson, C.R. (1982). Filter criteria for geotextiles: relevance and use. *ASCE Journal of Geotechnical Engineering*, **108**, No. 10, pp. 1301-1317

Luettich, S.M., Giroud, J.P., and Bachus, R.C. (1992). Geotextile filter design guide. *Geotextiles and Geomembranes*, **11**, 355 - 370.

Mlynarek J. (2000). Geo drains and geo filter-retrospective and future trends. *Filters and Drainage in Geotechnical and Geoenvironmental Engineering*, Balkema, Rotterdam, The Netherlands, pp. 27 - 47.

Munk, W. H. (1949). Surf beats. *EOS, Transactions,* American Geophysical Union, **30**, 849 - 859.

Ogink, H. J. M. (1975). Investigations on the hydraulic characteristics of synthetic fabrics. *Publication no. 146*, Delft Hydraulic Laboratory, Delft, The Netherlands.

Palmeira, E.M. and Fannin, R.J. (2002). Soil-geotextile compatibility in filtration. *Proceedings of the 7th International Conference on Geosynthetics*, Nice, France, pp. 853-872.

Pilarczyk, K. W. (2000). *Geosynthetics and geosystem in hydraulic and coastal engineering*. A.A. Balkema, Rotterdam, The Netherlands, 913 p.

Schober, W. and Teindl, H. (1979). Filter criteria for geotextiles, *7th European Conference on Soil Mechanics and Foundation Engineering*, Brighton, UK, Vol. 1, pp. 121-129.

2 Soil-Geotextile Compatibility Testing in Cyclic Flow[1]

2.1 Outline

Influence of filter ratio on soil-geotextile interaction is examined under conditions of cyclic flow. Seven different geotextiles and three non-plastic soils are tested in a cyclic gradient ratio test device, using a multistage test procedure with variables of confining stress and wave period. Mass loss per unit area in stages of cyclic flow increases with larger AOS/D_{85}. The empirical criterion of $AOS/D_{85} \leq 0.5$ for soil retention in cyclic flow is found conservative, both for nonwoven and woven geotextiles. Wave period and confining stress influence soil-geotextile filter compatibility, and those parameters, in combination with hydraulic gradient, require systematic study in order to understand the margin of safety that governs a confident use of the empirical criterion.

[1] A version of this chapter will be submitted for publication. Srikongsri, A., Fannin, R. J., Hawley, R. (2010). Soil-geotextile compatibility testing in cyclic flow.

2.2 Introduction

In the current state-of-practice, it is reasonable to observe that the behavior of geotextile filters in earthworks subject to unidirectional flow of groundwater seepage is well-understood and, consequently, that companion design criteria may be used with confidence. The confidence is predicated on a longstanding appreciation of the fundamental physical processes that govern compatibility (Lawson, 1982; Hoare, 1982). Subsequent recommendations for design criteria are wholly empirical and, importantly, assume the base soil through which seepage flow occurs is internally stable (Palmeira and Fannin, 2002).

In contrast to unidirectional seepage flow in routine filter applications, where a use of geotextiles is based on considerable field experience and many laboratory studies, the issue of bidirectional, reversing or cyclic flow is one for which our current understanding is more limited (Fannin, 2007). This may be attributed to several factors, including the relatively uncommon occurrence of reversing flow in routine engineering works, and corresponding lack of good documented field experience, coupled with a paucity of laboratory studies that address the specific nature of such flow regimes. Yet considerable challenges exist in the confident provision of filters for protection of civil infrastructure in estuarine and coastal environments, where a subtle distinction can be made between slow reversing flow, such as that of tidal

environments, and the relatively faster reversing flow that occurs in the presence of wave action. Fannin and Srikongsri (2007) provided a critical review of geotextile behavior in cyclic filtration experimental studies, with emphasis on governing factors and design criteria. Three factors, namely wave period, hydraulic gradient and confining stress were found to significantly influence compatibility of soil-geotextile filter.

A limited number of studies report on development of a laboratory test device for cyclic flow (Cazzuffi et al., 1999; Chew et al., 2000; Hameiri, 2000; Fannin and Pishe, 2001; Hawley, 2001; Hameiri and Fannin, 2002). Cazzuffi et al. (1999) described the influence of hydraulic gradient and confining stress on the performance of geotextile filters in cyclic flow, from test data on four combinations of two sandy soils and a woven and a nonwoven geotextile. Although the laboratory permeameter test device did not conform to specifications of the ASTM Gradient Ratio device, its configuration permitted a similar characterization of filtration compatibility with reference to a ratio of hydraulic gradient across the soil-geotextile interface to that within the base soil. Considerable quantities of mass loss were observed in test combination for which the woven geotextile opening size was relatively large ($AOS/D_{85} \approx 2.2$). At constant AOS/D_{85}, the general trend was characterized by greater mass loss with increasing hydraulic gradient or decreasing confining stress.

Effects of wave period in cyclic flow were examined by Chew et al. (2000), from tests on gravelly sand against a woven and a nonwoven geotextile. Once again, although their laboratory permeameter test device did not conform to specifications of the ASTM Gradient Ratio device, its configuration permitted measurement of hydraulic gradient across the soil-geotextile composite and within the soil. Mass loss was found to increase with the decrease of wave period, particularly from 15 s to 2 s. Recognizing the importance of wave period, they proposed an index value for rate of changing hydraulic gradient; $R_i = 2\Delta i/T$, where Δi = hydraulic gradient in each cycle and T is wave period. This index was recommended as a measure of hydraulic loading conditions.

The ASTM Gradient Ratio test (ASTM D5101) was originally conceived to evaluate compatibility of base soil and geotextile filter in steady unidirectional flow. Modifications to enable tests with cyclic flow are described by Hameiri and Fannin (2002). The modified Gradient ratio test device allows testing of a soil-geotextile specimen that is subject to axial confining stress, with gradient-control of seepage flow at a constant period, and collection of soil loss through the geotexile during a test.

Data obtained on soil-geotextile compatibility, using the modified Gradient Ratio test device with cyclic flow, are reported with the objective of evaluating its suitability as a performance test. Emphasis is placed on the utility of collecting soil that passes through the geotextile, where concern for filtration compatibility addresses a criterion

for soil retention. Evaluation of an empirical design criterion that employs the filter ratio AOS/D_{85} yields insight to the influence of effective stress on filtration compatibility.

2.3 Laboratory test program

The modified Gradient Ratio test device used in testing is equipped with a loading frame to apply axial force to the top surface of the specimen, and a conical trough to collect soil washed though the geotextile (Fig. 2.1a). A series of multistage cyclic flow tests, on specimens of reconstituted glass beads, was used to commission the laboratory test device (Hameiri, 2000): the utility of a modified value of gradient ratio (GR_8) was demonstrated, based on measurement of the hydraulic gradient across a gauge length of only 8 mm across the base soil and geotextile. The rationale for a relatively short gauge length is that any incompatibility of the filtration interface is most evident immediately upstream of the geotextile. An array of port locations on the side-wall of the permeameter (see Fig. 2.1b, with values in parentheses indicating height above the geotextile), define the ASTM Gradient Ratio (GR_{25}) and modified value (GR_8) respectively as:

$$GR_{25} = \frac{i_{57}}{i_{35}} \tag{1}$$

and

$$GR_8 = \frac{i_{67}}{i_{35}} \qquad (2)$$

where hydraulic gradient i_{35} is measured across the soil between ports P3 and P5, i_{57} is measured across the soil-geotextile zone between ports P5 and P7, and i_{67} across the same zone between ports P6 and P7. Details of the flow control and data acquisition have been summarized by Hameiri and Fannin (2002).

Hawley (2001) used the device to test three soils (see Fig. 2.2). Soil FR, a Fraser River sand with trace silt, has a D_{85} = 0.33 mm and coefficient of uniformity C_u = 1.8. Soil PC is also a river-deposited sand with some silt, for which D_{85} = 0.215 mm and C_u = 5.8. Soil MT, a processed mine tailings with some silt, has a D_{85} = 0.29 mm and C_u = 3.3. The mine tailings exhibited an angular grain shape, while both alluvial soils had sub-rounded grains. The gradation curves are evaluated as internally stable according to the method of Kenney and Lau (1985; 1986). Testing in the permeameter established a typical permeability of 0.025, 0.0015 and 0.0001 cm/s respectively for reconstituted specimens of soil FR, MT and PC.

Combinations of the three soils were tested against seven geotextiles, for which material properties are reported in Table 2.1. The two needle-punched nonwoven geotextiles have the same opening size of 0.212 mm, and the five woven geotextiles exhibit a range from 0.212 mm to 0.6 mm. Tests were conducted at an average

hydraulic gradient (i_{17}) of 4. Test variables examined were (i) the flow regime (unidirectional or cyclic), (ii) the imposed normal stress (0 or 25 kPa), and (iii) the period of cyclic flow reversal (50 or 10 s). A summary of the multistage test sequence followed in testing is given in Table 2.2. In principle, a relatively long stage of cyclic flow at T = 50 s (CYC 1) was followed by a shorter stage at T = 10 s (CYC 2), whereupon the normal stress was reduced from 25 kPa to zero, and the shorter stage at T = 10 s then repeated (CYC 3). In order to characterize filtration compatibility, each cyclic stage was preceded and followed by a stage of unidirectional flow. The rationale for choosing these test conditions is based on simulation of bank or shore protection structures that experience a low confining stress, and may be subject to a wide range of wave periods. A wave period T= 10 s is deemed "fast" reversing flow and recommended for simulation of wave action, while longer periods are deemed "slow" reversing flow typical of tidal environments

2.4 Results and discussion

Combinations of soil and geotextile examined in testing yield a filter ratio $0.6 \leq AOS/D_{85} \leq 2.1$ (see Table 2.3). For internally stable soil, a value of gradient ratio equal to one corresponds to a linear variation of head loss across the test specimen, believed indicative of excellent soil-geotextile compatibility; a value less than one implies a non-linear variation of head loss, in which the permeability of the soil-geotextile zone

(k_{57} or k_{67}) is less than that of the soil (k_{35}). Values of GR_{25} and GR_8 obtained in the last stage of unidirectional flow (UNI 4) generally diminish with increasing AOS/D_{85} (see Table 2.3 and Fig. 2.3), to a $GR_8 \leq 0.5$ at $AOS/D_{85} \geq 1.5$. The data suggest a relatively more permeable soil-geotextile interface develops with increasing pore size opening in the woven geotextiles. The needle-punched nonwoven geotextiles all have $AOS/D_{85} \leq 1$, and a $GR_8 > 0.5$ for the UNI 4 stage of testing.

Mass loss is reported separately for each stage of cyclic flow (see Table 2.3). Data for the first and last cyclic stage are plotted against AOS/D_{85} (see Fig. 2.4). Mass loss generally increases with greater AOS/D_{85}. The relation appears sensitive to opening size of the geotextile, given a loss smaller than 60 g/m^2 at $AOS/D_{85} \leq 1$ during the first stage of cyclic loading performed at a confining stress of 25 kPa (Table 2.2). Indeed, no mass loss was observed in any stage of cyclic flow in the three tests with AOS/D_{85} = 0.6, and a minimal loss ($m_p \leq 30$ g/m^2) was observed in only the initial stage of cyclic flow (CYC 1) in the three tests with AOS/D_{85} = 0.7 (see Table 2.3). The results describe the response of both nonwoven and woven geotextiles to cyclic flow. For these six tests with $AOS/D_{85} \leq 0.7$, inspection of gradient ratio values obtained in the last stage of unidirectional flow (UNI 4) establishes an average GR_{25} = 0.97 and GR_8 = 0.93. The finding implies consistency between the gradient ratio index value of relative permeability and absence of seepage-induced mass loss through the geotextile.

In contrast, the three test combinations with $AOS/D_{85} \geq 2$ yielded a cumulative mass loss $m_p \geq 1250$ g/m^2, which is much greater than that observed in all other tests. It was sufficiently large to cause early termination of the two tests with $AOS/D_{85} = 2$, given $m_p \geq 4000$ g/m^2. The nature of the response in these PC-G43aW and PC-G43bW tests, namely increased loss at reduced confining stress and wave period, appears consistent with the observations of Cazzuffi et al. (1999) and Chew et al. (2000). More generally, at greater values of AOS/D_{85}, the results show gradient ratio values (Fig. 2.3) consistent with the observations of mass loss (Fig. 2.4). Accordingly, values of $GR_8 \leq 0.5$ are attributed to piping of soil through the woven geotextiles examined in testing.

In filtration applications of dynamic, pulsating or reversing flow, Holtz et al. (1997) recommended an empirical design criterion of $AOS/D_{85} \leq 0.5$ for purposes of soil retention by a woven or nonwoven geotextile. The criterion evolved from an earlier expression based on O_{50}, rather O_{95}, that was based on a general review of filter design recommendation in several countries (Christopher and Holtz, 1985). A comparison of the empirical criterion for soil retention and laboratory test data (of Fig. 2.4) suggests the recommendation is conservative to design practice. In making this observation it should be noted that three factors, namely wave period, the hydraulic gradient and the confining stress are postulated to influence compatibility of soil-geotextile filter (Fannin and Srikongsri, 2007). Yet, none of these factors can be confidently addressed using the data of Fig. 2.4, and should be considered systematically in future studies in

order to properly understand the margin of safety that is implied in use of such empirical criteria.

2.5 Conclusions

The Gradient Ratio test was originally conceived to evaluate compatibility of base soil and geotextile filter in unidirectional flow. The test apparatus described has been configured to enable testing with unidirectional or cyclic flow, and to permit collection of soil that passes through the geotextile as a consequence of seepage flow. The following conclusions are made based on characterization of the soil (D_{85}), geotextile (AOS), soil-geotextile compatibility (GR_8) and mass of soil passing per unit area (m_p):

- test combinations of soil and geotextile that exhibit filtration compatibility in stages of cyclic flow, yield values of gradient ratio $0.5 \leq GR_8 \leq 2.0$ ($0.7 \leq GR_{25} \leq 1.6$) in a following stage of unidirectional flow;
- gradient ratio values diminish with larger AOS/D_{85};
- mass loss per unit area in stages of cyclic flow increases with larger AOS/D_{85};
- values of $GR_8 \leq 0.5$ are attributed to piping of soil through the woven geotextiles examined in testing.
- mass loss per unit area provides a very useful index of filtration compatibility for soil-geotextile combinations that exhibit piping (and a gradient ratio

significantly less than 1.0) rather than clogging (and a gradient ratio significantly greater than one), and should be reported to assist with test interpretation.

A negligible mass loss ($m_p \leq 30$ g/m^2) in only the first stage of cyclic flow at $AOS/D_{85} = 0.7$, and no mass loss ($m_p = 0$) in any stage of cyclic flow at $AOS/D_{85} = 0.6$, suggest:

- the empirical criterion of $AOS/D_{85} \leq 0.5$ for soil retention in cyclic flow is conservative, both for nonwoven and woven geotextiles.

An unacceptable mass loss ($m_p \geq 4000$ g/m^2) in the third stage of cyclic flow at $AOS/D_{85} = 2$, preceded by a relatively modest loss in the first two stages of cyclic flow, suggests:

- wave period and confining stress influence soil-geotextile filter compatibility, and those parameters, in combination with hydraulic gradient, require systematic study in order to understand the margin of safety that governs a confident use of the empirical criterion.

Table 2.1 Properties of the geotextiles

Geotextile (code)	Type	Mass / Unit Area	AOS (ASTM D4751)	Permittivity (ASTM D4491)	Permeability
	NW/W	(g/m^2)	(mm)	(sec^{-1})	(cm/s)
G21Na	NW	287	0.212	1.310	0.290
G21Nb	NW	185	0.212	1.192	0.134
G21W	W	218	0.212	0.511	0.021
G30W	W	225	0.300	0.769	0.049
G43Wa	W	282	0.425	0.881	0.080
G43Wb	W	304	0.425	2.003	0.194
G60W	W	453	0.600	0.366	0.061

Table 2.2 Multistage test procedure

Stage	UNI1	CYC1	UNI2	CYC2	UNI3	CYC3	UNI4
Normal Stress (kPa)	0	25	25	25	25	0	0
Wave Period (s)	0	50	0	10	0	10	0
Duration (min)	90	900	30	43	30	43	30
Number of cycles		1080		260		260	

Table 2.3 Test results

Test code	AOS/D_{85}	Mass loss (g/m^2)			UNI4	
		CYC1	CYC2	CYC3	GR_{25}	GR_8
FR-G21aN	0.6	≈ 0	≈ 0	≈ 0	1.0	0.8
FR-G21bN	0.6	≈ 0	≈ 0	≈ 0	1.3	1.1
FR-G21W	0.6	≈ 0	≈ 0	≈ 0	0.9	0.8
FR-G30W	0.9	≈ 0	≈ 0	≈ 0	1.1	1.3
FR-G43aW	1.3	≈ 0	≈ 0	≈ 0	1.0	1.0
FR-G43bW	1.3	6	≈ 0	≈ 0	1.3	1.3
FR-G60W	1.8	40	≈ 0	≈ 0	0.9	0.9
MT-G21aN	0.7	26	≈ 0	≈ 0	0.9	0.7
MT-G21bN	0.7	13	≈ 0	≈ 0	1.6	1.2
MT-G21W	0.7	4	≈ 0	≈ 0	0.9	1.0
MT-G30W	1.0	60	≈ 0	≈ 0	1.2	0.7
MT-G43aW	1.5	313	115	128	0.3	0.1
MT-G43bW	1.5	162	17	53	0.6	0.4
MT-G60W	2.1	1246	≈ 0	88	0.4	0.2
PC-G21aN	1.0	34	≈ 0	39	1.0	0.8
PC-G21bN	1.0	56	≈ 0	1	1.0	0.7
PC-G21W	1.0	49	≈ 0	28	1.2	2.0
PC-G30W	1.4	55	≈ 0	51	1.4	1.9
PC-G43aW	2.0	95	≈ 0	4349	N/A	N/A
PC-G43bW	2.0	239	165	4953	N/A	N/A

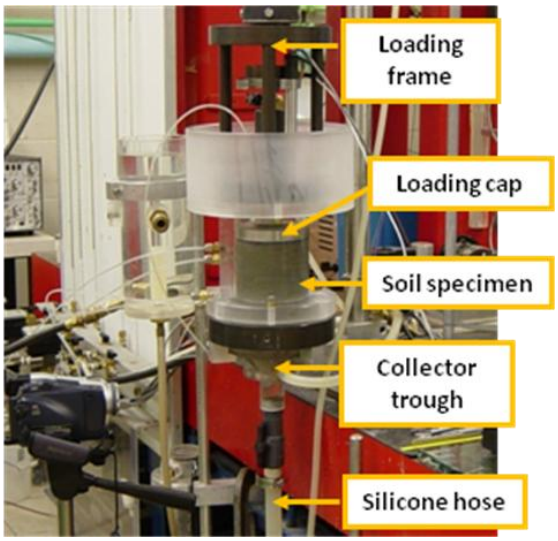

(a)

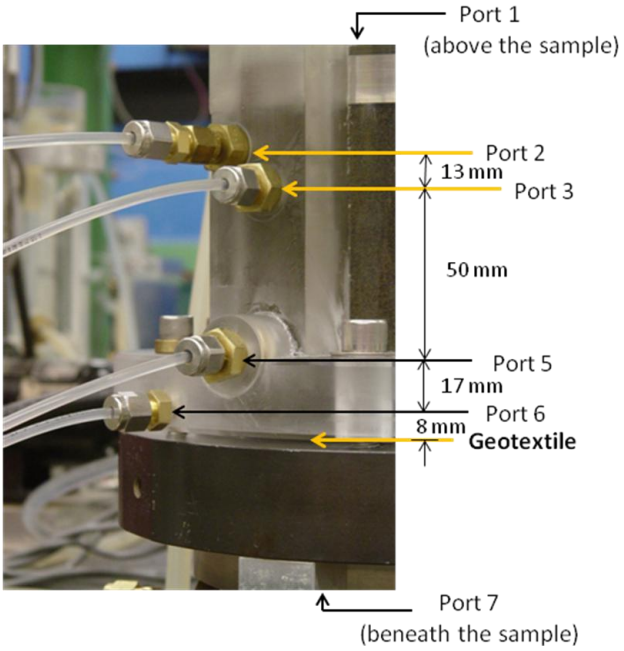

(b)

Figure 2.1 Cyclic Gradient Ratio test device: (a) permeameter assembly; (b) arrangement of sidewall ports

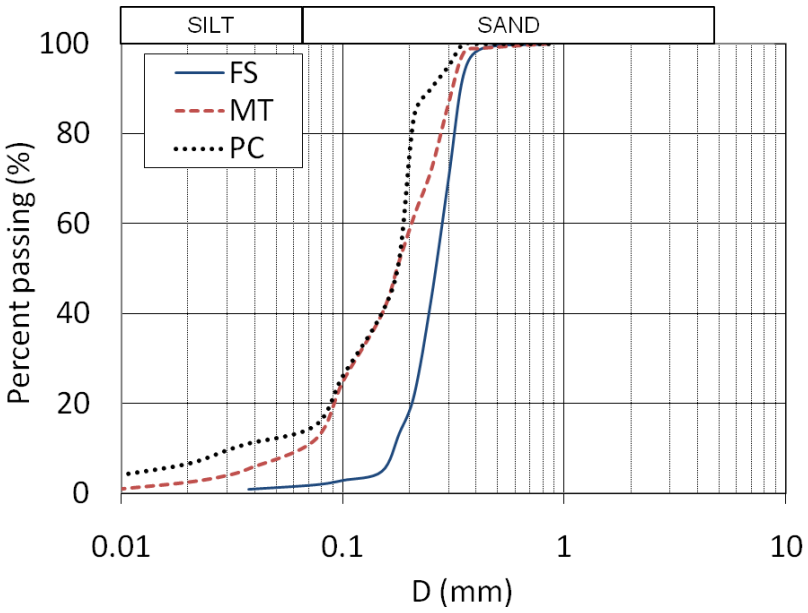

Figure 2.2 Grain size distribution curves

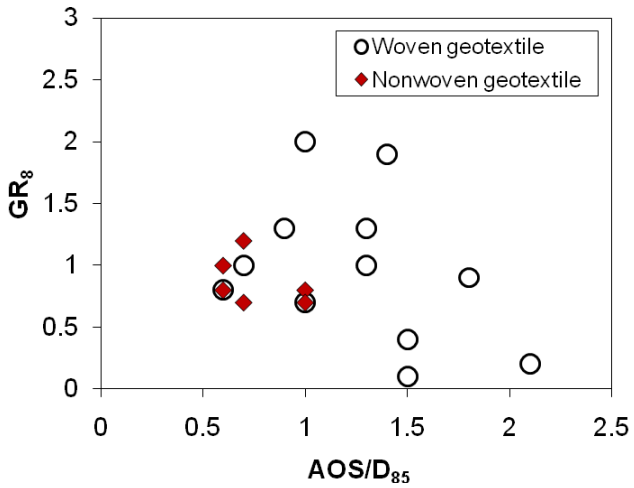

Figure 2.3 Relation between GR_8 (stage UNI4, see Table 2) and filter ratio AOS/D_{85}

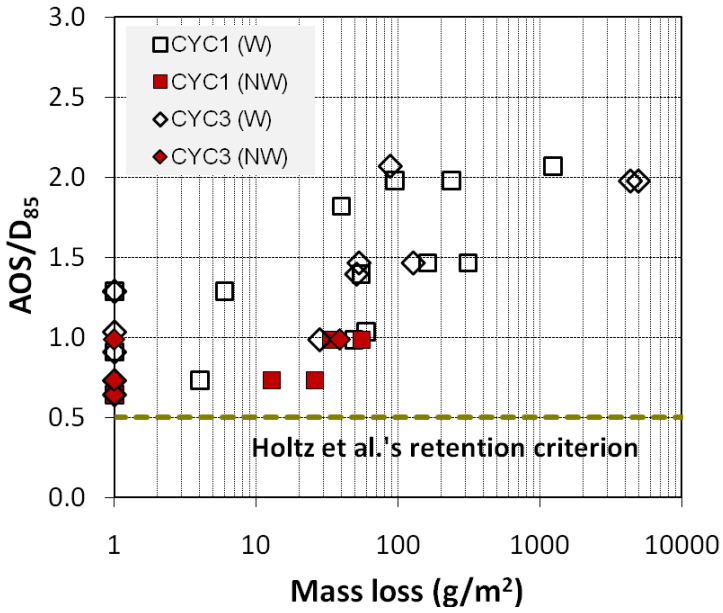

Figure 2.4 Relation between mass loss and filter ratio AOS/D_{85}

2.6 References

ASTM D 5101, *Standard Test Method for Measuring the Soil-Geotextile System Clogging Potential by the Gradient Ratio*, American Society for Testing and Materials, West Conshohocken, PA, USA.

Cazzuffi, D.A., Mazzucato, A., Moraci, N., & Tondello, M. (1999). A new test apparatus for the study of geotextiles behaviour as filters in unsteady flow conditions: relevance and use. *Geotextiles and Geomembranes,* **17**, 313 – 329.

Chew, S.H., Zhao, Z.K., Karunaratne, G.P., Tan, S.A, Delmas, P., and Loke, K.H. (2000). Revetment geotextile filter subjected to cyclic wave loading. *Proceedings of Geo-Denver 2000*, Denver, CO, USA, pp. 162 – 175.

Christopher, B.R., and Holtz, R.D. (1985), Geotextile engineering manual, *Report No. FHWA-TS-86/203*, Federal Highway Administration, D.C., USA, pp. 1044 p.

Fannin, R.J. (2007). Chapter 6: The use of geosynthetics as filters. *Geosynthetics in Civil Engineering*. Woodhead Publishing, Cambridge, UK, 295 p.

Fannin, R.J. and Pishe, R. (2000). Testing and specifications for geotextile filters in cyclic flow applications. *Proceedings of Geosynthetics 2001*, Portland, OR, USA, pp. 423-435.

Fannin, R.J., Vaid, Y.P., Palmeira, E.M. and Shi, Y.C., (1996). A modified gradient ratio device. *Recent Developments in Geotextile Filters and Prefabricated Drainage Geocomposites.* ASTM STP 1281, Philadelphia, PA, USA, pp. 100 – 112.

Fannin, R.J. and Srikongsri, A. (2007). Geotextile filters in cyclic flow: test results and design criteria. *Proceedings of Geosynthetics 2007*, Washington, D.C., USA, pp. 170-185.

Hameiri, A. (2000). Soil geotextile filtration behavior under dynamic conditions of vibration and cyclic flow. PhD Thesis, University of British Columbia, British Columbia, Canada, 270 p.

Hameiri, A. and Fannin, R.J. (2002). A cyclic gradient ratio test device. *ASTM Geotechnical Testing Journal*, **39**, 266-276.

Hawley, R. (2001). Filtration performance of geotextiles in cyclic flow conditions. MASc Thesis, University of British Columbia, British Columbia, Canada, 141 p.

Hoare, D.J. (1982). Synthetic fabrics as soil filters: a review. *ASCE Journal of Geotechnical Engineering*, **108**, 1230-1245.

Holtz, R.D, Christopher, B.R., and Berg, R.R. (1997). *Geosynthetic Engineering*. BiTech Publishers, British Columbia, Canada, 452 p.

Kenney, T. C. & Lau, D. (1985). Internal stability of granular filters. *Canadian Geotechnical Journal*, **22**, No. 2, 215-225

Kenney, T. C. & Lau, D. (1986). Internal stability of granular filters: Reply. *Canadian Geotechnical Journal*, **23**, No. 3, 420-423

Lawson, C.R. (1982). Filter criteria for geotextiles: relevance and use. *ASCE Journal of Geotechnical Engineering*, **108**, 1301-1317.

Palmeira, E.M. and Fannin, R.J. (2002). Soil-geotextile compatibility in filtration. *Proceedings of the 7th International Conference on Geosynthetics*, Nice, France, pp. 853-872.

3 Influence of Test Methodology on Soil-Geotextile Compatibility in Cyclic Flow Using Rigid-Wall Permeameter[2]

3.1 Outline

Cyclic flow is reproduced in two rigid-wall permeameters, of different size, to examine soil-geotextile filtration compatibility. The influence of test methodology is reported, from data on uniform sand and a monofilament and a multifilament woven geotextiles. Cyclic flow regime is characterized with reference to hydraulic gradient and wave period. Vertical effective stress at the soil-geotextile interface is obtained directly by measurement in the large permeameter, and indirectly by computation in the small permeameter taking into account side-wall friction. A new approach is proposed for data interpretation that considers both seepage pressure and stress history, using a value of mean effective stress at the soil-geotextile interface. No scale effect is apparent in results from the two permeameters. Values of gradient ratio, mass loss and volume change indicate a concern for soil retention at a filter ratio (AOS/D_{85}) between 2.0 and 2.8 that appears governed by effective stress and wave period.

[2] A version of this chapter will be submitted for publication. Srikongsri, A.and Fannin, R. J. (2010). Influence of test methodology on soil-geotextile compatibility in cyclic flow using rigid-wall permeameter.

3.2 Introduction

In filtration applications, reversing or pulsating seepage that yields a cyclic flow regime is encountered at river, lacustrine and marine protection works. The characteristics (i.e. wind wave, ship wave and tidal) of cyclic flow vary considerably with reference to spatial and temporal variations of hydraulic gradient, effective stress and period of flow reversal. Few systematic experimental studies of these variables are reported for granular filters (de Graauw et al., 1983 and de Graauw et al., 1984), and a very limited body of test data is reported for geotextile filters. No standard approach to testing is found in the literature, and design guidance for geotextile selection in applications of cyclic flow is, for the most part, unsupported by a firm understanding of the governing variables. Accordingly, the margin of safety inherent in use of empirical rules for such geotextile filtration design cannot be expressed with confidence.

Over a considerable period of time, research efforts on filtration applications in cyclic flow have sought to examine the influence of wave period, hydraulic gradient and effective stress. Laboratory permeameter test devices may be generally categorized in two sizes, namely a large permeameter of approximately 300 mm diameter, and a small permeameter of approximately 100 mm diameter. To date, issues of any scale effect in laboratory testing have not received attention. In particular, the variation in

effective stress along the length of a rigid-wall permeameter, under hydrodynamic conditions, is not well-understood due to limitations of the test device regarding the characterization of sidewall friction.

In a study of granular filters for storm surge barrier and coastal protection structures, de Graauw et al. (1984) reproduced a flow regime of in-plane cyclic flow (bi-directional flow parallel to the filter interface), and also cross-plane cyclic flow (bi-directional flow perpendicular to the filter interface). In contrast to in-plane cyclic flow, tests with cross-plane seepage resulted in movement of base soil into the filter layer. The later test series was conducted in a rigid-wall permeameter, 280 mm in diameter, employing the principle of head-control of seepage flow: a test performed at a constant differential water head across the soil sample to achieve the predetermined value of gradient. The specimen of base soil, and granular filter, were each approximately 350 mm in length. Importantly, a constant wave period (T) of 10 s, hydraulic gradient (i) from 1 to 8 and effective stress (σ) from 0 to 130 kPa were all examined as test variables. A sensitivity of the base soil, a fine sand, to arching phenomena at the filter interface was noted at a large filter ratio $D15_f/D50_b \approx 13$. Importantly, critical gradient at which instability occurred was found to increase with increasing stress. No consideration was given to sidewall friction in analysis of the results, and repeatability of filtration behaviour was not explicitly addressed.

Cazzuffi et al. (1999) developed a cross-plane cyclic flow device, employing the principle of flow-control to generate wave actions at a range of wave period 2 s $\leq$ T $\leq$ 20 s and hydraulic gradient 1.5 < i < 16. The flow-controlled system uses a cylindrical piston to push and pump the water seeping through the soil specimen in manner of a constant flow volume. Stress on the soil-geotextile interface was $0 \leq \sigma \leq 150$ kPa. The permeameter had a partially flexible wall that could accommodate axial compression of the test specimen, thereby reducing the influence of sidewall friction. The test specimen was 300 mm in diameter, and 400 mm in length. A ratio of hydraulic gradient across the soil-geotextile interface to that within the base soil was used to quantify the nature of filter compatibility, in an approach similar to that of the ASTM Gradient Ratio test. Retention capacity was characterized with reference to mass loss of base soil through the geotextile. The great loss (> 5000 g/m^2) that led to instability at very low stress ($\approx$ 0 kPa), associated with the high gradients of values greater than 3, was reported for the combination of uniform sand and woven geotextile at a filter ratio $O_{95}/D_{85} \approx 2.2$.

The work of Cazzuffi et al. (1999) led to development of very similar cyclic flow test devices, using a rigid-wall permeameter with slightly different dimensions (Chew et al 2000; Chen et al. 2008). In a study of wave period in the range 2s < T < 15s, Chew et al. (2000) tested a uniform sand in combination with a woven monofilament and a needle-punched nonwoven geotextile. A constant value of top stress 110 kPa was imposed on the specimen, of 315 mm diameter and 300 mm length, with no

consideration of sidewall friction effects governing stress at the interface. A wave period shorter than 10 s, most notably a value of 2s, was found to induce the greatest quantity of soil passing.

Chen et al. (2008) examined the effects of fines content in a uniformly-graded sand. The test specimen, 330 mm in diameter and 450 mm long, was subject to relatively slow cyclic flow at 300 s < T < 600 s, at a maximum hydraulic gradient of 10, and with a top vertical effective stress of 70 to 140 kPa. Grease was used to lubricate the soil-wall interface of the permeameter in order to reduce sidewall friction. However, an effectiveness of greasing on a reduction of sidewall friction was not addressed. Fines content, up to 10% of low plasticity silt, has a significant effect on the retention stability of a soil–geotextile system. Preferential piping channels are developed from washing out of the fines through the sand, and consequently the piping of sand particles.

Chen et al. (2009) used a smaller permeameter, 100 mm in diameter, to examine spatial variations of water head distribution in a plastic silt sample, 100 mm long. The specimen dimensions are identical to those of the ASTM Gradient Ratio test device. In this test series, the filter medium was a wire mesh screen of 0.5 mm in opening size. A cross-plane cyclic flow was reproduced using the principle of head-control, yielding a hydraulic gradient of 0.8, for a range of wave period 30 s < T < 3750 s. No vertical stress was applied to the top of the specimen. For wave periods shorter than 150 s, a

temporal hydraulic gradient developed at the filter interface was observed as greater than that within soil, and found to be influenced by the permeability of the soil.

Modifications to an ASTM Gradient Ratio test apparatus, to allow for testing with cyclic flow under head-control similar to that reported by de Graauw et al. (1984), are reported by Hameiri and Fannin (2002). The device was commissioned with a series of tests on glass beads (Hameiri, 2000) and subsequently used to examine the compatibility of various geotextiles and sandy soils in tests for wave periods of 10 s and 50 s, at a constant hydraulic gradient of 4, and a top axial stress of 25 kPa and 0 kPa (Hawley, 2001). A review of findings from this latter study is provided by Srikongsri et al. (2010: see chapter 2). The influence of wave period and confining stress was identified as important to geotextile filter compatibility, and found worthy of further systematic study in order to understand the safety margin of empirical design criteria.

In this study, the compatibility of soil and geotextile in cross-plane cyclic flow is examined using the small permeameter of Hameiri (2000) and the large permemater of Moffat (2005). The latter device was originally developed for study of seepage-induced internal instability of cohesionless soil in steady unidirectional flow, and therefore it was modified for the purposes of this study. A multi-stage test procedure is described, with sequences of cross-plane uni-directional and bi-directional flow, which enables characterization of soil-geotextile compatibility in cyclic flow. Use of two

permeameters allows for the reporting of observations on scale effect of the test device. An innovative component of the large permeameter leads to a novel approach to account for sidewall friction testing with a rigid-wall permeameter, and hence the influence of effective stress at the soil-geotextile interface. Experimental data, and a companion theoretical analysis, are presented in support of the test method and approach to data interpretation.

3.3 Test equipment

3.3.1 Small permeameter

The small permeameter is a Modified Gradient Ratio device that was designed and fabricated at UBC. It is a modified version of the ASTM device that allows for the application of unidirectional or cyclic flow, imposition of an axial stress to simulate in-situ confining pressures, and collection of particles passing through the geotextile. Additional measurements of water head along the sample length allow for a more comprehensive analysis of soil/geotextile compatibility. Details of the development and features of the design are reported by Fannin et al. (1996) and Hameiri (2000).

A schematic diagram of the gradient ratio device (Fig. 3.1a) illustrates the various modifications. The rigid-wall permeameter mounts on the bench top. It is made of 8

mm thick Plexiglas, which facilitates visual observation during testing (Fig. 3.1b). It accommodates a soil specimen of 101 mm diameter that is typically reconstituted to a length of approximately 105 mm. The specimen rests on the geotextile sample to be tested (Fig. 3.1c). The geotextile is supported on a perforated base plate, made of anodized aluminum, with 6 mm holes at 15 mm centre-to-centre spacing. A coarse wire mesh (opening size ≈ 1.5 mm) is inserted between the geotextile and the base plate to provide for unimpeded seepage across the geotextile. A collection trough, located below the base plate, collects soil particles that pass through the geotextile sample. The collection trough comprises an upper and lower section, where the upper section is made of a Plexiglas funnel with internal slope of 45° that directs particles passing through the geotextile into the lower section; the lower section is made of a flexible silicon tube with an internal diameter of 19 mm to facilitate the acquisition of discrete samples at any time during the test (Fig. 3.1d). Axial loading is applied by means of a piston and top plate made of anodized aluminum, to yield a value of normal effective stress on the top of the soil specimen (Fig. 3.1d).

Measurements of water head are taken at five port locations on the sidewall of the permeameter (Fig. 3.1a). Note that two additional port locations reported by Fannin et al. (1996) are redundant, and are found not necessary for purposes of data analysis and interpretation in this study. Port 1 is located on the top plate to establish the value of water head at the inlet (top of sample). Ports 3, 5 and 6 are located at 75 mm, 25 mm

and 8 mm above the geotextile. Port 7 is located on the upper part of the collection trough, and establishes water head at the outlet (bottom of sample). With reference to Fig. 3.1a, the value of Gradient Ratio (GR_{25}) and a companion modified value (GR_8) are calculated as:

$$GR_{25} = \frac{i_{57}}{i_{35}} \quad (1)$$

$$GR_8 = \frac{i_{67}}{i_{35}} \quad (2)$$

where i_{35} = hydraulic gradient within soil between ports 3 and 5

i_{57} = hydraulic gradient across soil-geotextile between ports 5 and 7

i_{67} = hydraulic gradient across soil-geotextile between ports 6 and 7

3.3.2 Large permeameter

The large permeameter was originally designed and fabricated at UBC for testing seepage-induced internal erosion of soil as a consequence of steady unidirectional flow, with application to earth dams (Moffat, 2005). Like the small permeameter, its design enables application of axial stress on the top of the specimen. In contrast to the small permeameter, axial load is measured at the top and also at the bottom of the specimen (Moffat and Fannin, 2006). For the purposes of the current study, a geotextile is located below the soil specimen. However, the configuration of the rigid-wall cell means that no special provision can be made to collect soil particles passing

through the geotextile during a test. Control of the permeameter was changed to enable application of a unidirectional or cyclic flow regime. Additional ports were added to the sidewall of the permeameter for measurements of water head along the specimen length at locations directly comparable to the small gradient ratio test device.

A schematic diagram of the large device (Fig. 3.2a) provides for a direct comparison with the smaller device. The large permeameter is floor-mounted. The rigid-wall cell, which seats in a steel reaction frame, is made of 13 mm thick Plexiglas that facilitates visual observation during testing (Fig. 3.2b). It accommodates a soil specimen of 280 mm diameter that was reconstituted to a length of approximately 105 mm, which is the same length used in the smaller device. As noted above, the specimen rests on the geotextile sample to be tested (Fig. 3.2c). The geotextile is supported on a perforated base plate, made of anodized aluminum, with 30 mm holes at 45 mm centre-to-centre spacings. Once again, a layer of two wire meshes, which are coarse (opening size $\approx$ 5 mm) and fine (opening size $\approx$ 1.5 mm), is inserted between the geotextile and the base plate to provide for unimpeded seepage across the geotextile. The base plate is part of an integral base reaction frame that seats onto a submersible load cell that is used to measure vertical stress at soil-geotextile interface (see Fig. 3.2c). In the absence of any collection trough that facilitates discrete collection of soil passing during a test, the lower chamber of the device was carefully washed at the end of a test, thereby permitting a final value to be calculated. Axial loading is applied by means of a piston and top plate made of anodized aluminum. Measurements of water head are taken at

five port locations on the sidewall of the permeameter (Fig. 3.2a), the locations of which reproduce those of the companion small permeameter. Accordingly, measurement of gradient ratio value is identical to that in the small permeameter.

3.3.3 Control and measurement system

In the small permeameter, vertical stress (σ'_{vt}) is applied to the top of the specimen by means of a pneumatic piston. The magnitude is controlled manually by a pressure regulator on the laboratory air-supply. Seepage flow is imposed by a hydraulic supply system that employs a principle of head-control. Three constant-head cylinders, with adjustable elevation, are used to impose either unidirectional or cyclic flow (Fig. 3.3). De-aired water is continuously supplied from a reservoir, by a peristaltic pump, to both the upper cylinder and the middle cylinder. The lower cylinder receives downward flow from the permeameter. Overflow water from all three constant-head cylinders is drained without recirculation.

In the large permeameter, vertical stress (σ'_{vt}) is similarly applied to the top of the specimen by means of a pneumatic piston that is controlled manually by a pressure regulator. Additionally, vertical stress at the bottom (σ'_{vb}) is established from readings by the submersible load cell. The hydraulic supply system is also head-controlled. However, in contrast to the small permeameter, the upper and middle cylinders (Fig. 3.3) are replaced by two floor mounted pressure-tanks with a capacity of

approximately 160 liters of de-aired water. In this case, water head across the specimen that is given by the differential head between ports 1 and 7 (H_{17}), is controlled manually by a pressure regulator that controls pressure applied to the air-membrane-water interface in the tanks. The lower cylinder is replaced with a floor-mounted overflow tank that is subject to atmospheric pressure.

The flow regime used in both the small and the large permeameter is reproduced using an identical flow operation. An equidistance system water head, namely +H and –H (Fig. 3.3) is adjusted to meet a pre-determined value of average hydraulic gradient across the specimen (i_{av}), defined as $i_{av} = H_{17}/Z$, where Z is a total length of specimen (see Figs. 3.1a and 3.1b). To impose a stage of downward unidirectional flow, seepage is controlled by water head +H across the specimen, from the middle cylinder to the lower cylinder. To impose cyclic flow, a programmable solenoid valve (3-way valve) is used to switch the direction of seepage at a pre-determined wave period (T), wherein the downward seepage controlled by +H is followed by upward seepage controlled by -H, associated with flow from the upper to the middle cylinder. Differential pressure transducers (DPT) provide a record of differential water head between each port location. A linear variable differential transformer (LVDT) is used to measure change in specimen length during a test (Figs. 3.1a and 3.2a). A data acquisition system records the output of each transducer and writes the data to storage in real-time. Discharge flow is measured periodically from the overflow of the lower cylinder (tank for the large permeameter) and used to deduce a value of hydraulic conductivity or

permeability. Soil passing through the geotextile may be collected at discrete intervals during soil placement and testing in the small permeameter, and at the end-of-test in the large permeameter, whereupon it is oven-dried in order to calculate mass loss per unit area.

3.4 Test methodology

The test methodology consists of preparing the geotextile and soil materials, reconstituting the soil specimen against the sample of geotextile, consolidation under the initial top vertical effective stress, performing the multi-stage seepage test, and collecting the soil, if any, that passes through the geotextile. The methodology is largely adapted from Hawley (2000), with some modifications to address the specific objectives of the current study.

3.4.1 Sample preparation

It is necessary in any fundamental study of soil properties and filtration compatibility involving a reconstituted specimen that the specimen preparation technique replicates a homogeneous specimen. A water pluviation technique is used in this study to create homogenous, saturated specimens of the same density. The technique is well-suited to uniform soils (Vaid & Negussey, 1986).

In all tests, the sample of geotextile is soaked in a bath of de-aired water and squeezed manually until there is no visual observation of air bubbles. Thereafter it is left in the bath overnight to further ensure saturation. In preparing the soil, water is added to a predetermined quantity of dry soil and the resulting slurry then boiled in a flask to remove any entrapped air. The soil for each specimen is prepared as a series of batches. The saturated soil is then allowed to cool in the flask to room temperature, which in the laboratory is consistently 23 – 24ºC.

The experimental routine involves assembly of the lower part of the permeameter, and back-filling the collection trough with de-aired water until the rising surface just reaches the perforated plate and wire mesh screen. The geotextile sample to be examined in testing is then transferred on to the wire mesh, and the permeameter cell mounted in position and immediately filled with de-aired water. After checking the saturation of each thin tube that connects a manometer port to its corresponding pressure transducer, soil is pluviated from the flask into the permeameter. During pluviation, the particles reach a terminal velocity at a very small drop height, and the resulting deposit is in a very loose state. Upon completing the process of reconstitution, the top surface is levelled to a targeted specimen length of approximately 100 - 105 mm. In order to prevent any significant filtration incompatibility at the top boundary, the surface was covered with a nonwoven geotextile (AOS = 0.08 mm) and a wire mesh (opening size ≈ 3 mm) before seating the

top loading platen against it. The experimental set-up is completed by assembling the upper components and connecting the top inlet-outlet valve to the middle constant-head supply.

3.4.2 Multi-stage test procedure

The test procedure is intended to recreate, in a general manner, conditions found at the soil-filter interface in bank or shore protection structures. The typical wave period of wind-generated waves recommended for purposes of design is in the range 2 to 10 s (Pilarczyk, 2000; USACoE, 2002). In contrast, infragravity waves typically generate a longer wave period in the range 50 to 350 s: the waves result from processes of energy conversion of gravity waves near the coastline. In addition, wave action creates a wide range of hydraulic gradient, which may attain values as large as 10 (Giroud, 1996). Accordingly, three wave periods (T) of 6, 60 and 120 s, and three average hydraulic gradients (i_{av}) of approximately 1, 5 and 10 were selected as test variables in the current study.

The multi-stage test procedure involves consolidation of the soil specimen to a targeted value of effective stress, whereupon it is subject to several stages of unidirectional and cyclic flow. Conditions at the filter interface in bank and shore protection structures are expected to invoke relatively low values of effective stress in the range 5 to 30 kPa (e.g. a stone armor layer of a typical thickness in the range 0.5 to

3 m, with a submerged unit weight of 10 kN/m^3). Accordingly, three values of vertical effective stress (σ'_{vt}) on the top surface of the soil were examined in testing; in the small permeameter, values of 66, 33 and 7 kPa and, in the large permeameter, values of 57, 28 and 7 kPa. The difference in values arises from the different aspect ratio (Z/D) of the specimen in the large permeameter (≈ 0.3) and the small permeameter (≈1): the influence of sidewall friction is expected less significant in the large permeameter and the selection of values was made with the objective of imposing an equal value of effective stress at the soil-geotextile interface, for purposes of data comparison. The selection was made based on reported experience from previous use of the large permeameter (Li, 2008) and the author's judgment based on use of the small permeameter. The combination of minimum top stress (≈ 7 kPa) and maximum hydraulic gradient (≈ 10) is anticipated to yield a very low value of vertical stress at the soil-geotextile interface.

The multistage test procedure is summarized in Fig. 3.4. In any particular test, all stages of cyclic flow are imposed at a constant value of wave period (T), yielding two test variables of effective stress (σ'_{vt}) and hydraulic gradient (i_{av}). A test commences with consolidation of the specimen to a value of σ'_{vt} = 66 kPa in the small permeameter, else 57 kPa in large permeameter. The first stage of cyclic flow (CYC1), at value of $i_{av} \approx 1$, is preceded and followed by a stage of unidirectional flow (UNI-1a and UNI-1b) at the same gradient $i_{av} \approx 1$: observations made during the stage

of unidirectional flow are used to characterize soil-geotextile filtration compatibility before, and after, the embedded stage of cyclic flow. Upon completion of the first stage of cyclic flow, the effective stress on the top of the specimen is reduced to a value of σ'_{vt} = 33 kPa in the small permeameter, else 28 kPa in large permeameter, and a second stage of cyclic flow (CYC2) then imposed at the same value $i_{av} \approx 1$: the same sequence is repeated for a third stage of cyclic flow (CYC3) at a value of σ'_{vt} = 7 kPa for either small permeameter. At this point in the test, the top effective stress is re-established at 66 kPa in the small permeameter, else 57 kPa in large permeameter, the value of hydraulic gradient increased to $i_{av} \approx 5$, and the imposed flow routine of CYC1 to CYC3 then repeated (Fig. 3.4). Upon completion, the top effective stress is re-established as before, the value of hydraulic gradient increased to $i_{av} \approx 9$, and the imposed flow routine of CYC1 to CYC3 then repeated for a third and last time.

All stages of unidirectional flow down through the specimen are imposed for a minimum of 30 mins, in order to observe any spatial and temporal variation in water head distribution. All stages of cyclic flow are imposed for exactly 90 mins, yielding 900 cycles per stage at T = 6 s (a total of 8100 cycles per test), 90 cycles per stage at T = 60 s (a total of 810 cycles per test), and 45 cycles per stage at T = 120 s (a total of 405 cycles per test). Typically, a test would take 3 to 4 days to complete in the small permeameter, and 7 to 10 days in the large permeameter. During testing, there was need for a periodic interruption that was usually timed to occur at the end of a

particular UNI stage, in order to recharge the supply reservoir of de-aired water. This interruption has no effect on the further stage of testing.

At any point in time during the test, the lower collection trough may be clamped at discrete intervals to separate and collect the soil passing through the geotextile (small permeameter only). Upon completion of the test (small and large permeameter), the soil is removed and its mass is determined. This information provides the basis of evaluating soil retention criteria for that specific geotextile/soil combination.

3.4.3 Test materials

The soil used in tests reported herein is a uniformly-graded alluvial sand, termed Alouette River sand. The soil is a very fine sand, which is believed as potentially problematic for soil erosion against selected geotextile filters. It has a D_{85} of 0.11 mm, a uniformity coefficient (C_u) of 1.8, and contains approximately 15% of non-plastic coarse silt. Microscopic inspection reveals the particles are sub-angular in shape. It is classified as silty sand (SM) according to the unified soil classification system, and found internally stable according to the method of Kenney and Lau (1985 and 1986). A water pluviation technique yields a saturated unit weight of 18 kN/m^3.

Direct shearbox tests were conducted in order to establish values for the angle of shearing resistance, to use in calculation of a lateral stress coefficient. The tests were

performed on reconstituted soil specimens in a standard shearbox, 100 mm x 100 mm in plan area, and 25 mm thick. The specimen was reconstituted by air pluviation with very small drop height, to yield a loose state believed representative of the permeameter test specimen. Specimens were consolidated at a normal effective stress in the range 5 to 100 kPa, and then sheared at a constant rate of 1 mm/minute. Results for the silty sand used in testing (termed soil C, in Appendix C) include a test that was repeated. The data exhibit a non-linear relation that is attributed to the influence of stress dependency at very low stress. Similar findings are reported in the literature for other soils at very low stress (e.g. Fannin et al. 2005). The maximum angle of shearing resistance (φ_{max}) was 38º, 40º and 44º for values of $40 \leq \sigma_n \leq 60$ kPa, $10 \leq \sigma_n \leq 40$ kPa and $\sigma_n \leq 10$ kPa, respectively.

Two geotextiles, a monofilament woven geotextile (W1) and a multifilament woven geotextile (W2), were examined in testing. These two geotextiles were designed and recommended for filtration applications involving coastal or bank erosion protection such as riprap revetment by the manufacturer (Ten Cate Geosynthetics). Properties of the geotextiles are given in Table 3.1: in combination with the sand they yield a filter ratio AOS/D_{85} of 2.0 and 2.8, respectively. Details of the test program are given in Table 3.2.

3.5 Results

A total of nine tests were performed on the soil and two geotextiles (Table 3.2). In the small permeameter, two tests at T = 6 s, namely W1-T6(S) and W2-T6(S) for which $AOS/D_{85} \approx 2$ and 2.8 respectively, may be compared with findings for the W2 geotextile with larger filter ratio at T = 60 and 120 s, from tests W2-T60(S) and W2-T120(S). In order to address issues of reproducibility in the experimental findings, tests W2-T6(S) and W2-T60(S) were repeated. In the large permeameter, three tests were performed, namely W2-T6(L) at T = 6 s, and W1-T60(L) and W2-T60(L) at T = 60s. These latter tests allow issues of scale effect to be addressed in interpretation of the data.

3.5.1 Hydraulic response in head-controlled system

The transition in test W2-T6(S), from stages UNI-1a to CYC1 (Fig. 3.5a) and CYC1 to UNI-1b (Fig. 3.5b) is typical of the hydraulic response observed in testing with head-control of seepage flow. The data are for a top stress of 66 kPa and $i_{av} \approx 9$, with the average gradient determined knowing H_{17} (see ports P1 and P7 in Figs. 3.1 and 3.2) and the specimen length (Z). Inspection shows the control system to yield an excellent transition from unidirectional to cyclic flow, and vice versa. The response during cyclic flow alone for the same W2 geotextile at T = 6 s, 60 s and 120 s (Fig. 3.6)

shows the short wave period of 6 s does not permit the water head across the soil-geotextile interface (H_{57}) and within the soil (H_{35}) to reach equilibrium (Fig. 3.6a). In contrast, there is a relatively short duration of steady flow evident at T = 60 s (Fig. 3.6b) that becomes longer at T = 120 s (Fig. 3.6c). The companion plots of water head along the specimen length depict the temporal variation over one flow reversal. It takes about 5 to 7 s to reach the equilibrium state (Figs. 3.6b and 3.6c) given the hydraulic conductivity of this soil (0.007 cm/s), which explains the absence of a steady flow regime in the data at T = 6 s (Fig. 3.6a). The response is typical of the cyclic flow in both the small and large permeameter. The variation of time to achieve equilibrium during the transient phase in each cycle of reversing flow, in soils of different permeability, has been demonstrated in the work of Hameiri and Fannin (2002).

Consider the general case of a soil element, which is subjected to upward seepage flow. The vertical effective stress at any depth *x*, below the top surface of the element is calculated by: $\sigma'_v = \gamma' x - i \gamma_w x$, where $= \gamma'$ is a submerged unit weight of the soil (kN/m^3), i is the hydraulic gradient across the entire soil element and γ_w is a unit weight of water (kN/m^3). If the applied gradient exceeds a critical value, seepage flow results in zero effective stress and the action of static liquefaction results in a condition of heave and boiling. This concept applies directly to the soil specimen in the permeameter, when flow reversal yields upward seepage flow component. The term $i\gamma_w x$ defines the pore water arising from the hydrodynamic component, which for

purposes of mechanical analysis (in further section), is defined herein as the "seepage pressure" (S).

Flow reversal produces a transient variation in water head distribution and hence hydraulic gradient, along the length of the test specimen. Inspection of the test data (Fig. 3.6a to 3.6c) yields a schematic representation of the transient hydraulic gradient (i_{tr}) at the lower part of the specimen, which exceeds the value of average hydraulic gradient (i_{av}) (see Fig. 3.6d). Over time, it diminishes to the value of i_{av}. The greater value of transient hydraulic gradient is likely to be the cause of seepage-induced instability. However, it acts over a length (Z′) shorter than the total length of the specimen (x = Z) and, the magnitude of Z′ cannot be defined accurately due to the limitation of port location on the permeameter. Accordingly, the term $i_{av}\gamma_w Z$ is used as an index parameter, in order to calculate seepage pressure for purposes of data analysis. Recognizing that the transient hydraulic gradient is greater than the average gradient, the approach is believed conservative in defining a limit to filtration incompatibility with reference to the general principle of hydromechanics.

3.5.2 Large permeameter test data

In the large permeameter, onset of seepage-induced soil loss is established from visual observations. During a test, compatibility of the soil-geotextile combination is characterized from volume change of the soil specimen and from Gradient Ratio

values in the soil-geotextile composite zone. Mass loss, obtained after completion of a test, is also reported.

At $AOS/D_{85} \approx 2$ and T = 60 s for test W1-T60(L), visual observations indicated no loss of soil in any stage of unidirectional (UNI) flow and, similarly, no loss in any cyclic (CYC) stage. No volume change was observed during the test, and therefore the cumulative mass loss of 94 g/m^2 recorded at the end is attributed only to loss during reconstitution of the soil specimen against the geotextile. Values of $GR_{25} \approx 1.1$ and $GR_8 \approx 1.2$, obtained in all UNI stages of the test, indicate a variation of water head distribution that is essentially linear across the length of the specimen. Accordingly, the test combination is deemed stable in both unidirectional and cyclic flow.

At $AOS/D_{85} \approx 2.8$ and T = 60 s for test W2-T60(L), visual observations again established no soil loss during any of the UNI stages. In the CYC stages, no losses occurred at $i_{av} \approx 1$, however small losses were noted for all CYC stages with $i_{av} \approx 5$ and found to increase at $i_{av} \approx 9$. The losses occurred as a pulsating action that was not restricted to any preferential location on the geotextile. The action was found transient, since each cycle of flow reversal yielding downward seepage was associated with the onset a soil loss that continued for approximately 7 s to 15 s, after which it diminished quickly to a negligible quantity. A volume change of 0.5% occurred over the duration of the test, associated with a cumulative mass loss of 959 g/m^2 that includes the component for specimen reconstitution. Values of $0.9 \leq GR_{25} \approx GR_8 \leq$

1.0 indicate a linear variation of head loss across the soil-geotextile composite zone. The results show the test combination to be stable in unidirectional flow, but provide evidence of a transition from stable to unstable response in cyclic flow.

At $AOS/D_{85} \approx 2.8$ and T = 6 s for test W2-T6(L), there was no mass loss in any of the UNI stages, however it did occur in all of the CYC stages. Rather than pulsating and transient, the action was found continuous at this shorter wave period. As for test W2-T60(L), the losses were observed across the entire surface area of geotextile, with no evidence of any preferential location. Observations suggest the losses increased with application of larger hydraulic gradient, and increased with reduction in effective stress applied to the top surface of the specimen. No preferential flow channel developed within the body of soil specimen. A volume change of 3% occurred over the duration of the test, associated with a cumulative mass loss of 5487 g/m^2, which again includes that for specimen reconstitution. Values of $GR_{25} = GR_8 = 1$ confirm a linear head loss across the soil-geotextile composite zone that appears common to all three tests, and is attributed to the uniform gradation of the soil. The test combination is deemed stable in unidirectional flow, but unstable in cyclic flow.

Axial load on the top and bottom surface of the test specimen are measured directly in the large permeameter. For the hydrostatic condition, a top vertical effective stress ($\sigma'_{vt(0)}$) of 57 kPa, 28 kPa and 7 kPa yielded values at the base ($\sigma'_{vb(0)}$) in the range 45 to 48 kPa, 22 to 24 kPa, and 4 to 6 kPa, respectively. In stages of unidirectional flow,

the downward seepage force resulted in a stress increase at the base of approximately 0.2 to 0.4 kPa, 2 to 3 kPa, and 4 to 5 kPa for values of $i_{av} \approx 1$, 5 and 9, respectively. In stages of cyclic flow at T = 60 s, upward flow yielded a corresponding reduction of similar magnitude in σ'_{vb}. Consequently, stress at the soil-geotextile interface is close to zero in the CYC3 stage when $\sigma'_{vt(0)} = 7$ kPa at $i_{av} \approx 9$ (see Fig. 3.7). Stress loss in the system that is influenced by sidewall friction is found to be about 20% to 45%. Stages of cyclic flow at T = 6s did not provide useful data on axial load at the base, because the reversing action is too fast.

3.5.3 Small permeameter test data

In the small permeameter, onset of seepage-induced losses is based not only on visual observations, but also on values of mass loss for each individual stage of loading. The additional data enable a more precise characterization of filtration compatibility.

At $AOS/D_{85} \approx 2$ and T = 6 s for test W1-T6(S), visual observations indicated no soil loss in any stage of unidirectional (UNI) or cyclic (CYC) flow. The finding is consistent with no volume change of the specimen. Only a mass loss of 65 g/m^2 was recorded during reconstitution of the soil specimen. Values of GR_{25} and GR_8 in the range 1.2 to 1.5 indicate a nearly linear variation of water head throughout the test. Accordingly, the test combination is considered stable in both unidirectional and cyclic flow.

At $AOS/D_{85} \approx 2.8$ and T = 6 s for test W2-T6(S), mass loss occurred in none of the UNI stages, but all of the CYC stages. At $i_{av} \approx 1$, the amount was reasonably similar ($m_{av} \approx 450$ g/m^2) for each value of top stress (σ'_{vt} = 66 kPa, 33 kPa and 7 kPa). Raising the gradient to $i_{av} \approx 5$ led to increased loss ($m_{av} \approx 800$ to 900 g/m^2). At the maximum gradient $i_{av} \approx 9$, the loss exceeds 1000 g/m^2. Reducing σ'_{vt} influences mass loss, particularly at 7 kPa where stress at the soil-geotextile interface is believed close to zero (see Table 3.3a). Although the losses were continuous, rather than pulsating, no preferential flow channels were evident in the soil. A volume change of 3.1 % during the test was associated with a cumulative mass loss of 7650 g/m^2. Of note is the finding that soil piping in each CYC stage did not affect the gradient ratio in the following UNI stage, for which values of GR_{25} and GR_8 in the range 0.9 to 1 were obtained. The test combination is deemed stable in unidirectional flow, but unstable in cyclic flow.

At $AOS/D_{85} \approx 2.8$ and T = 60 s for test W2-T60(S), collection of soil passing through the geotextile confirmed visual observations of no loss during any of the UNI stages, but occurrence of loss in all the CYC stages. The loss was very small ($m_{av} \leq 35$ g/m^2) at $i_{av} \approx 1$. Raising the gradient to $i_{av} \approx 5$ nearly doubled the loss, and raising it again to $i_{av} \approx 9$ produced another doubling of losses to a value of 115 g/m^2 (see Table 3.3b). Values of $0.9 \leq GR_{25} \approx GR_8 \leq 1.0$ are comparable to those of test W2-T6(S). At constant gradient, mass loss was found to increase with decreasing effective stress. As

for the large permeameter, losses occurred as a pulsating action that was not restricted to any preferential location on the geotextile. A volume change of 0.3 % during the test was associated with a cumulative mass loss of 473 g/m^2. The results show the test combination to be stable in unidirectional flow, but provide further evidence of a susceptibility to instability in cyclic flow like that reported from the companion W2-T60(L) test.

At AOS/D_{85} ≈ 2.8 and T = 120 s for test W2-T120(S), no visual observation was made of soil loss through the geotextile in UNI or CYC stages of flow. In CYC flow, no loss was measured at i_{av} ≈ 1, and very little mass loss (m_{av} ≤ 26 g/m^2) at i_{av} ≈ 5 and 9. In this regard, it appears the long wave period replicates behaviour found in unidirectional flow. A volume change less than 0.1% was associated with a very small cumulative mass loss of 83 g/m^2 (see Table 3.3b). Values of 1.1 ≤ GR_{25} ≈ GR_8 ≤ 1.3 imply a linear variation of head loss. Stability is again confirmed in unidirectional flow. In cyclic flow, it appears stable at relatively low hydraulic gradients, but may be susceptible at the highest gradient.

3.5.4 Reproducibility of findings

Test results at a filter ratio AOS/D_{85} ≈ 2.8 are used to examine issues of repeatability and scale effect in the laboratory data. Reproducibility of the findings is considered with reference to a qualitative assessment of general mass loss trends, and a

quantitative assessment of specific mass loss quantities and related volume change. Two tests were repeated in small permeameter, for T = 6 s and T = 60 s respectively. Tests W2-T6(S) and W2-T6(S)-R exhibit a similar trend of mass loss in response to change in gradient and vertical effective stress, and specific values of mass loss are also similar in comparable stages of testing (see Table 3.3a). For test W2-T6(s)-R (repeated test), a total volume change of 4.2 % during the test was associated with a cumulative mass loss of 6075 g/m^2. Tests W2-T60(S) and W2-T60(S)-R also exhibit a similar trend of mass loss, however the variation in specific values of mass loss is up to 40 % (see Table 3.3b). The difference is attributed the spatial variation of pore size opening in the fabric of the geotextile, from which each sample is selected, which is sufficient to yield a difference in the "local" response, but insufficient to influence the "general" response. A total volume change of 0.3 % during the test was associated with a cumulative mass loss of 287 g/m^2.

3.5.5 Scale effect

Scale effect manifests itself as a difference in cross-sectional area of the test specimen, and also volume of soil, examined in the large and small permeameter. Water head distribution in unidirectional flow is first used for evaluation of reproducibility, and the excellent agreement (see Fig. 3.8 for example) is very encouraging. This is reflected directly in values of gradient ratio, which also show good agreement (Fig. 3.9).

In considering reproducibility with reference to mass loss and volume change, focus is placed on the data for tests at T = 6 s which experienced a relatively large number of flow cycles (8100 in total) and therefore provide a sufficiently large volume change. In contrast, the data for T = 60 s (810 cycles) and 120 s (405 cycles) provide a relatively small volume change. In all three tests, volume change increases linearly with increasing cumulative mass loss for this uniform sand (see Fig. 3.10). Data for the large permeameter test plot between those of the repeated test in the small permeameter. Recall the cross-sectional area of test specimen in the large permeameter is approximately eight times greater than that in the small device. It is reasonable to expect the larger specimen would exhibit a response indicative of the average found in the smaller specimens, given the influence of spatial variations in pore size opening. The data support this expectation and, it is therefore reasonable to conclude that the two permeameter devices exhibit no significant scale effect. Accordingly, it may be necessary to repeat tests in the small permeameter that demonstrate seepage-induced soil piping through the geotextile. Comparable quantity of mass loss from the repeated test is used to ensure that the geotextile samples accommodate spatial variations in pore size opening and hence represent a larger sample size.

3.6 Stress in a rigid-wall permeameter

Stress exerts a controlling influence on filtration behaviour, especially in reversing or cyclic flow. Therefore, it is important to account for it in a mechanics-based interpretation of results in these filtration tests. Measured values of top and bottom stress in the large permeameter indicate a strong influence of sidewall friction, and a significant reduction in stress at the soil-geotextile interface. Accordingly, it is important to correct for this influence in the small device (for which the design yields a value of top stress only), because the ability of the small permeameter to provide multi-stage data on soil loss is instrumental to the main focus of the study. In this section, a simple force equilibrium approach is presented to account for the influence of sidewall friction, from interpretation of axial force measurements in both permeameters.

3.6.1 Vertical stress distribution

Taking a stress equilibrium at the base of the specimen, the relation between top vertical effective stress (σ'_{vt}) and basal stress ($\sigma'_{vb(0)}$) on the specimen, for the hydrostatic condition (no seepage) (Fig. 3.11a) is given by:

$$\sigma'_{vb(0)} = \sigma'_{vt} + \gamma' Z - \Delta\sigma'_{v(0)} \qquad (3)$$

where γ' is the buoyant unit weight of the soil (kN/m^3), $\Delta\sigma'_{v(0)}$ is the stress difference caused by sidewall friction (kPa) and Z is specimen length (m). Downward flow yields a stress increase at the base (Fig 3.11b) while, in contrast, upward seepage flow yields a decrease (Fig. 3.11c). Thus, vertical stress at the base for the hydrodynamic condition (seepage flow) σ'_{vb} is given by:

$$\sigma'_{vb} = \sigma'_{vt} + \gamma' Z - \Delta\sigma'_{v} \pm S \tag{4}$$

where $\Delta\sigma'_v$ is the stress difference (kPa), S is seepage pressure applied at the base (kPa) taken equal to $i_{av}\gamma_w Z$, where i_{av} is average hydraulic gradient across the specimen (negative for upward flow), and γ_w is the unit weight of water (kN/m^3).

Li (2008) simplified the solution (Eq. 3 and 4) by assuming a constant value of sidewall friction along the specimen, establishing the mean vertical effective stress at the mid-height of the specimen for hydrostatic ($\sigma'_{vm(0)}$) and hydrodynamic conditions (σ'_{vm}), respectively, as:

$$\sigma'_{vm(0)} = \sigma'_{vt} + 0.5(\gamma' Z - \Delta\sigma'_{v}) \tag{5a}$$

$$\sigma'_{vm} = \sigma'_{vt} + 0.5(\gamma' Z - \Delta\sigma'_{v} \pm S) \tag{5b}$$

The mean vertical effective stress was used by Li (2008) for mechanical analysis of internal soil erosion for the specimen tested in the large permeameter, and was also recommended for sidewall friction analysis.

3.6.2 Influence of sidewall friction

Sidewall shear is governed by lateral stress and a value of interface friction. The 'at-rest' condition is commonly assumed for a soil element in a rigid-walled device that inhibits development of lateral strain, primarily from studies on sidewall resistance in consolidation test cells (for example, Shirato *et al*. 1968 and, more recently Sivrikaya and Togol, 2005). Lateral strain in the rigid-wall permeameter is believed negligible, and leads to a similar assumption of K_0 for the lateral stress coefficient. Thus, average sidewall shear (τ_{av}) may be calculated with reference to mean vertical effective stress:

$$\tau_{av} = c + f\, K_0 \left(\sigma'_{vm(0)} \; or \; \sigma'_{vm}\right) \tag{6}$$

where c is a value of soil-wall adhesion (assumed zero in this study of cohesionless soil), and f is a coefficient of soil-wall interface friction. In theory, an upper-bound value of $f \leq tan\delta$ is mobilized with development of large relative displacement between the soil specimen and inside wall of the permeameter. However, in practice,

this does not occur over the full length of the specimen because of the zero displacement boundary on which it rests.

Considering force equilibrium (see Fig. 3.12) for the hydrostatic ($\Delta\sigma'_{v(0)}$) and the hydrodynamic condition ($\Delta\sigma'_v$) respectively, and introducing the aspect ratio (Z/D), yields:

$$\Delta\sigma'_{v(0)} = \frac{4Z}{D}\tau_{av} = \frac{4Z}{D}\sigma'_{vm(0)}K_0 f \tag{7a}$$

$$\Delta\sigma'_{v} = \frac{4Z}{D}\sigma'_{vm}K_0 f \tag{7b}$$

The test procedure of applied stress and cyclic flow during a multistage test imposes load-unload-reload sequences (see Fig. 3.4). Unloading at zero lateral strain affects the magnitude of K_0, which increases with value of over-consolidation ratio (OCR) in the specimen (Campanella and Vaid 1972; Mayne and Kulhawy 1982; Mayne and Kulhawy 1994).

Mayne and Kulhawy (1982) suggested a lateral stress coefficient at-rest (K_0) for unloading that is correlated with OCR and internal friction angle (φ), based on analysis of test data from 81 clays and 90 sands, expressed as:

$$K_0 = (1 - \sin\phi)\, OCR^{\sin\phi} \tag{8}$$

In the rigid-wall permeameter, and with reference to mean vertical effective stress, OCR is defined as:

$$OCR = \frac{\sigma'_{vm,\max}}{\sigma'_{vm}} \tag{9}$$

where $\sigma'_{vm,\max}$ is the maximum mean vertical effective stress experienced by the test specimen, and σ'_{vm} is mean the vertical effective stress at the current stage of testing.

3.6.3 Sidewall friction: large permeameter

Data from two tests in the large permeameter establish values of soil-wall interface friction coefficient that may be used in analysis and interpretation of data from the small permeameter. For the hydrostatic condition, stress difference ($\Delta\sigma'_{v(0)}$) is deduced from measurement of top stress, bottom stress and self weight of the specimen (see Eq. 3). For the hydrodynamic condition, and knowing the seepage pressure, the stress difference ($\Delta\sigma'_v$) is similarly deduced (see Eq. 4). In the absence of a condition of stress equilibrium fully developing in test W2-T6(L), as a consequence of the fast

cyclic flow, data from tests W1-T60(L) and W2-T60(L) only are used for purposes of stress analysis, and deduction of mobilized soil-wall interface friction.

3.6.3.1 Hydrostatic condition

The calculation is made in four steps: (a) determine the mean vertical effective stress ($\sigma'_{vm(0)}$) for σ'_{vt} = 57 kPa, 28 kPa and 7 kPa using Eq. 5a; (b) from known values of $\Delta\sigma'_{v(0)}$, calculate values of $K_0 f$ using Eq. 7a (see Fig. 3.13a and 3.13b); (c) knowing OCR = 1 at σ'_{vt} = 57 kPa, and recognizing that $\sigma'_{vm(0)}$ at σ'_{vt} = 57 kPa is the value of $\sigma'_{vm(0),max}$, determine OCR values (see Eq. 9) for unloading to σ'_{vt} = 28 kPa (OCR = 2.1) and 7 kPa (OCR = 9.1); (d) calculate K_0 (see Eq. 8) with $\varphi = 38^\circ, 40^\circ$ and 44° for σ'_{vt} = 57 kPa, 28 kPa and 7 kPa (see section 3.3.3), from which values of f may be deduced. The average value obtained for the tests without seepage flow is f = 0.32, 0.23 and 0.18, for σ'_{vt} = 57 kPa, 28 kPa and 7 kPa, respectively (see Fig. 3.14, at $S/\Delta\sigma'_{v(0)} = 0$).

3.6.3.2 Downward seepage flow

The calculation also consists of four steps: (a) knowing seepage pressure ($S = i_{av}\gamma_w Z$), calculate σ'_{vm} (see Eq. 5b) in order to determine an OCR value for the nine combinations of σ'_{vt} = 57 kPa, 28 kPa and 7 kPa, and $i_{av} \approx 1$, 5 and 9; (b) from known values of $\Delta\sigma'_v$, calculate values of $K_0 f$ using Eq. 7b (see Fig. 3.13a and 3.13b); (c) at a

given hydraulic gradient, and corresponding σ'_{vm}, determine OCR (see Eq. 9) for CYC1 (note that $\sigma'_{vm} = \sigma'_{vm,\max}$, and OCR = 1), CYC2 and CYC3; (d) knowing the value of OCR, calculate K_0 with reference to the same values of friction angle (φ) for the soil (see Eq. 8), allowing *f* to be deduced for different seepage conditions (see Fig. 3.14a).

3.6.3.3 Upward seepage flow

The calculation steps to deduce a value of *f* are identical to those for the case of downward flow, except for the need to account for a seepage pressure ($-S = -i_{av}\gamma_w Z$) that is negative in the first step of the calculation. The remaining three steps again enable a deduction of *f* for different seepage conditions (see Fig. 3.14b).

3.6.3.4 Coefficient of sidewall friction (*f*)

The relation between *f* and a normalized measure of seepage flow (see Fig. 3.14), from these large permeameter test data, depicts the combined influence of stress difference and hydraulic gradient. With downward flow (see in Fig. 3.14a), the value of *f* appears more sensitive to σ'_{vt} than magnitude of seepage flow. In contrast, upward flow (see Fig. 3.14b) yields a significant reduction in the magnitude of sidewall friction: negative values indicate a reversal of the direction is which sidewall friction is

mobilized at relatively large seepage flow. The response is consistent with observations reported by Li (2008) for the same test device.

The variety of seepage conditions examined in testing yield a range of $-0.4 \leq f \leq 0.4$ for the coefficient of interface friction, where $f \leq \tan \delta$. Proportionally, this represents between ½ and ⅔ $\tan \varphi$ for the friction angle of 44˚, 40˚ and 38˚ measured for the soil in direct shear box tests (section 3.3.3). The relation between f and $S/\Delta\sigma'_{v(0)}$ established from analysis of tests in the large permeameter, Figure 3.14, is assumed appropriate for stress analysis of tests data in the small permeameter. The assumption is made based on the use of an acrylic cell in each device.

3.6.4 Sidewall friction: small permeameter

In contrast to the large permeameter, effective stress at the soil-geotextile interface (σ'_{vb}) must be deduced for the small permeameter, since there is no provision to measure axial force on the lower boundary of the test specimen. Accordingly, the objective of the following stress analysis is to deduce a value of σ'_{vb} for the range of applied stress on the top boundary, namely 66 to 7 kPa. Note that the values of f deduced from the range 57 to 7 kPa in the large permeameter are assumed applicable to this range.

Since the value of stress difference arising from sidewall friction is unknown in the small permeameter, the mean effective stress for hydrostatic ($\sigma'_{vm(0)}$) and hydrodynamic conditions (σ'_{vm}) cannot be calculated directly by Eq. 5a or Eq. 5b. Thus, combining Eq. 7a with Eq. 5a and similarly Eq. 7b with Eq. 5b, yields the following new expressions:

$$\sigma'_{vm(0)} = \frac{\sigma'_{vt} + 0.5(\gamma' Z)}{\left(1 + \frac{2K_0 f Z}{D}\right)} \tag{10a}$$

$$\sigma'_{vm} = \frac{\sigma'_{vt} + 0.5(\gamma' Z \pm S)}{\left(1 + \frac{2K_0 f Z}{D}\right)} \tag{10b}$$

The stress analysis for the small permeameter is made in reverse order to that for the large permeameter (see Fig. 3.15): OCR is first obtained, and used to determine a value of K_0 that, knowing f (from Fig. 3.14, else Table 3.4), enables a calculation of mean vertical stress ($\sigma'_{vm(0)}$, or σ'_{vm}) and hence stress difference ($\Delta\sigma'_{v(0)}$, or $\Delta\sigma'_{v}$), which then allows for a calculation of bottom stress ($\Delta\sigma'_{vb(0)}$, or $\Delta\sigma'_{vb}$).

3.6.4.1 Hydrostatic condition

Consider, for illustrative purposes, a calculation for the case of σ'_{vt} = 33 kPa. The calculation is made in five steps: (a) for σ'_{vt} = 66 kPa, calculate K_0 from Eq. 8 (with φ = 38º, and OCR = 1); (b) calculate $\sigma'_{vm(0)}$ from Eq. 10a (with f = 0.32, and noting $\sigma'_{vm(0)} = \sigma'_{vm(0),\max}$); (c) for σ'_{vt} = 33 kPa, assume a trial value of OCR (= 66/33 ≈ 2) and calculate K_0 (with φ = 40˚, see section 3.3.3), and thereby determine $\sigma'_{vm(0)}$ from Eq. 10a (with f = 0.26); (d) calculate the OCR from Eq. 9 and compare with the assumed trial value (of step c), using iteration as a necessary to obtain agreement; (e) knowing $\sigma'_{vm(0)}$, calculate $\Delta\sigma'_{v(0)}$ from Eq. 7a, and deduce the bottom stress from Eq. 3.

3.6.4.2 Downward seepage flow

Like the hydrostatic condition, σ'_{vm} is unknown for stages with OCR greater than 1, until a value of K_0 is determined. Furthermore, OCR cannot be approximated from the top stress alone, or calculated from Eq. 9, rather a trial value must be established from:

$$OCR \approx \frac{\sigma_{vm,\max}}{(\sigma_{vm(0)} \pm 0.5S)} \tag{11}$$

Consider, for illustrative purposes, a calculation for the CYC2 stage (σ'_{vt} = 33 kPa) at i_{av} = ± 9 (S ≈ 8.8 kPa). In this case, use the value of $\Delta\sigma'_{v(0)}$, calculated earlier, to define

an $S/\Delta\sigma'_{v(0)}$ ratio that yields f from Fig. 3.14a, for conditions of downward flow. The calculation is made in five steps: (a) for σ'_{vt} = 66 kPa and S = +8.8 kPa, calculate K_0 from Eq. 8 (with φ = 38º, and OCR = 1); (b) calculate σ'_{vm} from Eq. 10b (noting σ'_{vm} = $\sigma'_{vm,\max}$); (c) for σ'_{vt} = 33 kPa, assume a trial value of OCR (Eq. 11) and calculate K_0 (with φ = 40˚), and thereby determine σ'_{vm} from Eq. 10b; (d) calculate the OCR from Eq. 9 and compare with the assumed trial value (of step c), using iteration as a necessary to obtain agreement; (e) knowing σ'_{vm}, calculate $\Delta\sigma'_v$ from Eq. 7b, and deduce the bottom stress from Eq. 4.

3.6.4.3 Upward seepage flow

The calculation steps to deduce a value of f are identical to those for the case of downward flow, except for the need once again to account for a seepage pressure ($-S$ = $-i_{av}\gamma_w Z$) that is negative in the first step of the calculation: $\sigma'_{vm,\max}$ has the same magnitude as that for downward flow. Importantly to note that Eq. 11 is invalid for a condition yielding a value 0.5S close to or in excess of $\sigma'_{vm(0)}$. There is only at the gradient ≈ 9 (0.5S ≈ 4.4 kPa) for the stage CYC3 (σ'_{vt} = 7 kPa and $\sigma'_{vm(0)}$ = 4.6 kPa) falling into this case. Thus, a trial OCR value of 10 is firstly assumed for OCR in the step c (see 3.6.4.2). The agreement from iteration is obtained at the OCR value of 14. At this stage, the calculation yields a bottom stress of about 0 kPa.

In summary, a corresponding vertical stress at the base or at the soil-geotextile interface (σ'_{vb}) is calculated for each measured value of top applied stress (σ'_{vt}) (see Fig. 3.16). Inspection shows σ'_{vb} to diminish with increasing i_{av} (negative value depicts upward flow). The relation between σ'_{vt} and σ'_{vb} appears non-linear, as a result of the influence of unloading, and therefore OCR, on K_0. For the same top stress, the calculations yield a value of interface stress for the small permeameter approximately 20 % lower than that for the large permeameter. The finding is attributed to the different aspect ratio of the respective test specimens. A summary of input parameters to the stress calculation, and resulting values deduced for *f*, is provided in Table 3.4.

3.7 Discussion

3.7.1 Size of geotextile sample

Size of the geotextile sample is found to influence quantity of mass loss per unit area, which differs in the small and large permeameter, a behaviour that is attributed to spatial variation of material properties. In contrast, no companion variation of water head distribution was observed at the soil-geotextile interface, as evident from similar values of hydraulic gradient ratio. The response is attributed to the uniform gradation of the soil. More generally, mass loss per unit area and consequent volume change are comparable, a finding that implies the system response in the small permeameter

replicates that in the large permeameter. Furthermore, a limited comparison of data indicates the large permeameter likely defines an average or typical response of the small permeameter (see Fig. 3.10). For this reason, it is recommended to repeat a test in the small permeameter where it is believed the soil and geotextile exhibit filtration incompatibility, and report an average of the experimental findings for purposes of analysis.

3.7.2 Influence of test procedure

The multi-stage test procedure is intended to challenge soil-geotextile compatibility, by means of reduced stress and increasing hydraulic gradient as the test progresses. As long as the specimen remains intact, it is believed the influence of stress and gradient can be examined in one test specimen. As shown by results at $AOS/D_{85} = 2.8$ in both the large and small permeameter, the GR_{25} and GR_8 values obtained in unidirectional flow, after a cyclic stage in which some piping or mass loss occurred, are unchanged from the initial values. It indicates the readiness of the test specimen for testing in the next stage: the finding is expected for a uniformly-graded soil. This protocol is very important to multi-stage testing, because the influence of these variables is examined by continued testing of the same geotextile sample. In this manner, test variables are examined without any spatial variation in geotextile properties. Furthermore it is efficient, in a systematic study of a large number of test combinations, to employ a multi-stage test procedure. Accordingly, the test procedure is believed well-suited to

testing of uniformly-graded soil, and is recommended for a systematic study of soil-geotextile compatibility that addresses stress and hydraulic gradient as well as wave period in cyclic flow reversal.

The loading routine, with load-unload-reload sequence, imposes a stress history on test specimen. Accordingly, the relation between vertical stress and lateral stress, which varies with stress history, has been addressed with reference to variation of mean vertical effective stress (see Fig. 3.17a) taking into account observations of Mayne and Kulhawy (1982). The point of $\sigma'_{vm,max}$ occurs for downward flow during the CYC1 stage at maximum gradient, and the point of $\sigma'_{vm,min}$ occurs for upward flow during the CYC3 stage at maximum gradient. Results for the small permeameter (see Fig. 3.17b) are provided for comparison: they underscore the difference between lateral stress and vertical stress in the rigid-wall permeameter. Inspection shows the values are comparable when vertical stress rebounds to a certain value, and shows that lateral stress exceeds vertical stress at relatively low values of vertical stress. The finding is meaningful because, if lateral stress influences a stress-based interpretation, then it must be addressed in data analysis and interpretation.

3.7.3 Significance of lateral stress

Particle movement within a porous medium is believed governed by confining stress in a plane normal to the direction of movement (Indraratna and Vafai 1997; Indraratna

and Radampola 2002). The configuration of the laboratory permeameter imposes one-dimensional vertical flow in either a downward or upward direction. Thus, the confining stress normal to the direction of movement is lateral stress. Theory and analysis suggest that lateral stress in a rigid-wall permeameter may be much lower than vertical stress when downward seepage occurs under a condition of normal consolidation and, in contrast, it may be much greater when upward seepage pressure reduces the stress level to yield a relatively large OCR (see Fig. 3.17). Accordingly, vertical stress alone is not believed sufficiently representative of the actual confining stress, and could result in misleading interpretations. For this reason, lateral stress should be accounted for in any mechanics-based analysis, and is explicitly addressed in this study.

More specifically, mean effective stress is proposed as an index value to account for the influence of vertical and lateral stress in the rigid-wall permeameter. At the soil-geotextile interface, it is taken as $p_i = \sigma'_{vb}[1+2K_0]/3$, where calculated values of $p_{i(0)}$ for the hydrostatic condition, and values of p_i for the hydrodynamic condition (upward flow) are illustrated in Fig. 3.18.

3.7.4 Influence of the test variables

Mass loss describes the combined influence of confining stress and hydraulic gradient. In a relatively open filter (AOS/D_{85} = 2.8), a particle bridging network is expected to

develop over the pore openings of the fabric. Its inherent stability relies on the contact resistance between individual grains of soil. It is evident that upward seepage pressure reduces confining stress at the soil-geotextile interface (see Fig. 3.7), which diminishes the integrity of the bridging network. If the confining stress is insufficient, is it postulated that flow reversal and the reinstating of downward flow may result in localized collapse of the network, whereupon the quantity of mass loss (mass per unit area per flow cycle) is governed by seepage velocity. Therefore, hydraulic gradient exerts an influence in triggering the onset of soil piping, whereas confining stress opposes the role of hydraulic gradient. This combined effect is believed significant to soil retention phenomena in a geotextile filter, especially in the presence of cyclic flow reversal.

Wave period appears to influence retention capacity of the woven geotextile. Consider, for example, results of all tests for geotextile W2 in the stage CYC3 at $i_{av} \approx 9$ (see Table 3.3). Reporting mass loss as an average value per cycle yields 1.4 g/m^2/cycle (average) for T = 6 s, 1.1 g/m^2/cycle for T = 60s and 0.6 g/m^2/cycle for T = 120 s. It appears the soil-geotextile interface stability is more sensitive to a shorter wave period than a longer wave period. This finding, from observation at T = 6 s, is tentatively attributed to a bridging network over the geotextile openings that cannot fully re-established itself before the onset of the next cycle of flow reversal. This apparent influence of wave period may explain why mass loss is greater and more continuous in the tests at the shortest wave period of T = 6 s.

From the test data reported for woven geotextiles, mass loss appears sensitive to a change in wave period, hydraulic gradient and stress. It is believed mass loss may be used to distinguish between a soil-combination that is compatible, versus incompatible in cyclic flow. In order to use this approach, more test data are required to characterize a greater range of AOS/D_{85}. Confidence in the approach also requires data for nonwoven geotextiles. This will enable development of an empirical soil retention rule for geotextile filter compatibility in cyclic flow that is based on principle of mechanics.

3.8 Conclusions

Wave period and confining stress influence soil-geotextile filter compatibility, and those two parameters, in combination with hydraulic gradient, require systematic study in order to understand the margin of safety that governs a confident use of empirical design criteria for applications of cyclic flow. Based on experimental results from the large and the small permeameter, for a uniformly-graded sand and two woven geotextiles, the following conclusions are drawn:

- measurement of axial load in the large permeameter indicates a reduction of 20% to 40% in vertical effective stress along the specimen length that is

attributed to interface friction, a finding that implies any stress-based interpretation of soil-geotextile compatibility in a rigid-wall permeameter must address the phenomenon of sidewall friction;

- mass loss-volume change relations in the large (280 mm diameter) and small (100 mm diameter) permeameter are attributed to a spatial variation of pore size opening in the geotextile specimen rather than a scale effect in the two permeameters, hence it is recommended to repeat a test in the small permeameter where it is believed the soil and geotextile exhibit filtration incompatibility, and report an average of the experimental findings for purposes of analysis; and,
- therefore the small permeameter is considered sufficient and more practical for a systematic study of test variables.

The experimental data and companion theoretical analysis show that:

- for the multi-stage test method, and corresponding variation of lateral stress in the rigid wall permeameter, mean effective stress at the soil-geotextile interface (p_i) is a better parameter for interpretation of performance than vertical stress; and

- soil retention is very sensitive to the upward component of cyclic flow that yields a reduction in mean effective stress and, it is postulated, thereby acts to destabilize arching in soil particles at the openings of the woven geotextile.

For the range of variables examined in testing, mass loss is negligible in cyclic flow at a filter ratio $AOS/D_{85} \approx 2$, but very significant at $AOS/D_{85} \approx 2.8$, where soil-geotextile retention incompatibility is sensitive to loading conditions governed by a combination of wave period, hydraulic gradient and confining stress. The findings suggest that mass loss may be used to distinguish between a soil-combination that is compatible, versus incompatible, in cyclic flow. More test data are required, both for woven and nonwoven geotextiles, to characterize a greater range of AOS/D_{85} and thereby enable development of an empirical soil retention rule for geotextile filter compatibility in cyclic flow that is based on principle of mechanics.

Table 3.1 Properties of the woven geotextiles

Geotextile	AOS (μm)	Percent open area (%)	Permittivity (sec^{-1})	Filter Ratio (AOS/D_{85})
W1	212	4	0.28	2.0
W2	300	4-6	0.51	2.8

Table 3.2 Test program

Small permeameter				Large permeameter		
Geotextile	T = 6 s	T = 60 s	T = 120 s	Geotextile	T = 6 s	T = 60 s
W1	W1-T6(S)	-		W1	-	W1-T60(L)
W2	W2-T6(S)	W2-T60(S)	W2-T120(S)	W2	W2-T6(L)	W2-T60(L)

Table 3.3 Mass loss (g/m^2)

Table 3.3a Wave period T = 6s (900 cycles)

Test code	W2(S)-T6			W2(S)-T6-R		
Stage	CYC1	CYC2	CYC3	CYC1	CYC2	CYC3
i_{av}	1.3	1.3	1.3	1.1	1.1	1.1
mass loss	465.4	460.0	430.8	322.8	551.3	643.6
i_{av}	5.7	5.7	5.7	5.1	5.1	5.1
mass loss	876.9	838.5	898.7	638.5	661.5	664.1
i_{av}	9.5	9.5	9.5	9.1	9.1	9.1
mass loss	1043.6	1159.0	1476.9	683.3	830.8	1079.5
Cum. loss	7648.7			6075.4		

Table 3.3b Wave period T = 60s (90 cycles) and T = 120s (45 cycles)

Test code	W2(S)-T60			W2(S)-T60-R			W2(S)-T120		
Stage	CYC1	CYC2	CYC3	CYC1	CYC2	CYC3	CYC1	CYC2	CYC3
i_{av}	1.1	1.1	1.1	1.0	1.0	1.0	1.2	1.2	1.2
mass loss	19.2	21.8	34.6	5.6	12.8	17.1	0	0	5.1
i_{av}	5.1	5.1	5.1	5.2	5.2	5.2	5.5	5.5	5.5
mass loss	38.5	37.2	64.1	21.8	34.2	40.6	6.4	10.3	11.5
i_{av}	8.9	8.9	8.9	8.7	8.7	8.7	9.3	9.3	9.3
mass loss	75.6	67.9	114.3	41.9	40.6	76.1	8.9	15.4	25.6
Cum. loss	473.3			286.8			83.3		

Table 3.4 Soil-geotextile interface stress (small permeameter): parametric values

$\pm i_{av}$		Hydrostatic			1			5			9		
σ'_{vt} (kPa)		66	33	7	66	33	7	66	33	7	66	33	7
$\Delta\sigma'_{v(0)}$ (kPa)		-	-	-	25.9	15.0	5.1	25.9	15.0	5.1	25.9	15.0	5.1
$\lvert\pm S/\Delta\sigma'_{v(0)}\rvert$		-	-	-	0.04	0.07	0.19	0.19	0.33	0.97	0.34	0.59	1.74
f		0.32	0.26	0.18	-	-	-	-	-	-	-	-	-
Down	f	-	-	-	0.34	0.26	0.19	0.34	0.27	0.21	0.35	0.29	0.22
	K_0	-	-	-	0.38	0.56	1.50	0.38	0.54	1.23	0.38	0.53	1.06
Up	f	-	-	-	0.32	0.25	0.15	0.31	0.21	0.05	0.3	0.17	-0.04
	K_0	-	-	-	0.38	0.57	1.73	0.38	0.59	1.80	0.38	0.62	1.89

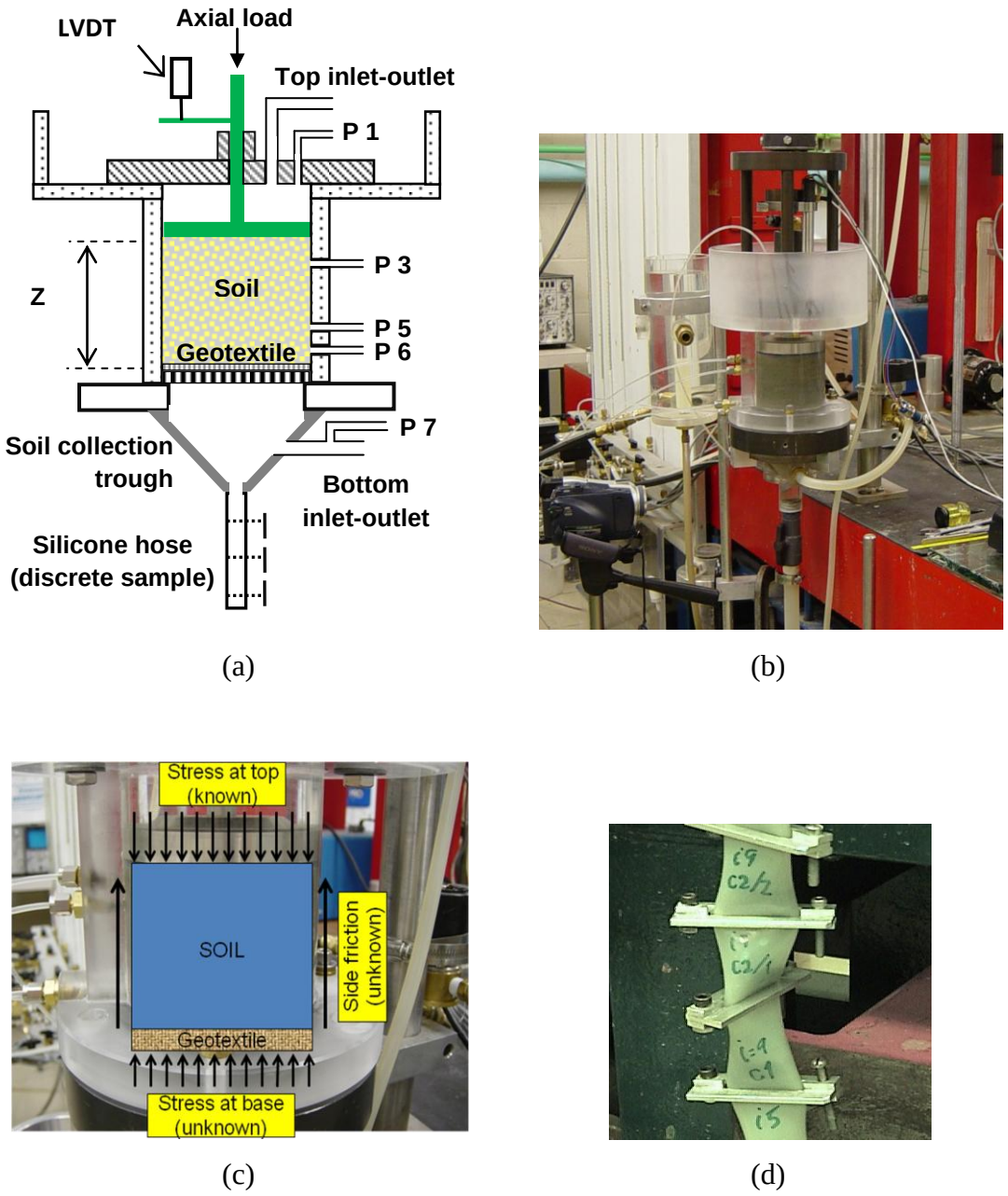

Figure 3.1 Small permeameter: a) schematic drawing; b) test device; c) test specimen; d) mass collection

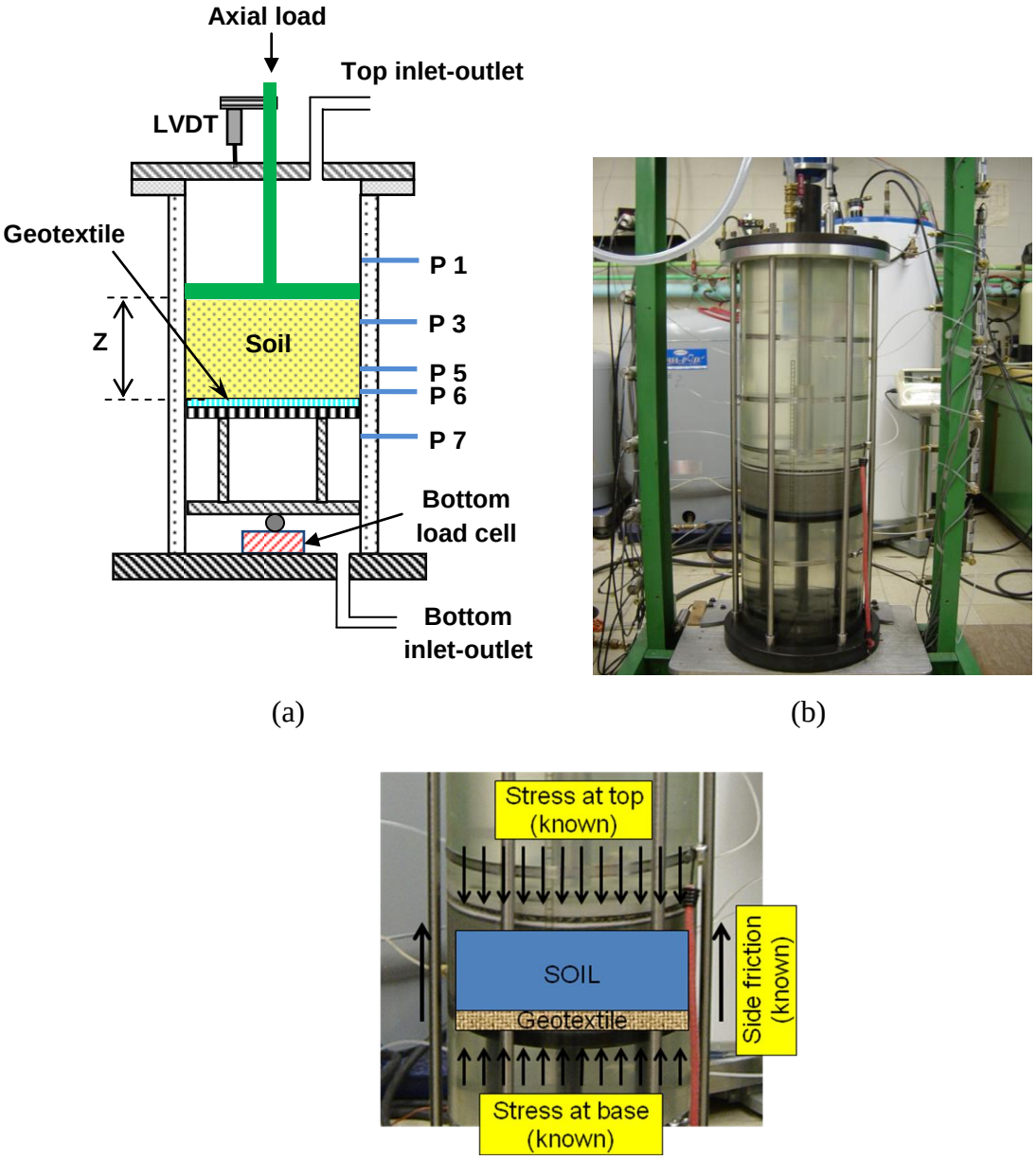

Figure 3.2 Large permeameter: a) schematic drawing; b) test device; c) test specimen

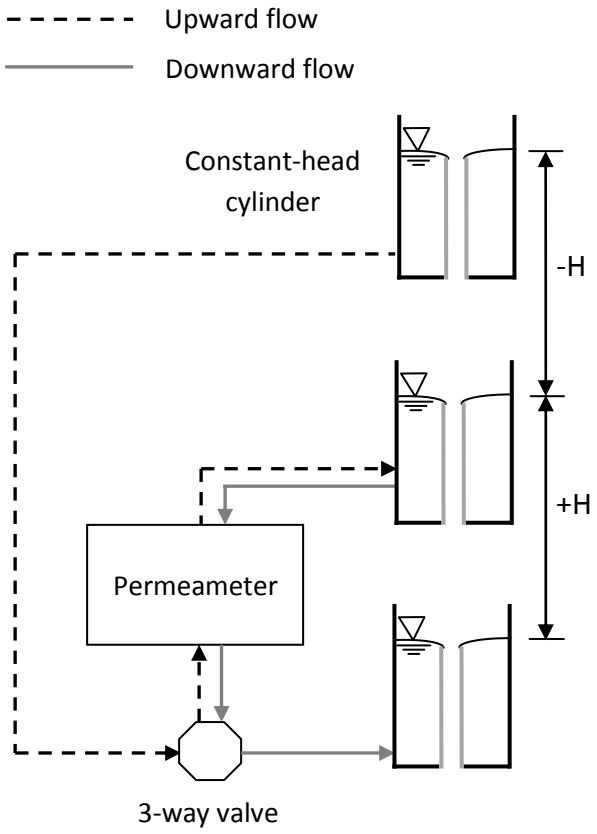

Figure 3.3 Schematic diagram of head-controlled system for cyclic flow

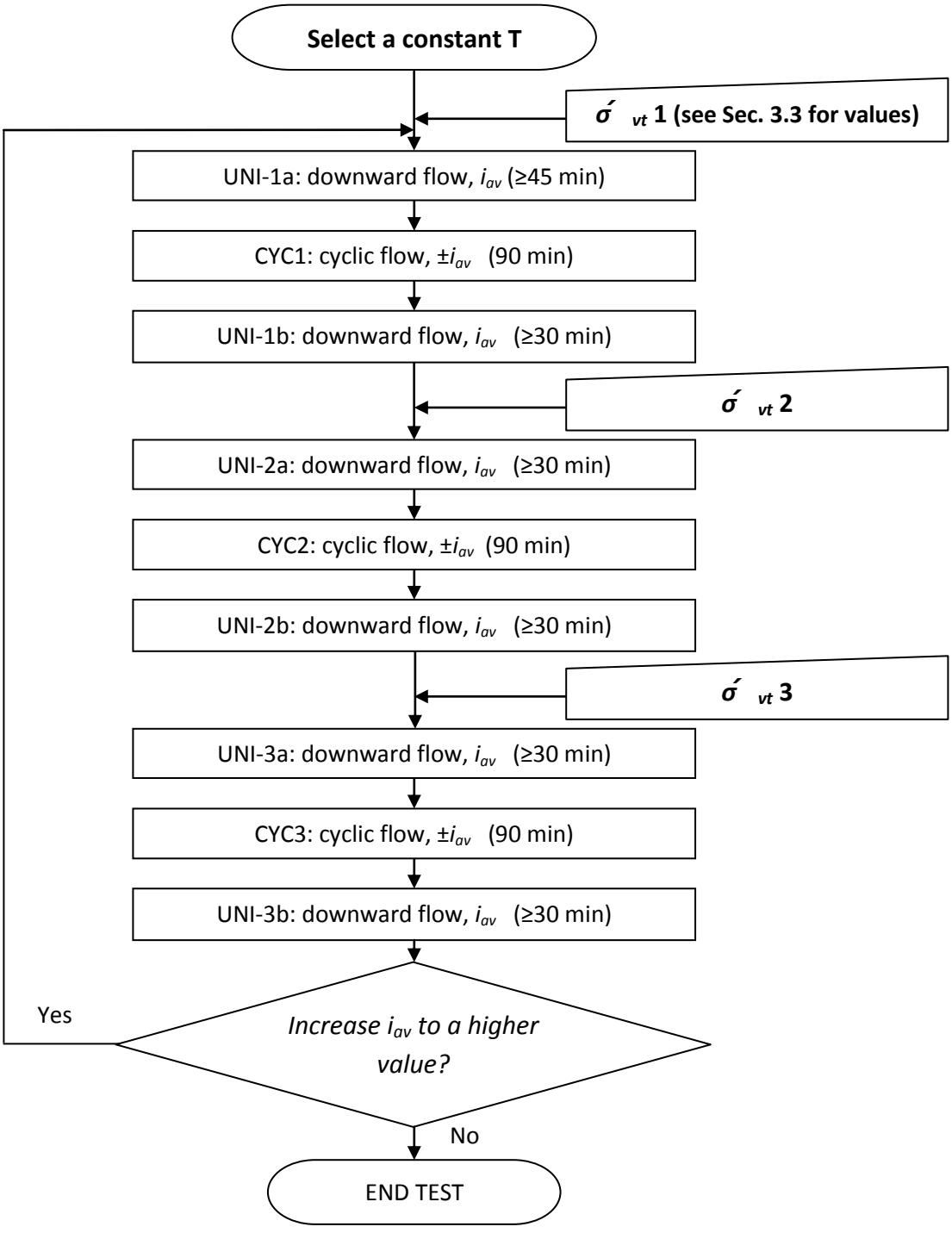

Figure 3.4 Flow chart of multistage test procedure

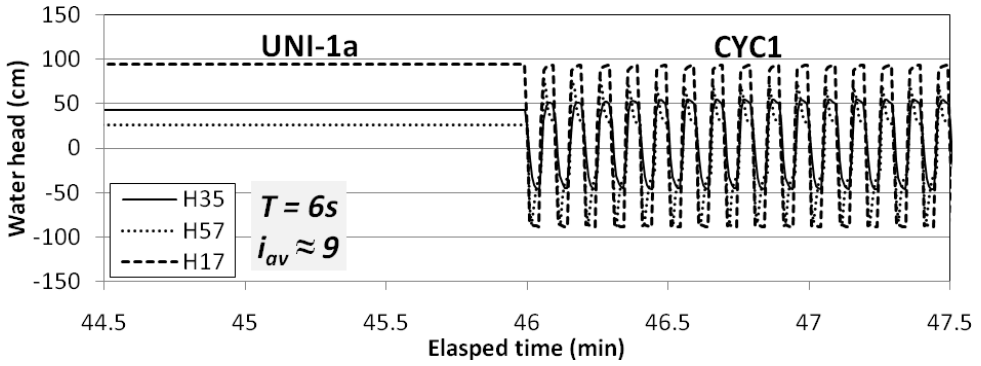

(a)

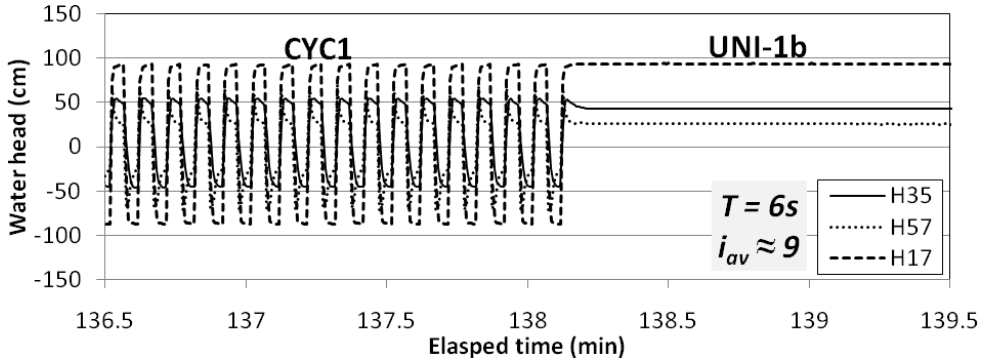

(b)

Figure 3.5 Water head distribution in test W2-T6(S): a) starting CYC1-stage and b) ending CYC1-stage

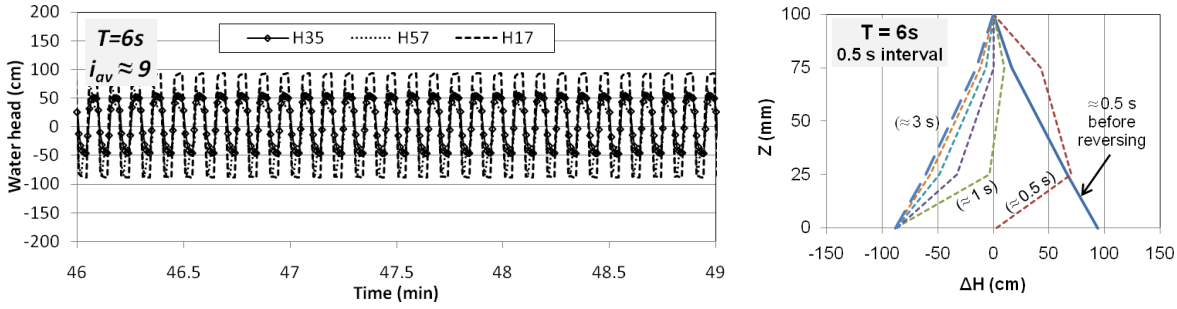

(a)

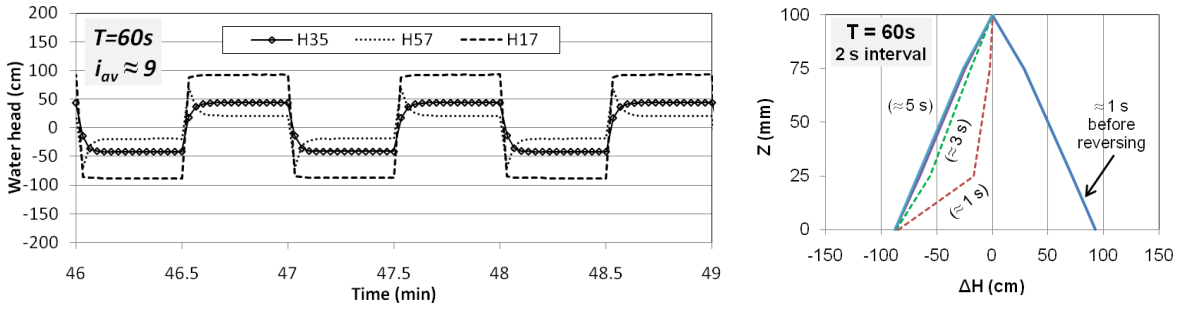

(b)

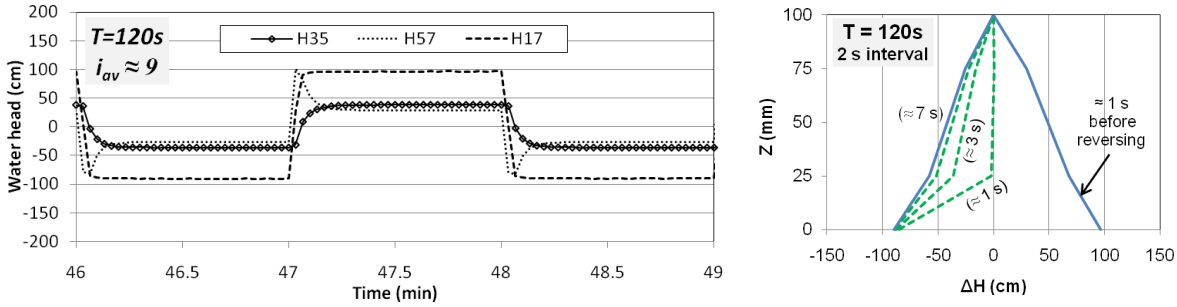

(c)

Figure 3.6 Water head distribution in tests W2-T6(S), W2-T60(S) and W2-T120(S): a) T = 6 s; b) T = 60 s; c) T = 120 s; d) schematic representation of transient hydraulic gradient

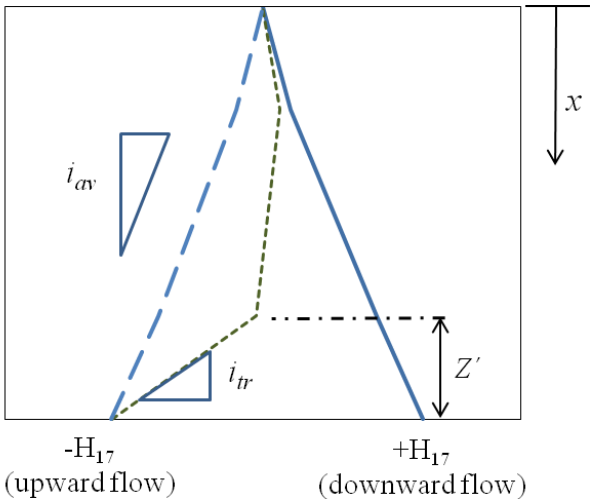

(d)

Figure 3.6 (continued)

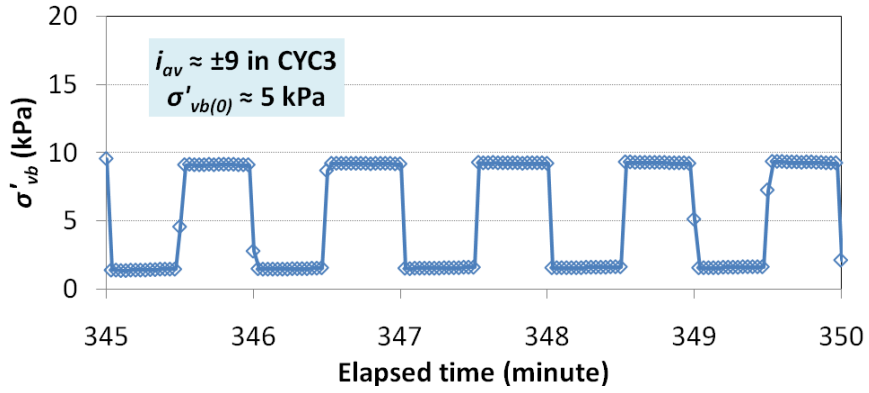

(a)

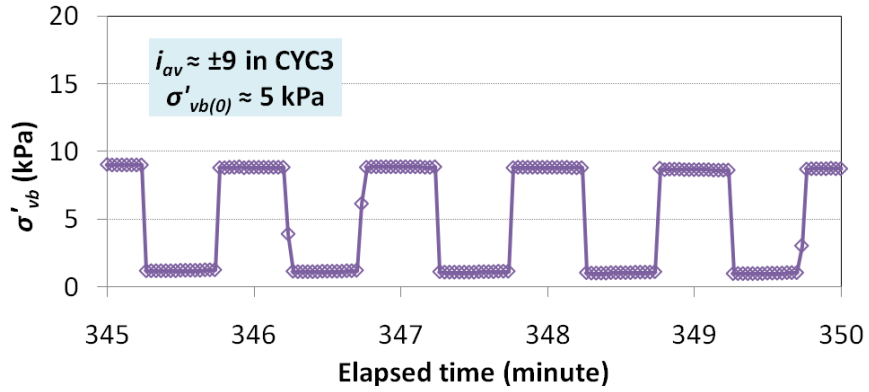

(b)

Figure 3.7 Measured stress at the soil-geotextile interface in the large permeameter: a) test W1-T60(L); b) test W2-T60(L)

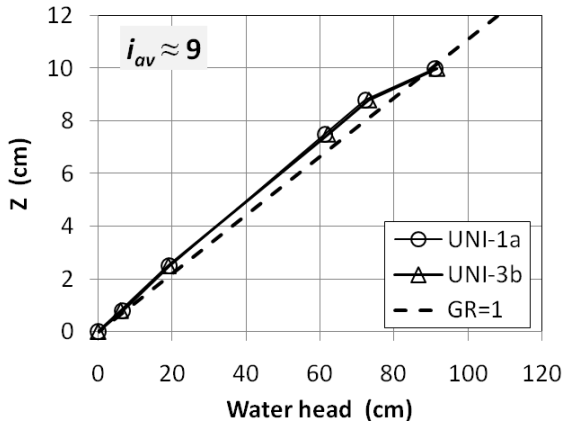

(a)

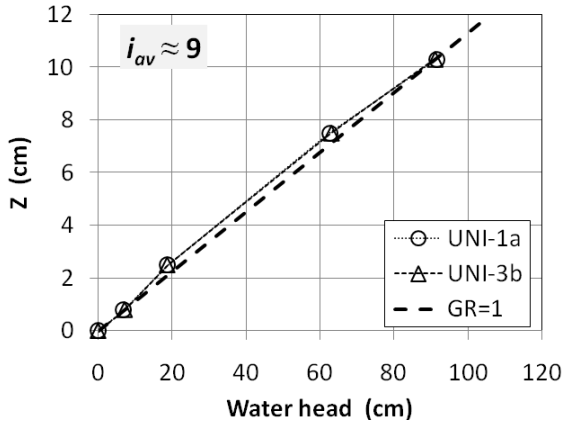

(b)

Figure 3.8 Water head distribution in unidirectional flow: a) test W2-T60(S) and b) test W2-T60(L)

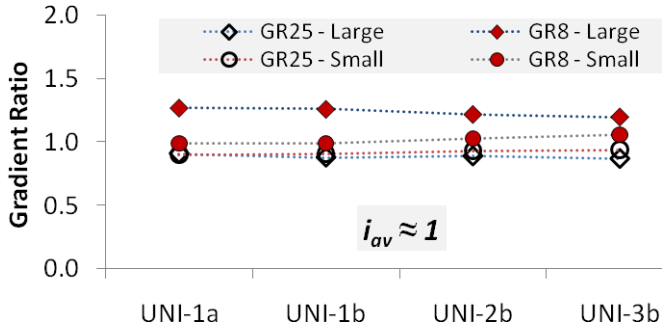

(a)

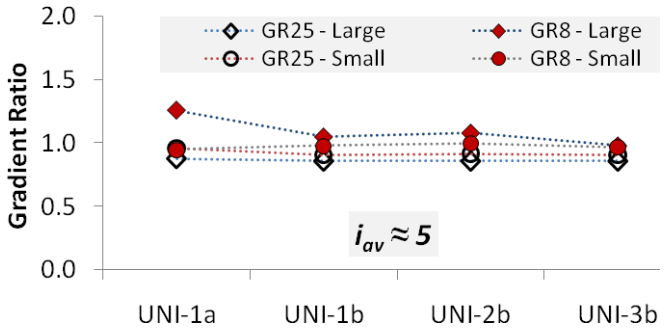

(b)

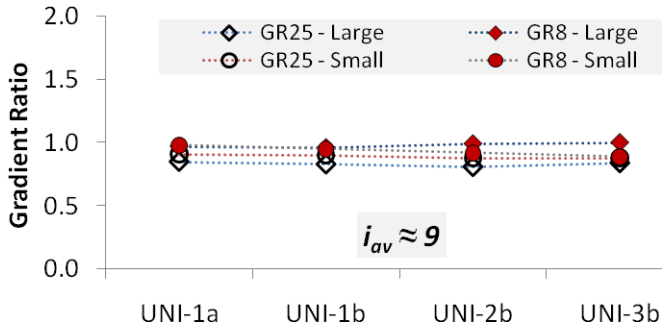

(c)

Figure 3.9 Gradient Ratio in tests W2-T60(S) and W2-T60(L): a) $i_{av} \approx 1$; b) $i_{av} \approx 5$; c) $i_{av} \approx 9$

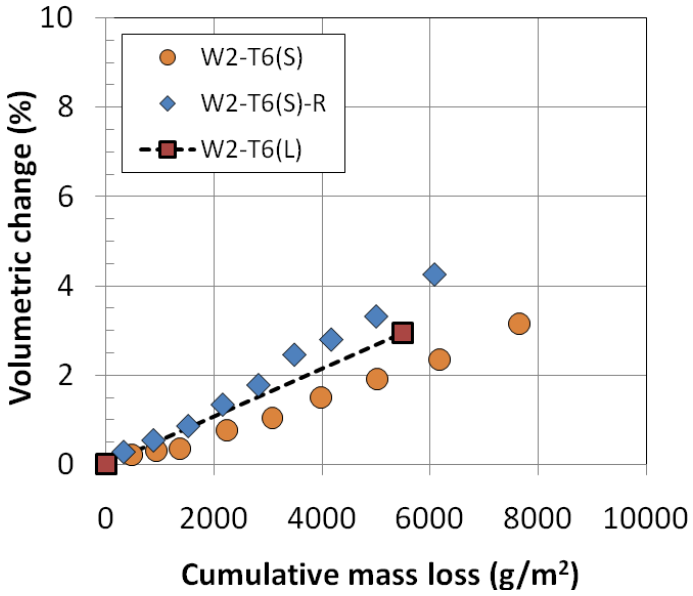

Figure 3.10 Comparison of mass loss and volume change in the small and large permeameter

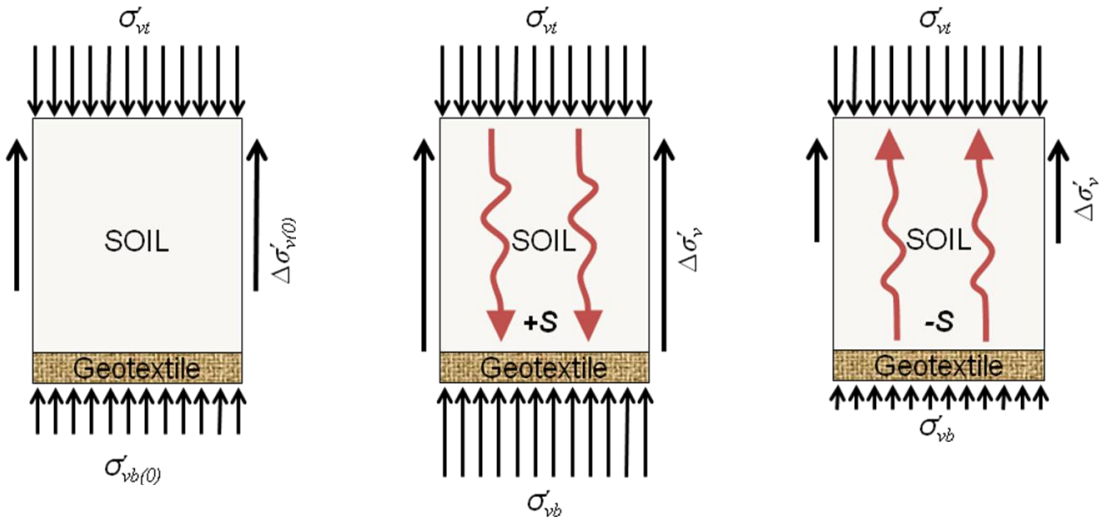

(a) (b) (c)

Figure 3.11 Schematic illustration of stress regime in the test specimen: a) hydrostatic; b) downward flow; c) upward flow

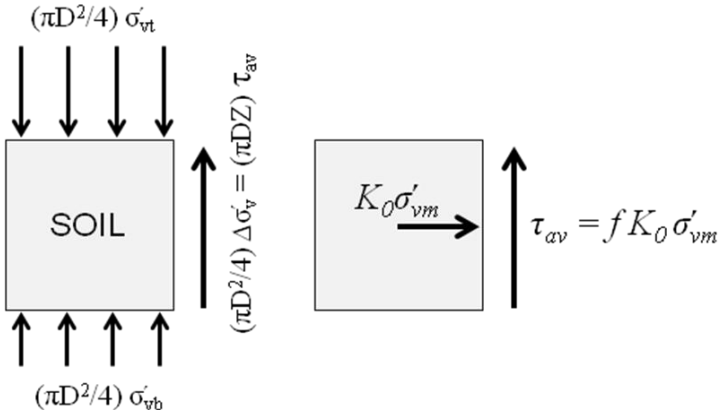

Figure 3.12 Relation of stress difference and average sidewall shear stress

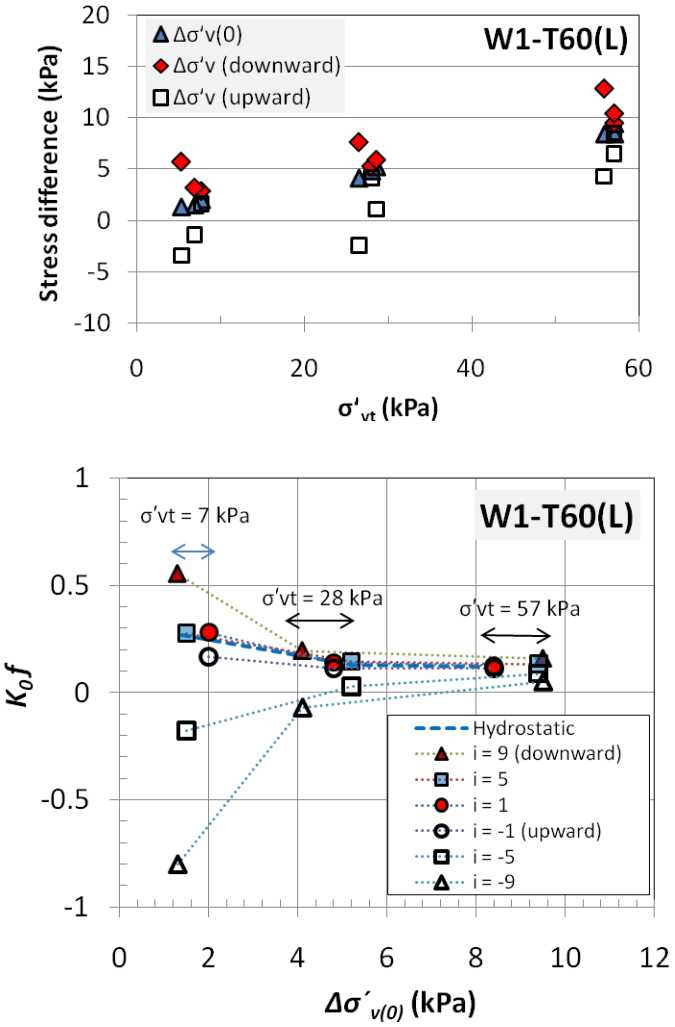

(a)

Figure 3.13 Stress analysis for large permeameter: a) test W1-T60(L); b) test W2-T60(L)

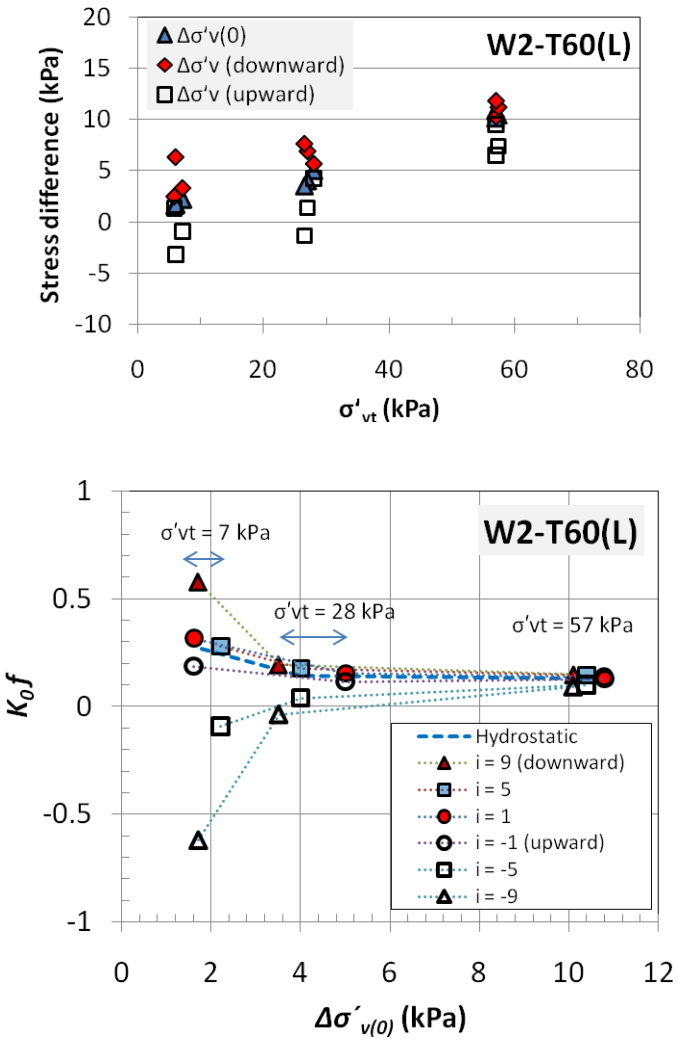

(b)

Figure 3.13 (continued)

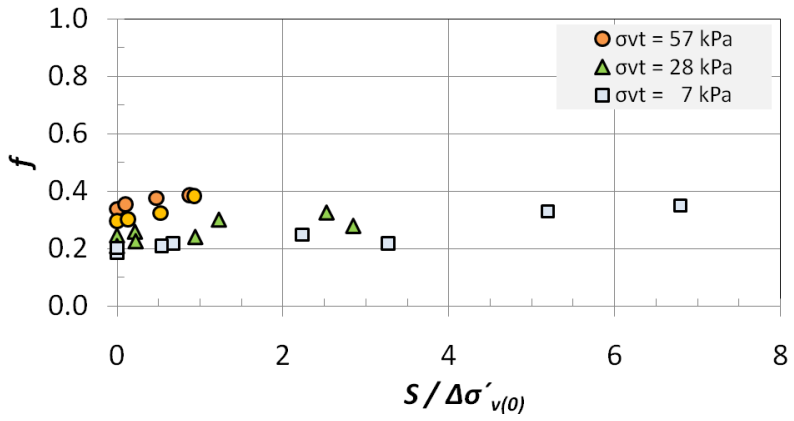

(a)

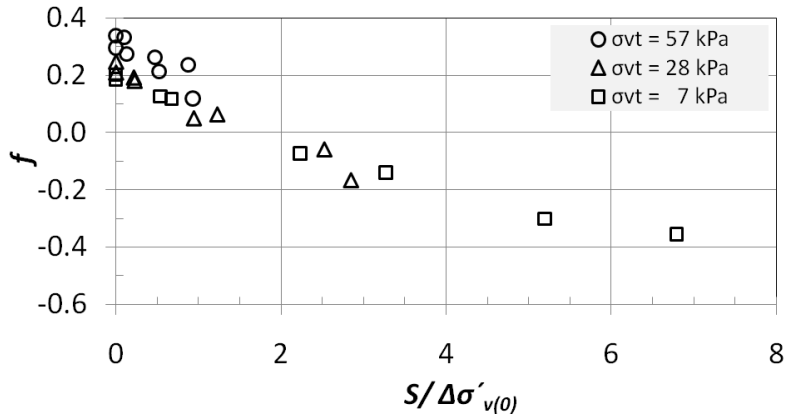

(b)

Figure 3.14 Back-analyzed values of *f*: a) downward flow; b) upward flow

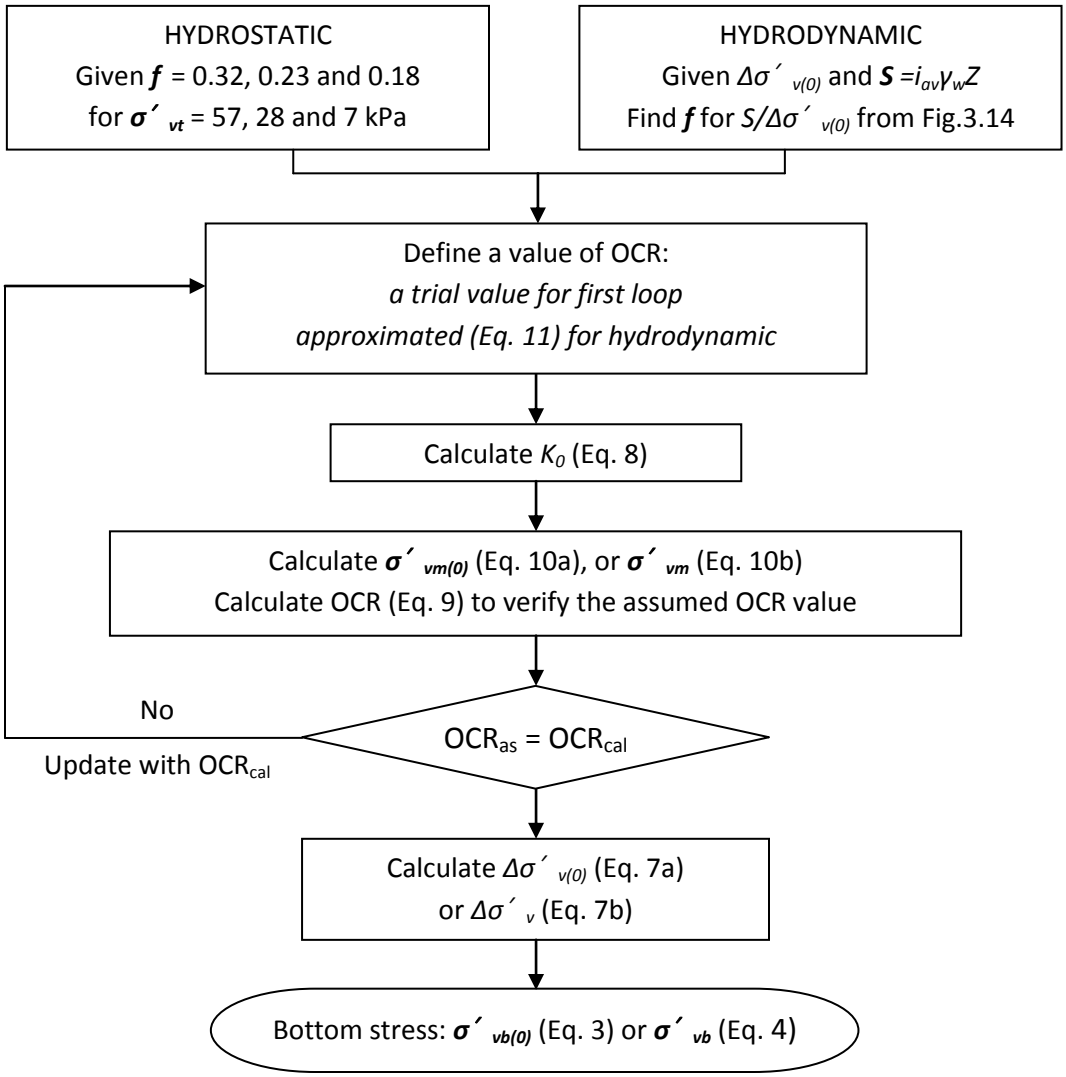

Figure 3.15 Stress calculation procedure for small permeameter

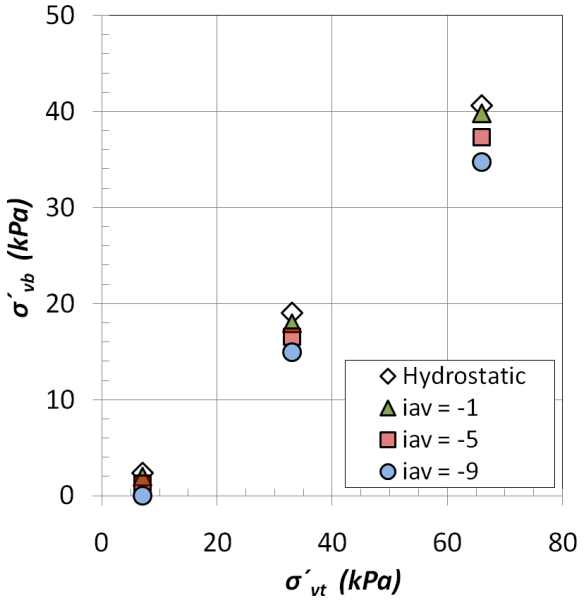

Figure 3.16 Vertical effective stress at soil-geotextile interface: small permeameter

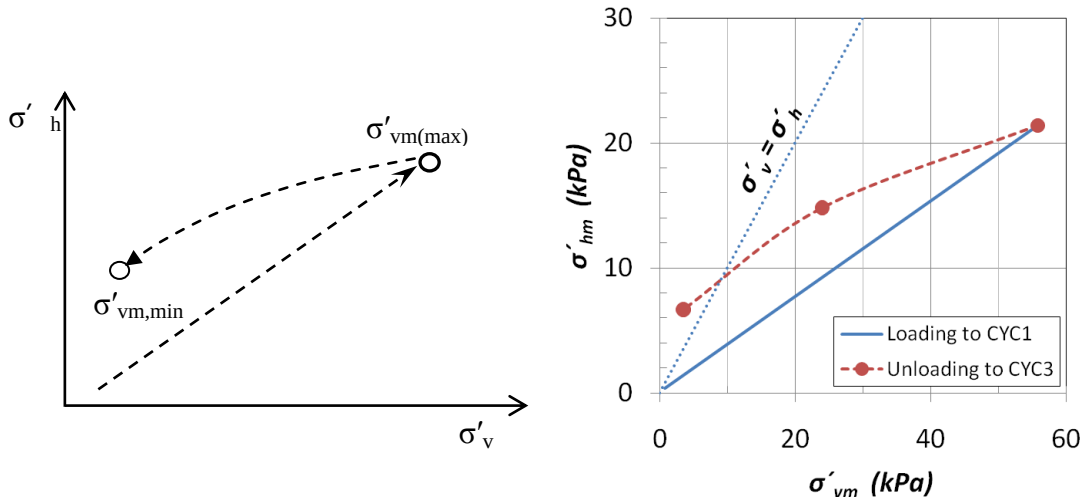

(a) (b)

Figure 3.17 Variation of vertical effective stress (at specimen mid-height) in a rigid-wall permeameter: a) typical response to unloading (modified from Mayne and Kulhawy 1982); b) analyzed response based on results of the large permeameter

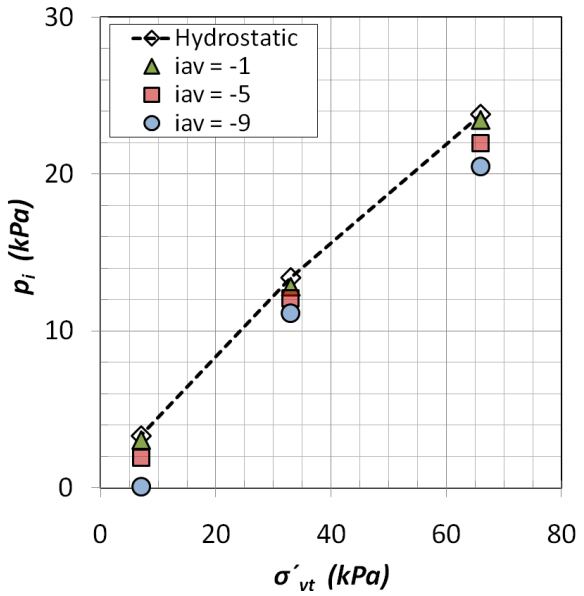

Figure 3.18 Mean effective stress at soil-geotextile interface: small permeameter

3.9 References

Campanella, R. G. & Vaid, Y. P. (1972). A simple K_0 triaxial cell. *Canadian Geotechnical Journal*, **9**, No.3, 249 – 260.

Cazzuffi, D. A., Mazzucato, A., Moraci, N., & Tondello, M. (1999). A new test apparatus for the study of geotextiles behaviour as filters in unsteady flow conditions: relevance and use. *Geotextiles and Geomembranes* **17**, No. 5-6, 313 - 329.

Chen, L., Zhuang, Y-F., Wang, Z. & Xu, Q. (2009). Hydraulic behavior of filter protected silt under cyclic flow. *Journal of Geotechnical and Geoenvironmental Engineering*, **135**, No. 8, 1161 – 1166.

Chen, R.-H., Ho, C.-C. & Hsu, C.-Y. (2008). The effect of fine soil content on the filtration characteristics of geotextile under cyclic flows. *Geosynthetics International*, **15**, No. 2, 95–106.

Chew, S. H., Zhao, Z. K., Karunaratne, G. P., Tan, S. A, Delmas, Ph., & Loke, K. H. (2000). Revetment geotextile filter subjected to cyclic wave loading. *Proceedings of Geo-Denver 2000*, Denver, CO, USA, pp. 162 – 175.

de Graauw, A., van der Meulen, T. & van der Does de Bye, M. (1983). Design criteria for granular filters. *Publication no. 278*, Delft Hydraulics Laboratory, The Netherlands, 25 p.

de Graauw, A., van der Meulen, T. & van der Does de Bye, M. (1984). Granular filters: design criteria. *Journal of Waterway, Port, Coastal and Ocean Engineering*, ASCE, **110**, No. 1, 80-96.

Fannin, R. J. & Srikongsri, A. (2007). Geotextile filters in cyclic flow: test results and design criteria. *Proceedings of Geosynthetics 2007*, Washington, D.C., USA, pp 170-185.

Fannin, R. J., Eliadorani, A. & Wilkinson, J. M. T. (2005). Shear strength of cohesionless soils at low stress, *Geotechnique*, **55**, No. 6, 467-478.

Fannin, R. J., Vaid, Y. P., Palmeira, E. M. & Shi, Y. (1996). A modified gradient ratio device. Recent Developments in Geotextile Filters and Prefabricated Drainage Geocomposites, *ASTM STP 1281*, Philadelphia, PA, USA, pp. 100 – 112.

Giroud, J. P. (1996). Granular filters and geotextile filters, *Proceedings of Geofilters'96 Conference*, Montreal, Quebec, Canada, pp 565-680.

Hameiri, A. (2000). Soil geotextile filtration behavior under dynamic conditions of vibration and cyclic flow. PhD Thesis, University of British Columbia, British Columbia, Canada, 270p.

Hameiri, A. & Fannin, R. J. (2002). A cyclic gradient ratio test device. *ASTM Geotechnical Testing Journal*, **39**, No.2, 266-276.

Hawley, R. (2001). Filtration performance of geotextiles in cyclic flow conditions. MASc Thesis, University of British Columbia, Vancouver, B.C., Canada, 141p.

Indraratna, B & Vafai, F (1997). Analytical model for particle migration within base soil-filter system, *Journal of Geotechnical and Geoenvironmental Engineering*, **123**, No. 2, 100-109.

Indraratna, B & Radampola, S. (2002). Analysis of Critical Hydraulic Gradient for Particle Movement in Filtration. *Journal of Geotechnical and Geoenvironmental Engineering*, **128**, No. 4, 347-350.

Kenney, T. C. & Lau, D. (1985). Internal stability of granular filters. *Canadian Geotechnical Journal*, **22**, No. 2, 215-225.

Kenney, T. C. & Lau, D. (1986). Internal stability of granular filters: Reply. *Canadian Geotechnical Journal*, **23**, No. 3, 420-423.

Li, M. (2008). Seepage induced instability in widely graded soils. Ph.D. thesis, University of British Columbia, B.C., Canada, 297 p.

Moffat, R. (2005). Experiments on the internal stability of widely graded cohesionless soils. Ph.D. thesis, University of British Columbia, B.C., Canada, 274 p.

Mayne, P.W. and Kulhawy, F.H. (1982). "K_o-OCR Relationships in Soil", *Journal of the Geotechnical Engineering Division*, ASCE, **108**, No. GT6, 851-872.

Mayne, P.W. and Kulhawy, F.H. (1994). Discussion of "The Coefficient of Earth Pressure At-Rest", *Canadian Geotechnical Journal*, **31** No.5, pp. 788-790.

Moffat, R.A. and Fannin, R.J. (2006). A large permeameter for study of internal stability in conhesionless soils. *ASTM Geotechnical Testing Journal*, **29**, No. 4, pp. 273-279.

Pilarczyk, K. W. (2000). *Geosynthetics and Geosystem in Hydraulic and Coastal Engineering*. A.A. Balkema, Rotterdam, The Netherlands, 913 p.

Shirato, M., Aragaki, T., Mori, R. & Sawamoto, K. (1968). Predictions of constant pressure and constant rate filtrations based upon an approximate correction for side wall friction in compression permeability cell data. *Journal of Chemical Engineering of Japan*, **1**, No. 1, 86-90

Sivrikaya, O. & Togrol, E. (2005). Measurement of side friction between specimen and consolidation ring with newly designed oedometer cell. *ASTM Geotechnical Testing Journal*, **29**, No. 1, 1-8.

Srikongsri, A. and Fannin, R.J. (2010). Soil-geotextile compatibility testing in cyclic flow. *Manuscript prepared for publication (chapter 2).*

U.S. Army Corps of Engineers (2002). *Coastal Engineering Manual*, EM 1110-2-1100, Washington, DC., USA.

Vaid, Y.P. and Negussey, D. (1988) Preparation of reconstituted sand specimens, *Advanced Triaxial Testing of Soil and Rock,* ASTM STP 977, ASTM, Philadelphia, pp. 405 – 417.

4 Geotextile-Soil Retention in Cyclic Flow[3]

4.1 Outline

Unidirectional and cyclic flow regimes are reproduced at laboratory scale using a cyclic Gradient Ratio device, in order to examine the influence of filter ratio AOS/D_n from combinations of four uniformly-graded soils and seven geotextiles. All combinations were found retention compatible for unidirectional flow. In cyclic flow, mass loss (g/m^2/100 cycles) indicates a strong influence of wave period, hydraulic gradient and effective stress at $3 \leq AOS/D_{50}$ and $2.5 \leq AOS/D_{85}$. A novel analytical approach is proposed, to unify AOS/D_n and a normalized value of seepage pressure ($S/p_{i(0)}$). The hydromechanical approach appears to distinguish between mass loss by washout, in contrast to the more problematic action of piping, in response to cyclic flow. Comparison of the laboratory data with empirical design criteria using AOS/D_{50} or AOS/D_{85} reveals a considerable margin of safety for applications to uniformly-graded soil.

[3] A version of this chapter will be submitted for publication. Srikongsri, A.and Fannin, R. J. (2010). Soil-geotextile retention in cyclic flow.

4.2 Introduction

Dynamic flow regimes are complex phenomena, yet cyclic flow (repeating cross-plane reversing flow) is often of major concern as it typically presents a severe challenge for filtration compatibility. In the absence of a standard test method for cyclic flow, a paucity of appropriate laboratory studies, and a lack of well-documented field performance data, the selection of a geotextile for protection against dynamic flow-induced erosion of a base soil is made with reference to empirical criteria that are believed very conservative (Srikongsri and Fannin, 2009). The criteria define a relation between characteristic value of pore size opening in the geotextile (AOS), and indicative particle size of the base soil (D_n), termed the filter ratio (AOS/D_n). The conservatism arises from recommendation of a small filter ratio, likely unnecessarily small, given uncertainty in thresholds for soil retention in dynamic flow. Retention criteria in cyclic flow are derived from judgement based on practical experience, with few reported data to support the selection process. Yet, over a considerable period of time, those criteria have not been evaluated in a systematic manner (Pilarczyk, 2000).

Consider the relatively simple case of unidirectional flow through a base soil. Openings of the companion filter layer may be selected as large relative to the grain size of the base soil, and the selection made with reasonable confidence, because the margin of safety can be easily determined in a laboratory filtration test or indeed

verified through simulation. In contrast, examining the boundary for soil retention in cyclic flow is considerably more difficult, because dynamic flow regimes are not easily reproduced in a simple test device and the mechanism is governed by several factors (Fannin, 2007). Stress and hydraulic gradient have been demonstrated to govern the movement of soil particles in a granular filter (Indraratna and Vafai, 1997; Indraratna and Radampola, 2002). Similarly, soil passing through the geotextile is influenced by stress and hydraulic gradient (Cazzuffi et al. 1999), and has been found more sensitive to shorter wave periods (Chew et al. 2000).

More specifically, Srikongsri et al. (2010a: see chapter 2) reviewed the experimental work of Hawley (2001), which determined the empirical criterion of $AOS/D_{85} \leq 0.5$ for cyclic flow was overly conservative for the soils examined in testing, given that excessive mass loss through the geotextile was only first encountered at filter ratios $AOS/D_{85} \approx 2$. Consequently, a systematic study was recommended to explore more fully the threshold to seepage-induced instability. In undertaking the systematic study, the need was quickly established to understand better the spatial variation of stress in a rigid-wall permeameter. Furthermore, the need for a standardized multi-stage test procedure and interpretation also became evident. Variation of stress in a rigid-wall permeameter is believed a function of applied stress level, seepage pressure, stress history, soil properties and soil-wall interface shear. An approach to analysis and interpretation of test data is proposed that involves mean effective stress at the soil-geotextile interface (Srikongsri and Fannin, 2010b: see chapter 3).

Two empirical criteria used for soil retention in conditions of dynamic, pulsating or cyclic flow, namely O_{95} or AOS < D_{50} (Luettich et al., 1992), else O_{95} or AOS < $0.5D_{85}$ (Holtz et al., 1997), are often referenced in conference publications, book chapters and specialist design guidance (see for example, Koerner 1998; Pilarczyk 2000; Reddi 2003; Shukla and Yin 2006; Fannin 2006). Hence these two criteria are selected for evaluation in this systematic laboratory study, with the objective of establishing the margin of safety with regard to filter incompatibility.

The Luettich et al. (1992) criterion, for severe hydraulic loading conditions, is based on the earlier proposal of Heerten (1982). In providing guidance on geotextile filter selection against clogging, namely a permeability criterion, Heerten (1982) suggested an approach that was developed from forensic evaluation of 12 needle-punched nonwoven and 4 woven geotextile samples, all of which were exhumed from in-land waterways and sea dikes constructed between the years 1970 - 1977. Comparison was made of clogging in exhumed nonwoven geotextiles, with emphasis on properties of the virgin geotextile and the exhumed geotextile (pore space clogging, reduced porosity and reduced permeability). From these field studies, and more specifically the issue of soil retention, the suggested approach was simply to adopt a conservative value for "sand-tightness": it led to the soil retention criterion of O_{90} < D_{50} for non-plastic soils subject to dynamic loading conditions given by high turbulent flow, wave attack or pumping phenomenon. Accordingly, the empirical criterion is based on

experience that is both appropriate and valuable, but it was not developed from any fundamental study of soil retention and filtration compatibility.

The Holtz et al. (1997) criterion is modified from earlier work reported by Christopher and Holtz (1985). It transpires the origin of the criterion takes the form of $O_{50} < 0.5D_{85}$, and is based on a simple, and intentionally conservative, reduction of a companion filter ratio criterion for unidirectional flow. The objective was to provide for a greater, albeit unknown, margin of safety for more challenging applications in dynamic flow. At the time of the Christopher and Holtz (1985) contribution, few systematic studies were available to support design practice using geosynthetics, hence it is reasonable to find the criterion was not supported by any fundamental study of soil-geotextile behaviour in dynamic, pulsating or cyclic flow. The modified version of $AOS < 0.5D_{85}$ has subsequently been adopted in the Canadian Foundation Engineering Manual (CFEM).

The objective of the current study is to examine the inherent margin of safety in the empirical criteria for geotextile selection in applications of cyclic flow. A systematic experimental program is followed, based on testing of soil-geotextiles combinations in a gradient ratio device, in order to reproduce cyclic flow regimes at laboratory scale. A broad range of filter ratio ($0.7 \leq AOS/D_{85} \leq 3.7$) or ($0.9 \leq AOS/D_{85} \leq 4.6$) is evaluated, from combinations of four uniformly-graded soils against five needle-punched nonwoven geotextiles and two types of woven geotextile. The test results are

interpreted based on values of Gradient Ratio in the soil-geotextile filtration zone, mass loss through the geotextile, and volume change of the soil specimen. Soil retention is then characterized with reference to principles of hydromechanics, through which recognition is given to the influence of hydraulic gradient (i), stress (σ) and wave period (T) on filtration compatibility. The findings address confidence in geotextile selection criteria, and margins of safety in use of empirical criteria for engineering design.

4.3 Experimental methodology

4.3.1 Soils

Four uniformly-graded soils, termed A, B, C and D (see Fig. 4.1 and Table 4.1), were used to examine retention compatibility with seven different geotextiles. The gradations are derived from Fraser River sand (A and B) and Alouette River sand (C and D), taken from borrow sources located in the Vancouver Lower Mainland of British Columbia. Soils A and B are poorly graded sand (SP), soil C is a poorly graded silty sand (SM) and soil D is a non-plastic sandy silt (ML), according to the Unified Soil Classification System. The grain size distribution curves represent soils at the finer end of the coarse-grained size range, and are believed characteristic of problematic erodible soils in marine environments.

Permeability was determined from outflow measurements during test stages of unidirectional flow in the laboratory permeameter, yielding average values between 4 x 10^{-3} cm/s for soil D and 2 x 10^{-2} cm/s for soil A (see Table 4.1). Direct shearbox testing was conducted on dry specimens, reconstituted to a loose condition, at relatively low values of normal effective stress ($\sigma'_n \leq 50$ kPa). The objective was to determine the angle of shearing resistance at large displacement (φ) at stress levels equal to those encountered in the permeameter test device, for purposes of stress analysis at the soil-geotextile interface. The values of φ are found to be very similar in magnitude, and exhibit an apparent stress-dependency (see Table 4.1).

4.3.2 Geotextiles

Seven geotextiles, with Apparent Opening Size (AOS) ranging from 0.06 to 0.30 mm, were examined in the program of testing (see Table 4.2). Five needle-punched nonwoven geotextiles, termed NW1 to NW5, are manufactured from continuous filaments of polypropylene. They all exhibit a permeability, defined by the product of permittivity and thickness, greater than that of the four soils. The woven monofilament (W1) and woven multifilament (W2) geotextile are also made of polypropylene yarn. They have a percent open area (POA) greater than or equal to 4 %, and values of permeability comparable to those of soils A and B, and greater than

soils C and D. All seven geotextiles were manufactured and supplied by Ten Cate Geosynthetics.

Altogether, 15 combinations of soil and geotextile were examined (see Table 4.3), in a total of 27 tests at a wave period of 6, 60 or 120 s. All test combinations were examined at T = 6 s, with additional testing at T = 60 s and 120 s for the case of soil loss or for occasional comparative checks on compatibility. In reporting the laboratory data, the test code employed (e.g. C-W2-T6) declares the sequence of soil gradation (C), geotextile type (W2) and wave period (T6). Given the grain size distribution of soils, and opening size of geotextiles, the variety of soil-geotextile combinations yielded a range in filter ratio of $0.7 \leq AOS/D_{85} \leq 3.7$ ($0.9 \leq AOS/D_{50} \leq 4.6$). The smallest filter ratio is similar to that recommended in design guidance for applications of cyclic flow, while the largest is significantly greater than that recommended for unidirectional flow.

4.3.3 Test device and procedure

A cyclic gradient ratio test device was used to characterize soil-geotextile compatibility (see Fig. 4.2a). The device is configured to apply stress on the top of the specimen, to record the distribution of water head along the test specimen, to measure change in specimen length, and to collection of soil loss through the geotextile in discreet quantities. Water head distribution is used to calculate a value of Gradient

Ratio: port 1 is located on the top plate; ports 3, 5 and 6 are located at 75 mm, 25 mm and 8 mm above the geotextile; port 7 is located beneath the geotextile sample (see Fig. 4.2a). Gradient Ratio, GR_{25} and a modified value GR_8 are calculated as:

$$GR_{25} = \frac{i_{57}}{i_{35}} \tag{1}$$

$$GR_8 = \frac{i_{67}}{i_{35}} \tag{2}$$

where i_{35} = hydraulic gradient within the soil between ports 3 and 5

i_{57} = hydraulic gradient across the soil-geotextile interface between ports 5 and 7

i_{67} = hydraulic gradient across the soil-geotextile interface between ports 6 and 7

Cyclic flow is imposed by a head-controlled system (see Fig. 4.2b). Average hydraulic gradient (i_{av}), in either downward or upward flow, is controlled by an equidistant spacing of constant head tanks (+H and -H). The gradient is defined by head loss between ports 1 and 7 (H_{17}), expressed as $i_{av} = H_{17}/Z$, where Z is length of the specimen. Frequency of flow reversal is controlled using a 3-way solenoid valve programmed to switch at an interval t = T/2 sec, where T is the wave period. Further details of the test device are reported by Hameiri (2000) and Hameiri and Fannin (2002).

Preparation of the geotextile sample, reconstitution of the soil specimen, and imposition of seepage in stages of unidirectional (UNI) and cyclic flow (CYC) followed exactly the routine described by Srikongsri and Fannin (2010b: see chapter 3). A test was conducted with cyclic flow at constant wave period (T = 6, 60 or 120 s). Three values of gradient ($i_{av} \approx 1$, 5 and 9) were imposed sequentially, with vertical effective stress on the top of the specimen changed to yield values of confining stress reducing from $p_{i(0)}$ = 23 kPa to 14 kPa and then 3 kPa at each value of i_{av}. The nature of the loading routine for test C-W2-T6 is illustrated schematically for $i_{av} \approx 9$ (see Fig. 4.3), in order to demonstrate how stages of unidirectional (UNI) flow were used to bound stages of cyclic (CYC) flow, yielding values of gradient ratio (GR_8 and GR_{25}).

Consider the matter of stress distribution in the test specimen. Vertical effective stress at the soil-geotextile interface (σ'_{vb}) is less than that applied at the top (σ'_{vt}), as a consequence of sidewall friction (see Fig. 4.2c). The relation between σ'_{vt} and σ'_{vb} has been quantified (Srikongsri and Fannin, 2010b: see chapter 3) with respect to its variation in a multi-stage loading sequence identical to that of the program of testing reported herein. Recognizing the importance of overall confining stress on geotextile filtration compatibility, the relation established between σ'_{vt} and initial mean effective stress ($p_{i(0)}$) at the soil-geotextile interface is illustrated for soil C (see Fig. 4.2d). The relation was established for the initial hydrostatic condition: it is assumed to quantify the initial hydrostatic stress condition for tests on soils A, B and D given the similar properties of all four uniformly graded materials.

4.4 Results

The five needle-punched nonwoven geotextiles were all tested at the relatively fast cyclic flow (T = 6 s), in a total of eight combinations of soil and geotextile that yield a filter ratio $0.7 \leq AOS/D_{85} \leq 2.3$. In presenting the data, results are examined over two distinct ranges of filter ratio, firstly for $0.7 \leq AOS/D_{85} \leq 1$, and secondly for $1 < AOS/D_{85} \leq 2.3$. The two woven geotextiles, which exhibit a relatively larger opening size than the nonwoven geotextiles (see Table 4.3), were also tested at the relatively fast cyclic flow of T = 6 s and, in several cases at T = 60 s and 120 s, with tests exhibiting significant soil loss then repeated. A total of seven combinations of soil and geotextile yield a filter ratio $1.2 \leq AOS/D_{85} \leq 3.7$. The data are again presented over two ranges of filter ratio, namely $1.2 \leq AOS/D_{85} \leq 2$ and $2 < AOS/D_{85} \leq 3.7$, in order to distinguish between subtle aspects of filtration compatibility.

The generalized nature of filtration compatibility is summarized in Table 4.4, and examined herein with reference to type of geotextile and filter ratio. A general trend is evident in the experimental findings, with the nonwoven geotextiles yielding no mass loss, and the more open woven geotextiles yielding mass loss at larger filter ratio (see also Table 4.4). The general trend is best illustrated by the relation between mass loss and AOS/D_{85}, for all test specimens, induced by cyclic flow in the CYC2 stage at the

same confining stress $p_{i(0)}$ = 14 kPa (σ'_{vt} = 33 kPa) at $i_{av} \approx 1$ (Fig. 4.4a) and $i_{av} \approx 5$ (Fig. 4.4b). Mass loss per unit area is reported for 100 cycles of flow reversal (g/m^2/100 cycles): it is an average value for tests at T = 6 s (with 900 cycles/stage) and an extrapolated value for tests at T = 60 s (with 90 cycles/stage) and T = 120 s (with 45 cycles/stage). It appears the filter ratio $2 \leq AOS/D_{85} \leq 3$ exerts a governing influence on filtration compatibility, and deserves careful evaluation.

4.4.1 Nonwoven geotextiles

4.4.1.1 Filter ratio: $0.7 \leq AOS/D_{85} \leq 1.0$

Four soil-geotextile combinations with $AOS/D_{85} \leq 1$ (tests A-NW4-T6, C-NW3-T6, D-NW1-T6 and D-NW2-T6, see Table 4.3), all exhibited a similar response in testing at T = 6 s. No soil was observed to pass through the geotextile during the process of soil reconstitution by water pluviation. Visual observations indicated no loss of soil in any stage of unidirectional (UNI) flow and, similarly, no loss in any cyclic (CYC) stage, and none was found in the silicone collection hose (see Fig. 4.2a). No volume change was observed in the specimen during the test. Gradient ratio values in the range $0.9 \leq GR_{25} \leq 1.4$ and $0.9 \leq GR_8 \leq 1.7$, for all stages of unidirectional flow, confirm the homogeneity of the test specimen. Accordingly, these test combinations are deemed stable in both unidirectional and cyclic flow.

4.4.1.2 Filter ratio: $1.0 < AOS/D_{85} \leq 2.3$

Consider the two soil-geotextile combinations with AOS/D_{85} = 1.7 (tests C-NW4-T6 and C-NW5-T6), which again were tested at T = 6 s. No soil loss occurred during specimen reconstitution, and subsequent visual observations indicated no loss of soil in any stage of unidirectional (UNI) or cyclic (CYC) flow. The observations are consistent with no measurable accumulation of soil in the collection hose, and no volume change during the test. Values of GR_{25} and GR_8 in the range 0.9 to 1.0 indicate an almost linear variation of water head distribution along the length of the specimen. Accordingly, both tests reveal a very similar response, and the combinations are deemed stable in both unidirectional and cyclic flow.

The two soil-geotextile combinations with AOS/D_{85} = 2.3 (tests D-NW4-T6 and D-NW4-T60, and D-NW5-T6) include one test at T = 60 s, in addition to those at T = 6 s. Although some soil loss was observed at the beginning of specimen reconstitution, the amount was too small to measure. Visual observations indicated no loss of soil in any stage of unidirectional (UNI) flow and, similarly, no loss in any cyclic (CYC) stage, which is consistent with no recorded volume change in the specimens. Values of GR_{25} and GR_8 ranging from 0.9 to 1.3 imply a water head distribution that is essentially linear along the specimen. Accordingly, these test combinations are also deemed stable in both unidirectional and cyclic flow.

Scanning Electron Microscope (SEM) images from D-NW4-T6 and D-NW5-T6, taken after testing (Figs. 4.5b and 4.5d), are compared to images of the geotextiles before testing (Figs. 4.5a and 4.5c). Note the geotextiles must be dried before imaging, and experience moderate disturbance as a consequence of preparation for the imaging process. In contrast to the specks of dust evident on the untested geotextile, the post-test specimens reveal particles of soil D embedded within the fabric of the geotextile. The particles, ranging in size up to 100 microns, illustrate clearly the manner in which soil retention is mobilized within the tortuous array of pore size openings and constrictions in the nonwoven material of $AOS/D_{85} = 2.3$.

4.4.2 Woven geotextiles

4.4.2.1 Filter ratio: $1.2 \leq AOS/D_{85} \leq 2.0$

Four soil-geotextile combinations were examined with $1.2 \leq AOS/D_{85} \leq 2.0$ (see Table 4.3). No soil was observed to pass through the geotextile during specimen reconstitution of tests A-W1-T6 and A-W1-T60 ($AOS/D_{85} = 1.2$), and B-W1-T6 and B-W1-T60 ($AOS/D_{85} = 1.4$). In contrast, tests B-W2-T6, B-W2-T60 and C-W1-T6 ($AOS/D_{85} = 2$) yielded a mass loss between 50 and 100 g/m^2. Thereafter, visual observations indicated no loss of soil in any stage of unidirectional (UNI) flow and, similarly, no loss in any cyclic (CYC) stage. Additionally, no volume change was measured in the specimen length during these tests. Gradient ratio values in the range

$1.0 \leq GR_{25}$ and $GR_8 \leq 1.5$ confirm the homogeneous nature of the test specimen. Accordingly, the test combinations for $AOS/D_{85} \leq 2.0$ are deemed stable in both unidirectional and cyclic flow.

4.4.2.2 Filter ratio: $2.0 < AOS/D_{85} \leq 3.7$

In total, five tests were performed on soil D and geotextile W1 ($AOS/D_{85} = 2.6$) for wave periods of T = 6, 60 and 120 s and, similarly, five tests on soil C with geotextile W2 ($AOS/D_{85} = 2.8$) at the same values of wave period. One test was performed at the largest filter ratio, that for soil D and geotextile W2 ($AOS/D_{85} = 3.7$), at T = 6 s. A significant soil loss was found during specimen reconstitution, in the range 200 to 400 g/m^2 for $2.6 \leq AOS/D_{85} \leq 2.8$, and 450 g/m^2 for $AOS/D_{85} = 3.7$. In providing a detailed description of soil loss during cyclic flow (see Figs. 4.6 to 4.12), reference is made to imposed seepage pressure $S = \pm i_{av}\gamma_w Z$ (kPa), where γ_w is unit weight of water and Z is length of the test specimen, when discussing the influence of hydraulic gradient.

For $AOS/D_{85} = 2.6$, at T = 6 s (test D-W1-T6), mass loss occurred in none of the UNI stages, but all of the CYC stages. The loss was not found particularly sensitive to $S \approx \pm 1$ kPa for each of the three values of confining stress ($p_{i(0)}$ = 23 kPa, 14 kPa and 3 kPa), but appears more sensitive at $S \approx \pm 5$ and ± 9 kPa (see Fig. 4.6). The response to seepage flow appears consistent, given repetition of the test on a different sample of

the same geotextile: average mass loss (m_{av}) varies from 10 to 90 g/m^2/100 cycles (see Fig. 4.6a), and from 10 to 150 g/m^2/100 cycles (see Fig. 4.6b). The modest difference in values is believed a consequence of spatial variation in pore size distribution in the two samples tested. Visual observation indicates the losses were continuous, rather than pulsating, a response that is attributed to the relatively short wave period of 6 s. No preferential flow channels were found to develop in the soil specimen.

Increasing the wave period to T = 60 s (test D-W1-T60) at the same AOS/D_{85} = 2.6, again yielded no mass loss during the UNI stages of flow, and a loss in all of the CYC stages. The general trend found in testing at T = 6 s is also apparent in testing at T = 60 s (compare Figs. 4.7 and 4.6). At the same value of confining stress, soil loss increases with greater seepage pressure (from S ≈ ± 1 kPa to S ≈ ± 5 kPa and S ≈ ± 9 kPa, see Fig. 4.7a); likewise, at the same condition of seepage pressure, mass loss increases with reduction in confining stress. In contrast to the experience at T = 6 s, the losses at T = 60 s occurred as a pulsating action that dimished to zero loss over the duration of each flow reversal. The loss was not restricted to any preferential location on the geotextile filter. The trend in mass loss is again confirmed by the repeated test (see Fig. 4.7b), where the same influence of spatial variation in geotextile opening size is believed evident (compare Figs. 7a and 7b). The losses at T = 60 s appear slightly smaller than those at T = 6 s.

Increasing the wave period to T = 120 s (test D-W1-T120) confirmed, once again, no soil loss through the geotextile in the UNI stages of flow. Furthermore, no loss was measured at S ≈ ± 1. Thereafter, some loss (25 g/m^2 < m_{av} ≤ 55 g/m^2/100 cycles) was observed at S ≈ ± 5 and ± 9 kPa (see Fig. 4.8). In this regard, it appears the relatively long wave period does not replicate the responses at T = 6 and 60 s.

All tests at this filter ratio gave values of GR_{25} and GR_8 between 1.0 and 1.3, which confirms the homogeneity of the test specimen throughout the multi-stage test procedure. Hence, to summarize the findings for tests at AOS/D_{85} = 2.6, the soil-geotextile combination is deemed stable in unidirectional flow. However, given the greater value of soil loss, the soil retention and consequent nature of stability achieved in cyclic flow requires further analysis in order to characterize it more definitively.

Consider now the data acquired for AOS/D_{85} = 2.8, which are re-plotted from Srikongsri and Fannin (2010a). No mass loss was observed during stages of unidirectional flow. In cyclic flow, test C-W2-T6 (see Fig. 4.9a) and the companion repeated test (see Fig. 4.9b) at T = 6 s both exhibit the general trend evident in data for the smaller filter ratio of 2.6 at the same relatively short wave period (see Fig. 4.6). Values of m_{av} vary from 50 to 160 g/m^2/100 cycles, which slightly exceeds those for the corresponding test at AOS/D_{85} = 2.6. The finding is attributed to the slightly larger filter ratio.

Increasing the wave period to T = 60 s (test C-W2-T60) at the same AOS/D_{85} = 2.8, again yielded no mass loss as a consequence of unidirectional flow. Losses during stages of cyclic flow in this test (see Fig. 4.10a) and the companion repeated test (see Fig. 4.10b) again increase with greater seepage pressure, and increase with reduction in confining stress. Values of m_{av} recorded in the two tests do not appear to differ significantly, ranging from 25 to 125 g/m^2/100 cycles and 10 to 80 g/m^2/100 cycles, respectively. As was the case for AOS/D_{85} = 2.6, the losses at T = 60 s appear slightly smaller than those at T = 6 s.

Increasing the wave period to T = 120 s (test C-W2-T120) yields a response (see Fig. 4.11) almost identical to that reported for D-W1-T120 (see Fig. 4.8). Comparison of the data shows the general pattern of soil loss with variation of seepage pressure and confining stress is very similar, with $m_{av} \leq 55$ g/m^2/100 cycles in all stages of cyclic flow.

All tests at this filter ratio gave values of GR_{25} and GR_8 between 1.0 and 1.5, which like the previous filter ratio, confirms the homogeneity of the test specimen throughout the multi-stage test procedure. Hence, to summarize the findings for tests at AOS/D_{85} = 2.8, the soil-geotextile combination is deemed stable in unidirectional flow. However, given the greater value of soil loss, and its variation with wave period, soil retention and the consequent nature of stability achieved in cyclic flow requires further analysis in order to properly characterize it.

One test (D-W2-T6) was performed for the largest filter ratio AOS/D_{85} = 3.7, at T = 6 s. Unlike all of the preceding tests at relatively smaller filter ratios, it was terminated before completion of the multi-stage procedure. More specifically, the test was stopped after completion of the stage at $i_{av} \approx 5$ and $p_{i(0)} \approx 14$ kPa (CYC2), due to excessive mass loss through the geotextile and a corresponding loss of integrity in the test specimen itself. Again, in contrast to all of the preceding tests, mass loss was observed in every stage of unidirectional flow that was applied, and measured to be in the range 30 to 80 g/m^2. Visual observations confirm the losses to occur over a relatively short time period after transition from cyclic to unidirectional flow, typically no longer than one minute, whereupon the downward seepage flow did not yield further loss and the system appeared "meta-stable". Values of GR_{25} and GR_8 in the range 0.7 to 0.8, which being less than 1.0, suggest a zone of slightly lower hydraulic conductivity at the soil-geotextile interface that is consistent with significant washout of soil particles. Accordingly, the soil-geotextile combination is believed close to a limiting value of filter ratio for soil retention in unidirectional flow. In the five stages of cyclic flow that were imposed (see Fig. 4.12a), mass loss was found to be much greater than in previous tests (Fig. 12a). More specifically, m_{av} varied from 150 to nearly 320 g/m^2/100 cycles, which resulted in development of significant voids in the body of soil specimen (see Fig. 4.12b). The AOS/D_{85} = 3.7 filter ratio is deemed unstable in cyclic flow, given the very clear evidence of retention incompatibility.

In summary, significant quantities of soil loss were only observed from tests on the two woven geotextiles, with soils C and soil D, for values of filter ratio in the range $2.6 \leq AOS/D_{85} \leq 3.7$. Loss occurs with cyclic flow alone at the lower end of the range, and with both unidirectional and cyclic flow at the higher end of the range. Variations in mass loss are evident at different values of confining stress, hydraulic gradient and wave period.

Scanning Electron Microscope (SEM) images from D-W1-T6 and C-W2-T6, taken after testing (see Figs. 4.13a and 4.13b, respectively) illustrate the very different structure of the woven monofilament and multifilament fabrics. The AOS of geotextile W1 (210 microns) is smaller than geotextile W2 (300 microns), and both values are larger than those of the nonwoven geotextiles examined in testing (see Table 4.2). A common feature of both is the absence of a tortuous path, comprising many pore size openings and constrictions, across the plane of the fabric. It is in marked contrast to the nonwoven geotextile (see Fig. 4.5). The SEM images illustrate well the regular configuration of fibres and openings of a woven geotextile that does not allow particles to lodge within the fabric (see Fig. 4.13).

It is believed that retention stability in these soil-geotextile combinations of filter ratio greater than 1 is a consequence of soil bridging over the filter opening (see Fig. 4.14). The range between $2.0 < AOS/D_{85} < 2.6$ appears very important with regard to the onset of filtration incompatibility in cyclic flow. The work of Valdes and Santamarina

(2008) demonstrates, for spherical particles and a single circular orifice or opening, a series of conceptual regimes for particle bridging. The effect of particle shape on the formation of bridges across an orifice of diameter d_0 is illustrated in Figure 4.14a. The conceptual regime for glass beads at $2 \leq d_0/d \leq 3$ is further illustrated in Figure 4.14b: it suggests that for spherical particles and a single orifice, the onset of bridging instability may occur at $d_0/d \approx 3$. The contribution of Valdes and Santamarina (2008) suggests the ratio d_0/d increases with particle angularity. Likely, this fundamental study (with vibration, not cyclic flow) represents an upper threshold to the case for soil grains against a mesh or filter with many closely-spaced openings. Hence, the onset of filtration incompatibility in cyclic flow at $2.0 \leq AOS/D_{85} \leq 2.6$ observed in the current study appears consistent with the findings reported by these conceptual regimes.

4.5 Analysis and discussion

The behaviour of soil-geotextile combinations in the range $2.6 \leq AOS/D_{85} \leq 3.7$ provides the basis for a hydromechanics-based analysis. More specifically, the measured soil loss and associated volume change may be used to quantify filtration compatibility with reference to soil retention. The analytical approach first involves defining an acceptable threshold for seepage-induced loss or washout through the geotextile, and then defining a retention criterion that accounts for the influence of wave period, hydraulic gradient and confining stress. Findings of the analysis are

reported for the complete set of laboratory data ($0.7 \leq AOS/D_{85} \leq 3.7$, else the equivalent $0.9 \leq AOS/D_{50} \leq 4.6$). Discussion addresses the issue of a margin of safety in design guidance.

4.5.1 Soil washout

In order to achieve stability in a relatively open filter, some amount of seepage-induced mass loss may be necessary, recognizing washout contributes to the formation of a stable bridging network at the filter openings. A threshold value for the associated losses may be established from consideration of volume change over time (or number of flow cycles): a constant or increasing rate of volume change is taken to denote a piping action.

A preliminary consideration of volume change in the three soil-geotextile combinations that exhibit mass loss suggests a value of m_{av} greater than about 60 g/m^2/100 cycles is likely not a case of washout. More specifically, consider the data for tests D-W1-T6 and C-W2-T6. The response at T = 6 s is selected for analysis because volume loss at T = 60 s (90 cycles) and 120 s (45 cycles) is insufficient for systematic study, compared to the 900 cycles imposed at T = 6 s. The relation between volume change and number of flow cycles for these two tests (including test repetition), from the CYC1 stage at $i_{av} \approx 5$, reveals three clustered responses (see Fig. 4.15). A nearly constant rate of loss occurs for 70 g/m^2/100 cycles $\leq m_{av} \leq$ 100

g/m^2/100 cycles (see Fig. 4.15a), whereas the rate appears to diminish for 35 g/m^2/100 cycles $\leq m_{av} \leq$ 50 g/m^2/100 cycles and clearly results in zero volume change after about 500 cycles for $m_{av} \leq$ 30 g/m^2/100 cycles (Fig. 4.15b). It is proposed the curves for 36, 38 and 52 g/m^2/100 cycles represent a transition from washout to a piping action, which may be reasonably associated with a volume change less than 0.5 %. It therefore appears an upper threshold to washout, leading to stability in soil retention, is defined by the range 30 g/m^2/100 cycles $\leq m_{av} \leq$ 50 g/m^2/100 cycles (or total mass loss of 270 to 450 g/m^2, at 900 cycles). Comparison shows the range is similar to the mass loss of 200 g/m^2 to 400 g/m^2 through the geotextile that was observed during reconstitution of the soil specimen by water pluviation.

4.5.2 Soil retention: a hydromechanical approach

A normalized seepage pressure ($S/p_{i(0)}$), which accounts for both the initial stress condition and hydraulic gradient, is evaluated for its potential to explain the variation of mass loss during various stages of seepage flow in the multi-stage test procedure. The stress ratio serves as an index for intensity of the imposed hydromechanical loading condition. A low $S/p_{i(0)}$ value, significantly less than unity, represents relatively mild or moderate hydraulic loads. In contrast, if the ratio $S/p_{i(0)}$ exceeds a value of one, it implies that effective stress at the soil-geotextile filter interface is approaching zero. The range of variables examined in testing (see Table 4.5) yields a range of normalized seepage pressure $0.05 \leq S/p_{i(0)} \leq 3$.

4.5.2.1 Onset of piping for $2.6 \leq AOS/D_{85} \leq 3.7$: woven geotextiles

For $AOS/D_{85} \approx 2.6$, mass loss data obtained at T = 6 s (18 values from Fig. 6a and 6b) and at T = 60 s (18 values from Fig. 4.7a and 4.7b) is reported as an average value per 100 cycles (yielding 9 values for each wave period), and reproduced with reference to the normalized seepage pressure (see Fig. 4.16a). Data for T = 120 s (from Fig. 4.8) are also included, with the results from 45 cycles reported as an equivalent rate per 100 cycles. The influence of wave period is generally evident: data at T = 6 s represent the most sensitive response, characterized by greatest increase of mass loss with normalized seepage pressure, compared to data at T = 60 s and T = 120 s, with the latter yielding a relatively small increase in soil loss. It is reasonable to conclude the short wave period of T = 6 s governs retention stability in the range 6 s ≤ T ≤ 120 s. Inspection of the T = 6 s data, at the threshold range of 30 – 50 g/m^2/100 cycles for washout, suggests the onset of soil piping through the geotextile is triggered at values of $S/p_{i(0)}$ approximately 0.1 to 0.2.

For $AOS/D_{85} \approx 2.8$, mass loss data are obtained in the same manner (see Fig. 4.16b), using data at T = 6 s in (Figs. 4.9a and 4.9b), T = 60 s (Figs. 4.10a and 4.10b) and T = 120 s (Fig. 4.11). Inspection of the plot confirms the data at T = 6 s again demonstrate the greatest increase of mass loss, and govern the retention stability. Indeed a subtle, yet clear difference, is evident in the relative plotting positions of the response at each

of three wave periods. Inspection of the T = 6 s data, at the threshold range for washout, suggests the onset of soil piping is triggered at values of $S/p_{i(0)}$ approximately 0.04 to 0.08.

For $AOS/D_{85} \approx 3.7$, data for only five stages at T = 6 s (Fig. 12) are available (see Fig. 4.16c) given early termination of the test. They general trend of mass loss with $S/p_{i(0)}$ is consistent with that observed for the two smaller filter ratios (see Figs. 4.16a and 4.16b). The five data points locate significantly above the threshold range for washout, providing further evidence that the soil-geotextile combination experienced a severe piping action in response to seepage flow. The finding is consistent with the visual observation of voids within the body of the soil specimen (see Fig. 4.12b). Extrapolation of the data toward the origin of the plot, and therefore into the threshold range for washout, suggests the onset of soil piping is likely triggered at values of $S/p_{i(0)}$ approximately 0.01 to 0.02.

The general relation between mass loss and normalized seepage pressure, in combination with a criterion for washout progressing to onset in piping, is found to be an appropriate technique for characterizing soil retention in cyclic flow. It addresses the most critical test variables and, although subjective in part, lends itself to quantification of the system response. Importantly it brings a hydromechanical framework to evaluation of soil-geotextile filtration compatibility, which has potential for general application (see Fig. 4.16d).

4.5.2.2 Hydromechanical influence: a unified plot

The experimental data indicate the short wave period T = 6 s governs stability in soil retention, a response that is attributed to the more aggressive nature of this flow condition. Accordingly, it is reasonable to use the response at that wave period to unify the influence of hydromechanical constraint at the soil geotextile interface, characterized by $S/p_{i(0)}$, and the influence of geometric constraint from the filter medium, characterized either by AOS/D_{85} or AOS/D_{50} in various design guidance. The experimental findings on $S/p_{i(0)}$ values at the onset of piping are plotted against $2.6 \leq AOS/D_{85} \leq 3.7$ (see Fig. 4.17). Additionally the finding for $AOS/D_{85} = 2.0$, from test C-W1-T6 that exhibited essentially no loss for $S/p_{i(0)} \leq 3$, is included for purposes of trends analysis. The dashed curve represents the lower boundary (30 g/m^2/100 cycles) to washout through the geotextile. The error bar represents the range between lower and upper bound values of $S/p_{i(0)}$ to washout. It should be noted that inspection of the error bars, derived from the postulated washout threshold in Fig. 4.16, implies a greater sensitivity to value of the threshold limits rather than value of effective stress at the soil-geotextile interface. At a particular value of $S/p_{i(0)}$, if a value of AOS/D_{85} plots above the curve, it implies there is susceptibility to soil piping.

Consider now the data for a wave period longer than T = 6 s, namely 60 s and 120 s, which are available at $AOS/D_{85} = 2.6$ and 2.8: the threshold range is associated with

larger values of $S/p_{i(0)}$ for T = 60 s and 120 s (see Figs. 4.16a and 4.16b). The influence of wave period is evident in the unified plot (Fig. 4.17). The phenomenon may be explained through a consideration of the duration of steady flow condition between each cycle of flow reversal, in association with the rate of change of seepage pressure (i.e. ΔS, kPa – s^{-1}). For tests at T = 6 s, the soil-geotextile interface is continuously subjected to an unsteady flow condition yielding turbulent pressure fluctuations: the relatively short duration of each cycle is not sufficient to allow the value of ΔS, which is a function of the rate of change of gradient (Δi), to diminish to zero before the next flow reversal (see chapter 3). In contrast, tests at T = 60 and 120 s experience a transient condition of steady flow between each flow reversal, and consequently the soil bridging network can stabilize between periods of instability. The plotting position of the data at T= 60 s and 120 s is attributed to this importance of wave period. Furthermore, the rate of change of seepage pressure is also found to influence the onset of incompatibility.

Consider now the error bars for the data at AOS/D_{85} = 2.6 and 2.8, on the semi-log plot (Fig. 4.17), which depict values of $S/p_{i(0)}$ associated with a condition of washout (30 g/m^2/100 cycles) and onset of retention incompatibility from piping action (50 g/m^2/100 cycles). The range of $S/p_{i(0)}$, from a condition of washout through to onset of piping action, is found to be relatively small in tests at T = 6 s, nearly twice as large at T = 60, significantly larger again at T = 120 s (see also Fig. 4.16). In each case, $\Delta S/p_{i(0)}$ increases by approximately 100%. The finding suggests that the rate of change

of seepage pressure is more important to soil retention for conditions of relatively fast cyclic flow. Hence, the threshold boundary at T = 6 s yields a conservative relation between $S/p_{i(0)}$ and AOS/D_{85} for the onset of incompatibility in soil retention.

4.5.2.3 Unified plot for AOS/D_{85}

The hydromechanical influence examined in Fig. 4.17, for data on woven geotextiles only, is expanded to include data for all soil-geotextile combinations examined in the test program (see Fig. 4.18a). Recall that filter ratios of $1.2 \leq AOS/D_{85} \leq 2.0$ are for woven geotextiles, and $0.7 \leq AOS/D_{85} \leq 2.3$ are for needle-punched nonwoven geotextiles, yielding a variety of geotextile type at a filter ratio $AOS/D_{85} \approx 2$. The data for no soil loss are also plotted as a minimum and maximum range of $S/p_{i(0)}$, for any given AOS/D_{85}: the minimum value is that for the first stage of cyclic loading (CYC1) at a lowest gradient ($i_{av} \approx 1$), and the maximum value is obtained in the third stage (CYC3) at the highest gradient imposed in the test.

A general inspection of Fig. 4.18a reveals three characteristic responses to cyclic flow. At relatively large filter ratio ($AOS/D_{85} \geq 3.5$), the onset of piping that occurs at a very low value of $S/p_{i(0)} \leq 0.05$ means a gentle flow reversal is capable of triggering retention instability, and implies the filter ratio is close to a limit at which unidirectional flow alone could lead to filter incompatibility. In contrast, no soil loss is found with $AOS/D_{85} \leq 2.0$ for a woven geotextile, and with $AOS/D_{85} \leq 2.2$ for a

nonwoven geotextile. The interval between these two contrasting responses yields a third range of filter ratio wherein washout and piping are found very dependent on the influence of hydraulic gradient on the magnitude of effective stress. Within this range, a filter ratio $2.0 \leq AOS/D_{85} \leq 2.5$ is likely to result in washout, with increasing susceptibility to piping at higher seepage pressures; a filter ratio $2.5 \leq AOS/D_{85} \leq 3.5$ is likely to result in piping, with a small change in filter ratio being very sensitive to changes in the hydromechanical influences of stress and gradient.

The design criterion O_{95}/D_{85} or $AOS/D_{85} \leq 0.5$ is suggested for applications of cyclic, pulsating or reversing flow (Holtz et al., 1997; CFEM, 2006). From inspection of the laboratory data (see Fig. 4.18a), it appears the criterion provides a substantial safety margin, given no soil loss in any stage of unidirectional or cyclic flow in a woven or nonwoven geotextile with $AOS/D_{85} \leq 2$.

4.5.2.4 Unified plot for AOS/D_{50}

The same database for all soil-geotextile combinations is also reported with reference to the alternate filter ratio of AOS/D_{50} (see Fig. 4.18b). Once again, the data for soil loss are plotted with the threshold range of $S/p_{i(0)}$ for onset of piping, and the data with no soil loss are plotted with a minimum and maximum range of $S/p_{i(0)}$ imposed in testing. Given the uniform gradation of the four soils examined in testing, the distribution $0.7 \leq AOS/D_{85} \leq 3.7$ is now expressed as $0.9 \leq AOS/D_{50} \leq 4.6$.

The same three characteristic responses to cyclic flow identified previously (in Fig. 4.18a) are again evident in Fig. 18b. At relatively large filter ratio ($AOS/D_{50} \geq 4.0$), the onset of piping at a very low value of $S/p_{i(0)} \leq 0.05$ implies a filter ratio that is close to filter incompatibility in unidirectional flow alone. In contrast, no soil loss is found with $AOS/D_{50} \leq 2.4$ for a woven geotextile, and with $AOS/D_{85} \leq 2.7$ for a nonwoven geotextile. The third range of filter ratio now yields values of $2.5 \leq AOS/D_{50} \leq 3.0$ that are likely to result in washout and increasing susceptibility to piping at higher seepage pressures, and a filter ratio $3.0 \leq AOS/D_{50} \leq 4.5$ that is likely to yield piping, again with a small change in filter ratio being very sensitive to hydromechanical influences.

The design criterion O_{95}/D_{50} or $AOS/D_{50} \leq 0.5$ is an alternate suggestion for applications of cyclic, pulsating or reversing flow (Luettich et al., 1992). From inspection of the laboratory data (see Fig. 4.18b), it appears this criterion also provides a substantial safety margin, given no soil loss in any stage of unidirectional or cyclic flow in a woven or nonwoven geotextile with $AOS/D_{50} \leq 2.5$. As before, the finding is appropriate to filtration of uniformly-graded soils.

4.5.3 Soil retention in cyclic flow

Analysis of the laboratory data identifies a general relation between normalized seepage pressure $S/p_{i(0)}$, and a normalized characteristic opening size of the geotextile AOS/D_n (Fig. 4.18c). It provides for a distinction between three domains of (i) no loss, (ii) washout and (iii) piping through the geotextile. The concept is predicated on a $S/p_{i(0)}$ characterizing the hydromechanical demand of the flow regime, and AOS/D_n describing the geometric resistance of the filter zone. The threshold boundary between the domains of no loss and washout appears governed mainly by AOS/D_n. In contrast, the threshold boundary between domains of washout and piping appears to be governed by both AOS/D_n and $S/p_{i(0)}$. In addition, transition from no loss to piping is very sensitive to a change of AOS/D_n when seepage pressure exceeds the initial mean effective stress ($S/p_{i(0)} > 1$).

The novel analytical framework is developed from results of a systematic laboratory study, involving head-control of one-dimensional seepage flow, with testing on reconstituted specimens of uniformly-graded soil. In this regard, it has been developed from a limited database of experience. Accordingly, it is recommended that confidence in the findings be established from applying the framework to explain the response of other soils and geotextiles reported in the literature.

4.6 Conclusions

A systematic experimental study was conducted on a broad range of filter ratios in the cyclic Gradient Ratio device. Filtration compatibility was evaluated for conditions of unidirectional and cyclic flow under controlled conditions of hydraulic gradient and effective stress, in order to understand the fundamental mechanism of geotextile-soil retention incompatibility. The findings relate to applications of woven and needle-punched nonwoven geotextiles with uniformly-graded base soil (fine sands, silty sand and coarse sandy silt). With reference to a characteristic opening size AOS and an indicative particle size D_n, the following conclusions are drawn:

- For unidirectional flow at $i_{av} < 10$, no unacceptable mass loss was observed for nonwoven geotextiles at $0.7 \leq AOS/D_{85} \leq 2.3$ ($0.9 \leq AOS/D_{50} \leq 2.7$), and woven geotextiles at $1.2 \leq AOS/D_{85} \leq 3.7$ ($1.3 \leq AOS/D_{50} \leq 4.6$). The finding implies retention compatibility;
- For cyclic flow at $i_{av} < 10$, with nonwoven geotextiles at $0.7 \leq AOS/D_{85} \leq 2.3$ ($0.9 \leq AOS/D_{50} \leq 2.7$), and with woven geotextiles at $1.2 \leq AOS/D_{85} \leq 2.0$ ($1.3 \leq AOS/D_{50} \leq 2.5$), there was again no unacceptable mass loss observed, which also implies retention compatibility.

However for woven geotextiles at $AOS/D_{85} > 2.0$, mass loss was observed in some cyclic loading conditions, which suggests:

- From interpretation of specimen volume change, a value $30 \leq m_{av} \leq 50$ g/m^2/100 cycles defines a threshold for soil arching at openings of the geotextile that describes the boundary between washout and onset of incompatibility;
- At $2.0 < AOS/D_{85} \leq 2.5$ ($2.5 \leq AOS/D_{50} \leq 3.0$), a transition occurs from retention compatible to retention sensitivity;
- At $2.5 < AOS/D_{85} \leq 3.7$ ($3.0 \leq AOS/D_{50} \leq 4.6$), soil retention is found very sensitive to loading conditions that are governed by hydraulic gradient, stress and wave period;

A hydromechanics-based interpretation is proposed to account for the combined influence of hydraulic gradient and effective stress. A normalized value of seepage pressure at the soil-geotextile interface ($S/p_{i(0)}$) appears to explain the nature of mass loss through pore size openings of the geotextile. For woven geotextiles, data analysis implies that T = 6 s governs the filtration compatibility, for the range 6 s ≤ T ≤ 120 s. The fundamental mechanism of soil retention, from interpretation based on the threshold range of m_{av} (g/m^2/100 cycles), for the test data at T = 6 s, suggests:

- A threshold boundary between no loss and washout is governed by AOS/D_n;
- A threshold boundary between washout and piping is governed by AOS/D_n and $S/p_{i(0)}$;
- Transition from no loss to piping is very sensitive to a change of AOS/D_n when seepage pressure exceeds the initial mean effective stress ($S/p_{i(0)} > 1$).

The findings of the laboratory experimental program on uniformly-graded soils indicate filtration compatibility in cyclic flow for a nonwoven geotextile at $AOS/D_{50} \leq 2.7$ or $AOS/D_{85} \leq 2.3$, and the onset of retention incompatibility for woven geotextile when $AOS/D_{50} > 2.5$ or $AOS/D_{85} > 2$. Accordingly, the design criterion $AOS/D_{50} \leq 1$ (Luettich et al., 1992), or alternatively $AOS/D_{85} \leq 0.5$ (Holtz et al., 1997; CFEM, 2006), appears to provide a very adequate margin of safety for applications involving uniformly graded soil.

The novel analytical framework is developed from results of a systematic laboratory study, involving head-control of one-dimensional seepage flow, with testing on reconstituted specimens of uniformly-graded soil. In this regard, it has been developed from a limited database of experience. Accordingly, it is recommended that confidence in the findings be established from applying the framework to explain the response of other soils and geotextiles reported in the literature.

Table 4.1 Properties of soils

Soil	D_{85} (μm)	D_{50} (μm)	44μm < D < 75μm (%)	C_u	$\gamma_{t,avg}$ (kN/m^3)	k_{av} (cm/s)	φ (degree)		
							50 kPa	25 kPa	< 10 kPa
A	180	160	-	1.5	18	0.020	39	41	45
B	150	130	-	1.5	18	0.014	39	41	45
C	106	85	30 †	1.8	18	0.007	38	40	44
D	80	65	80 †	1.4	18	0.004	37	40	43

† Non-plastic coarse silt

Table 4.2 Properties of geotextiles

Geotextile code	Fabric structure	AOS (O_{95}) (microns)	POA (%)	ASTM Permittivity (s^{-1})	Thickness (mm)	Unit mass (g/m^2)
NW1	NW-NP	60	N/A	2.5†	4.0	1200
NW2	NW-NP	75	N/A	1.0	4.0	500
NW3	NW-NP	80	N/A	8†	4.5	600
NW4	NW-NP	180	N/A	1.7	2.5	285
NW5	NW-NP	180	N/A	1.1	2.3	278
W1	W-M	210	4-6	0.3	N/A	190
W2	W-MT	300	4	0.5	N/A	170

Remarks: NW-NP = needle-punched nonwoven geotextile,

W = woven, M = monofilament, MT = multifilament

N/A = data not available, † = according to ISO standard

Table 4.3 Test combinations (and AOS/D_{85})

Geotextile (AOS) / Soil	NW1 (60μm)	NW2 (75μm)	NW3 (80μm)	NW4 (180μm)	NW5 (180μm)	W1 (210μm)	W2 (300μm)
A				T6 (1.0)		T6, T60 (1.2)	
B						T6, T60 (1.4)	T6, T60 (2.0)
C			T6 (0.7)	T6 (1.7)	T6 (1.7)	T6 (2.0)	**T6**, **T60**, T120 (2.8)
D	T6 (0.8)	T6 (0.9)		T6,T60 (2.3)	T6 (2.3)	**T6**,**T60**, T120 (2.6)	T6 (3.7)

Remarks: 1) Test code: A-W1-T6 describes soil A and geotextile W1, at T = 6 s.

2) Bold letter denotes a repeated test

Table 4.4 Summary of modified values of Gradient Ratio (GR_8) and qualitative observation of mass loss

<table>
<tr><th>Geotextile (AOS) / Soil</th><th>NW1 (60µm)</th><th>NW2 (75µm)</th><th>NW3 (80µm)</th><th>NW4 (180µm)</th><th>NW5 (180µm)</th><th colspan="3">W1 (210µm)</th><th colspan="3">W2 (300µm)</th></tr>
<tr><td>A</td><td></td><td></td><td></td><td>0.9
No</td><td></td><td colspan="3">1.2
No</td><td colspan="3"></td></tr>
<tr><td>B</td><td></td><td></td><td></td><td></td><td></td><td colspan="3">1.3
No</td><td colspan="3">1.1
No</td></tr>
<tr><td rowspan="2">C</td><td rowspan="2"></td><td rowspan="2"></td><td rowspan="2">1.7
No</td><td rowspan="2">0.9
No</td><td rowspan="2">0.9
No</td><td colspan="3" rowspan="2">1.5
No</td><td colspan="3">0.9 – 1.1</td></tr>
<tr><td>T6
Yes</td><td>T60
Yes</td><td>T120
Yes</td></tr>
<tr><td rowspan="2">D</td><td rowspan="2">1.4
No</td><td rowspan="2">0.9
No</td><td rowspan="2"></td><td rowspan="2">1.0
No</td><td rowspan="2">1.3
No</td><td colspan="3">1.0 - 1.3</td><td colspan="3" rowspan="2">0.7
T6
Yes</td></tr>
<tr><td>T6
Yes</td><td>T60
Yes</td><td>T120
Yes</td></tr>
</table>

Remarks: "No" denotes for no loss or negligible cumulative quantity (< 0.2 g ≈ 25 g/m^2)
Bold denotes test repeated

Table 4.5 Average mass loss (m_{av}) in CYC stages (g/m^2/100 cycles)

Test code		T=6s for confining stress, $p_{i(0)}$ (kPa)			T=60s for confining stress, $p_{i(0)}$ (kPa)			T=120s for confining stress, $p_{i(0)}$ (kPa)		
		23	14	3	23	14	3	23	14	3
C-W2	i_{av}	1.3	1.3	1.3	1.1	1.1	1.1	1.2	1.2	1.2
	m_{av}	52	51	48	21	24	38	0	0	11
	i_{av}	5.7	5.7	5.7	5.1	5.1	5.1	5.5	5.5	5.5
	m_{av}	97	93	100	43	41	71	14	23	26
	i_{av}	9.5	9.5	9.5	8.9	8.9	8.9	9.3	9.3	9.3
	m_{av}	116	129	164	84	76	127	20	34	57
C-W2 (repeated)	i_{av}	1.1	1.1	1.1	1.0	1.0	1.0			
	m_{av}	36	61	72	6	14	19	-	-	-
	i_{av}	5.1	5.1	5.1	5.2	5.2	5.2			
	m_{av}	71	74	74	24	38	41	-	-	-
	i_{av}	9.1	9.1	9.1	8.7	8.7	8.7			
	m_{av}	76	92	120	47	45	85	-	-	-
D-W1	i_{av}	1.1	1.1	1.1	1.2	1.2	1.2	1.1	1.1	1.1
	m_{av}	11	11	13	9	10	17	0	0	20
	i_{av}	5.2	5.2	5.2	5.3	5.3	5.3	5.4	5.4	5.4
	m_{av}	38	78	81	16	24	44	23	26	34
	i_{av}	9.5	9.5	9.5	9.4	9.4	9.4	9.6	9.6	9.6
	m_{av}	76	78	91	47	67	78	26	29	57
D-W1 (repeated)	i_{av}	1.1	1.1	1.1	1.0	1.0	1.0			
	m_{av}	15	27	30	21	34	43	-	-	-
	i_{av}	5.3	5.3	5.3	5.2	5.2	5.2			
	m_{av}	67	69	90	46	77	85	-	-	-
	i_{av}	9.7	9.7	9.7	9.7	9.7	9.7			
	m_{av}	103	116	143	97	104	131	-	-	-
D-W2	i_{av}	1.3	1.3	1.3						
	m_{av}	150	203	228	-	-	-	-	-	-
	i_{av}	5.4	5.4							
	m_{av}	299	316	-	-	-	-	-	-	-
	i_{av}									
	m_{av}	-	-	-	-	-	-	-	-	-

Remark: highlights denote data plotted in Figure 4.15

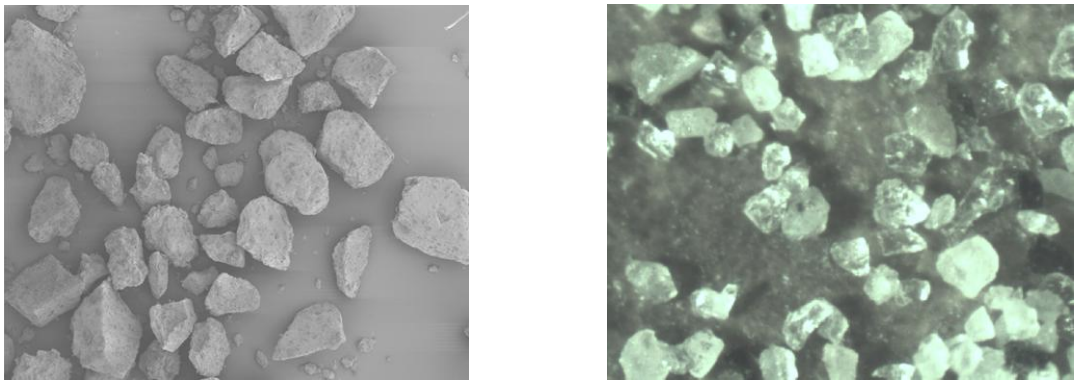

(a) (b)

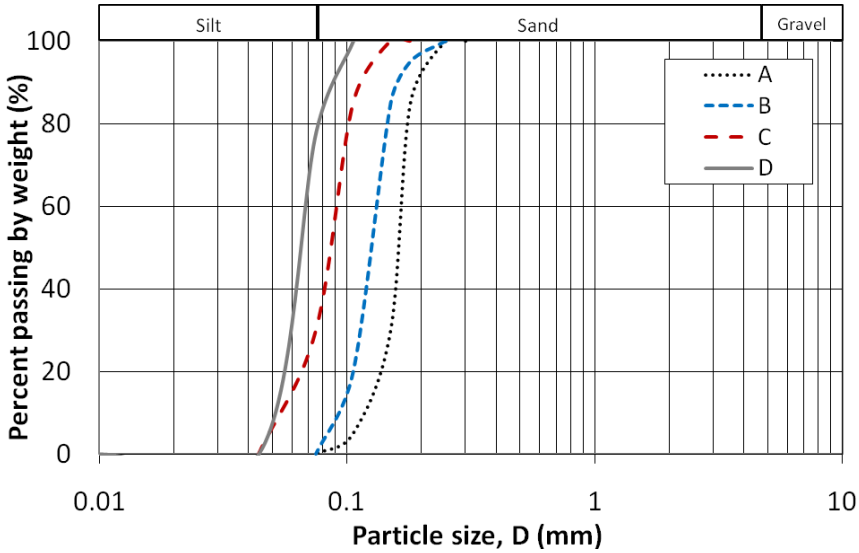

(c)

Figure 4.1 Soils: a) photograph of Fraser River sand; b) photograph of Alouette River sand; c) grain size distribution curves

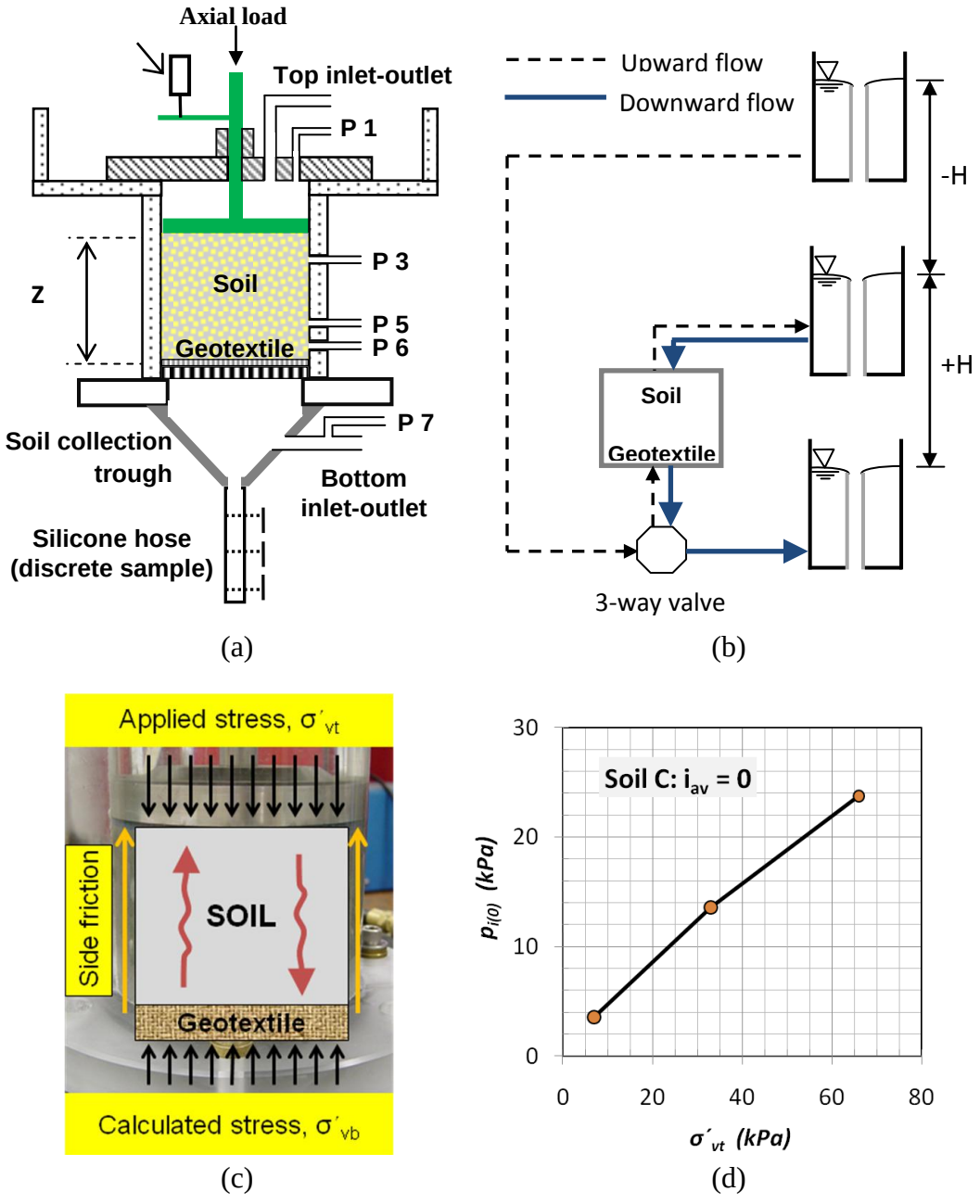

Figure 4.2 Cyclic Gradient Ratio device: a) permeameter; b) head-control system; c) schematic stress distribution; d) relation between top stress on the specimen and mean stress at the soil-geotextile interface (after Srikongsri and Fannin, see chapter 3)

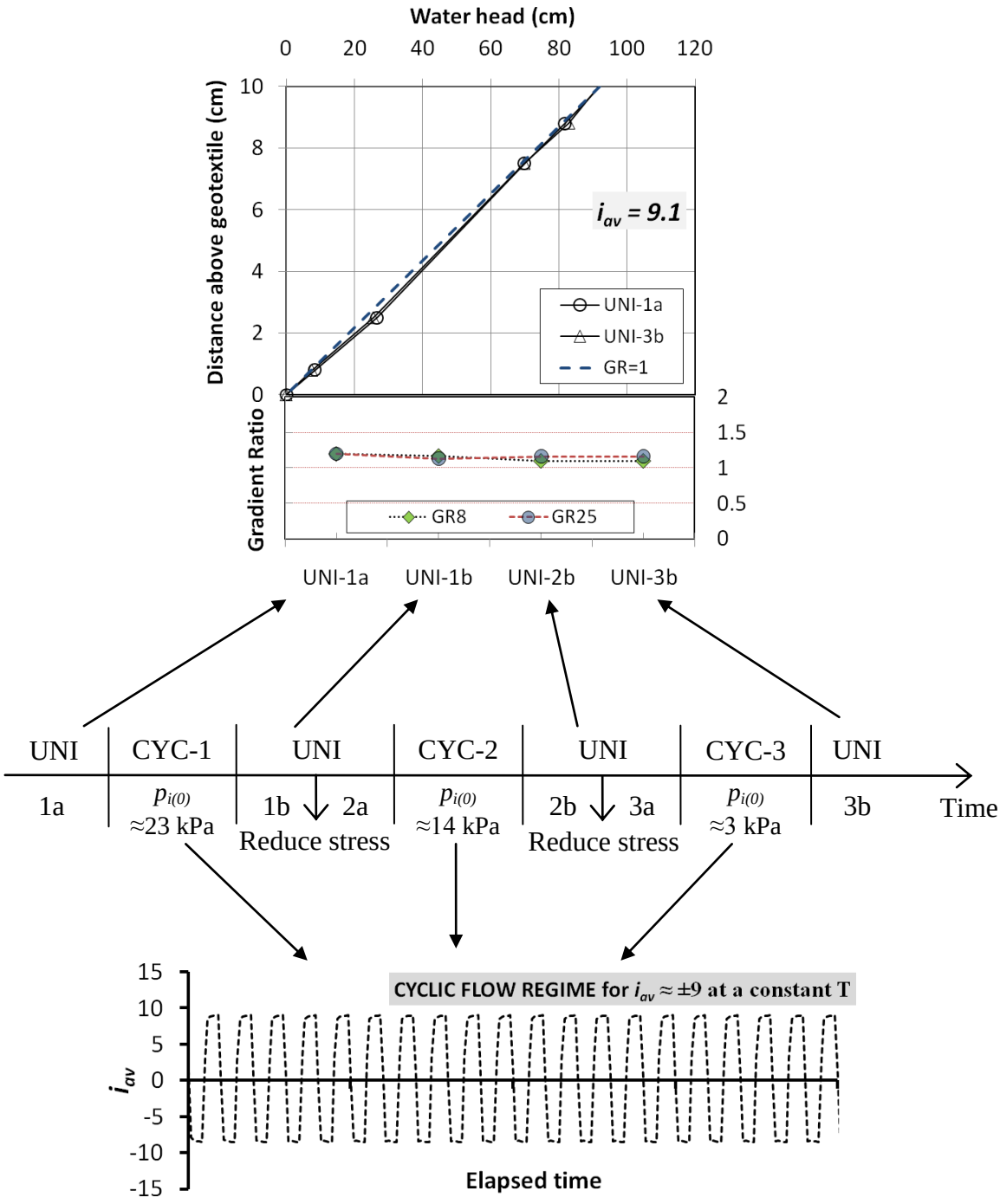

Figure 4.3 Multi-stage test procedure (test C-W2-T6) at $i_{av} \approx 9$

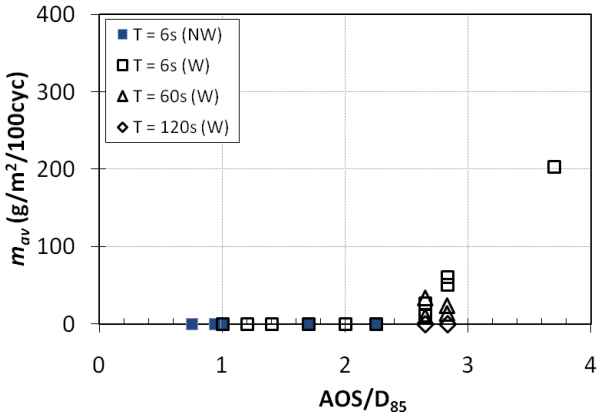

(a)

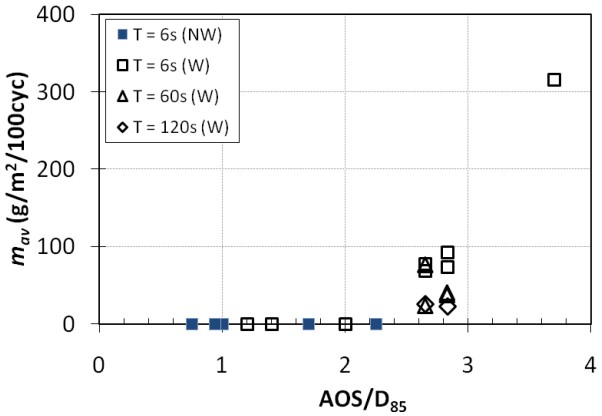

(b)

Figure 4.4 Relation between soil passing and filter ratio for stage CYC2: a) at i_{av} = 1 and b) at $i_{av} \approx 5$

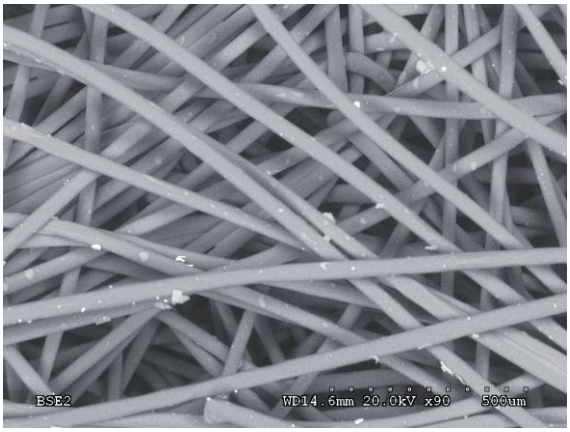

(a)

(b)

Figure 4.5 SEM images of needle-punched geotextiles: a) new NW4; b) tested NW4 (from D-NW4-T6); c) new NW5; d) tested NW5 (from D-NW5-T6)

(c)

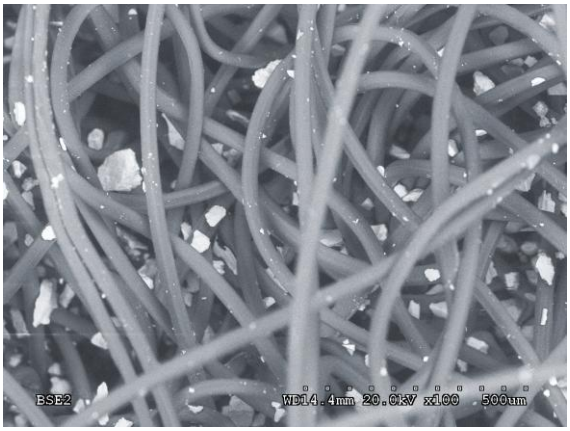

(d)

Figure 4.5 (continued)

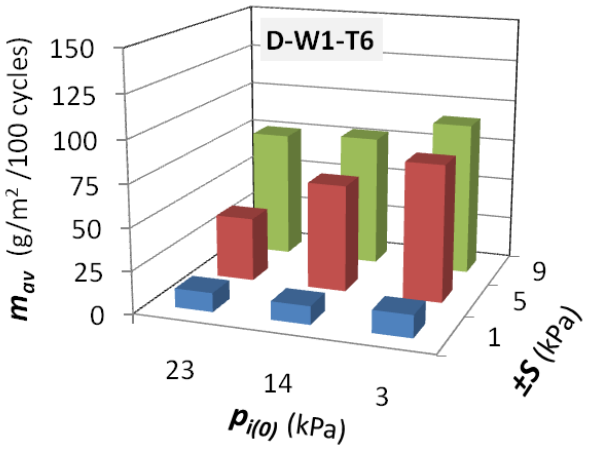

(a)

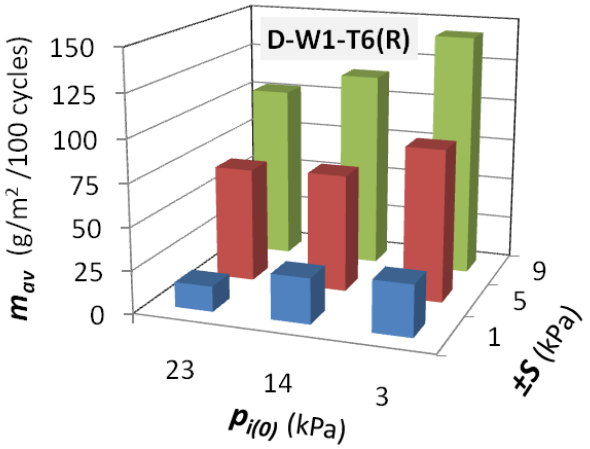

(b)

Figure 4.6 Mass loss at AOS/D_{85} = 2.6 for T = 6 s: a) test D-W1 and b) repeated D-W1

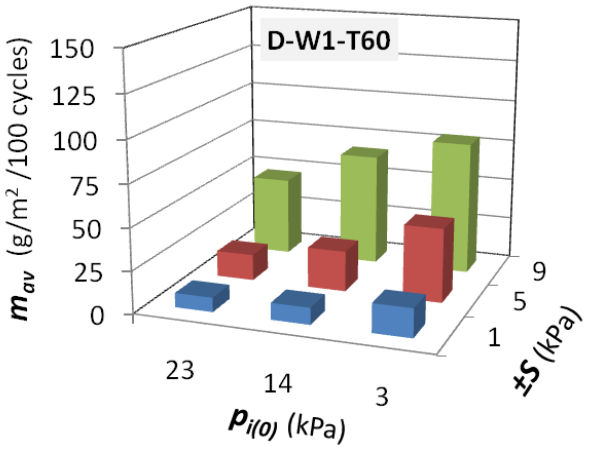

(a)

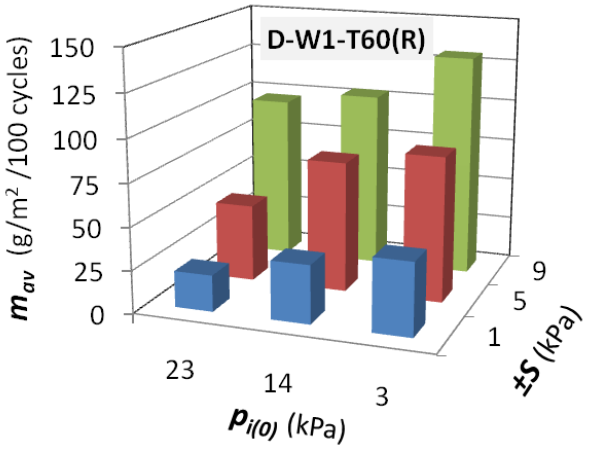

(b)

Figure 4.7 Mass loss at AOS/D_{85} = 2.6 for T = 60 s: a) test D-W1-T60 and b) repeated D-W1-T60

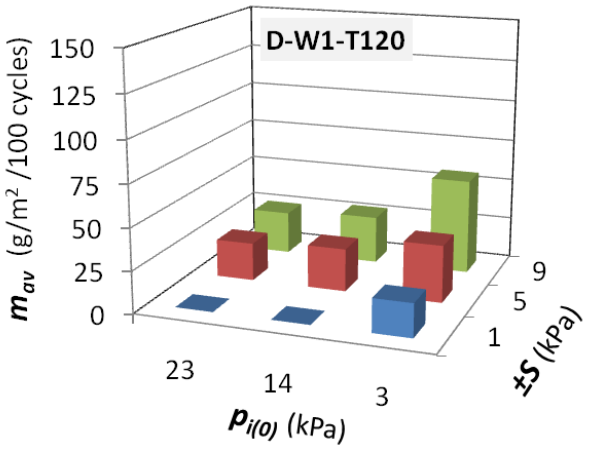

Figure 4.8 Mass loss at AOS/D_{85} = 2.6 for test D-W1-T120

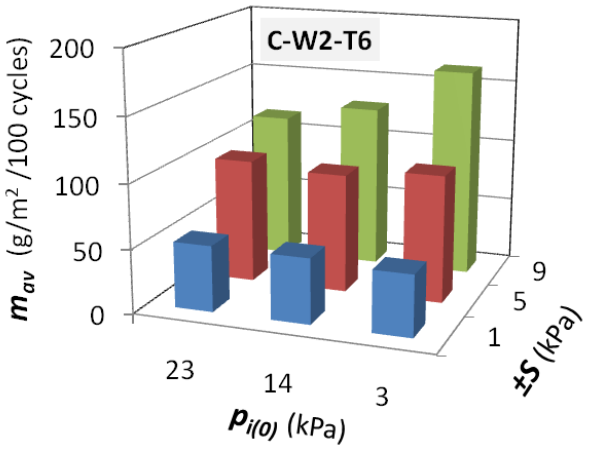

(a)

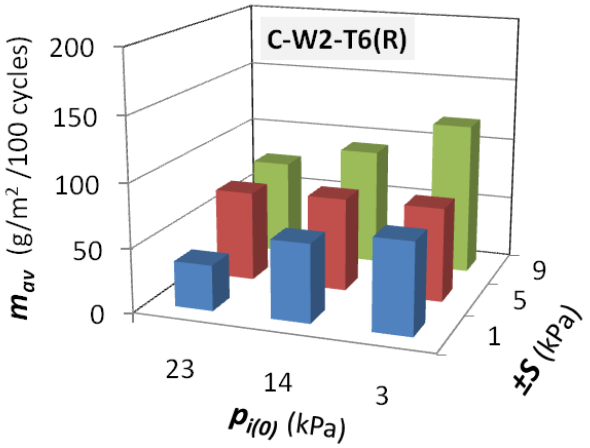

(b)

Figure 4.9 Mass loss at AOS/D_{85} = 2.8 for T = 6 s: a) test C-W2-T6 and b) repeated C-W2-T6

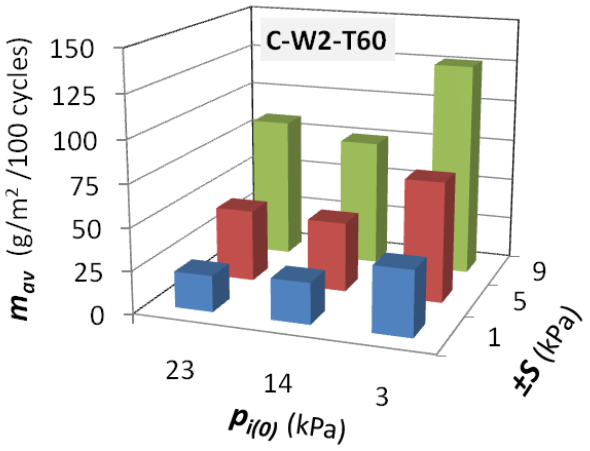

(a)

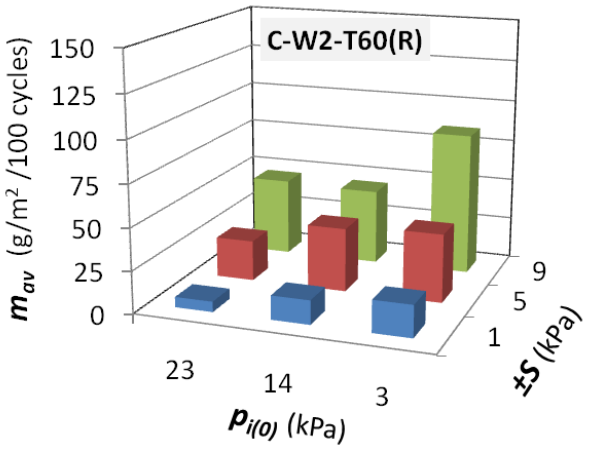

(b)

Figure 4.10 Mass loss at AOS/D_{85} = 2.8 for T = 60 s: a) test C-W2-T60 and b) repeated C-W2-T60

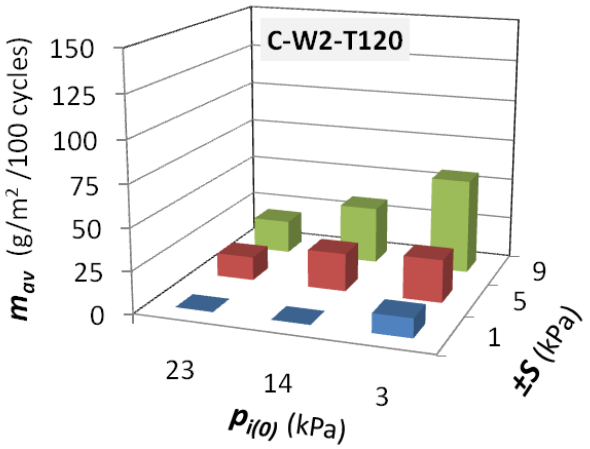

Figure 4.11 Mass loss at AOS/D_{85} = 2.8 for test C-W2-T120

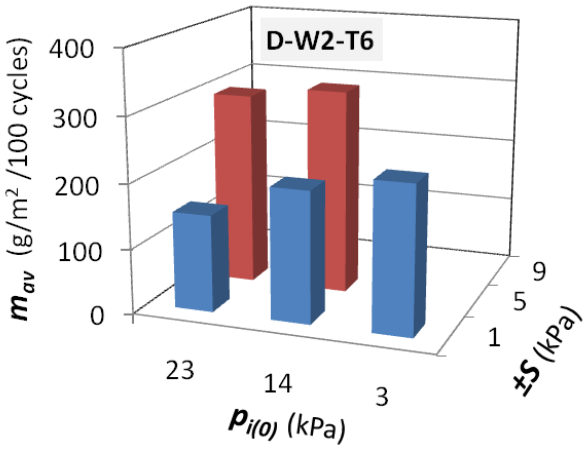

(a)

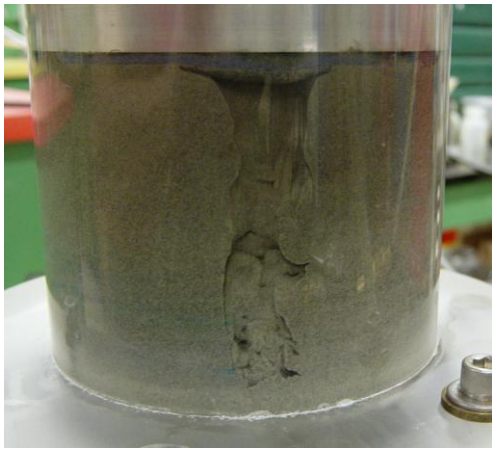

(b)

Figure 4.12 results at AOS/D_{85} = 3.7 for test D-W2-T6: a) mass loss; b) end-of-test photograph

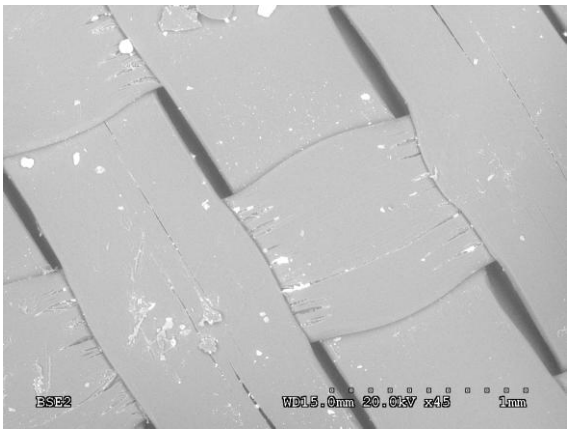

(a)

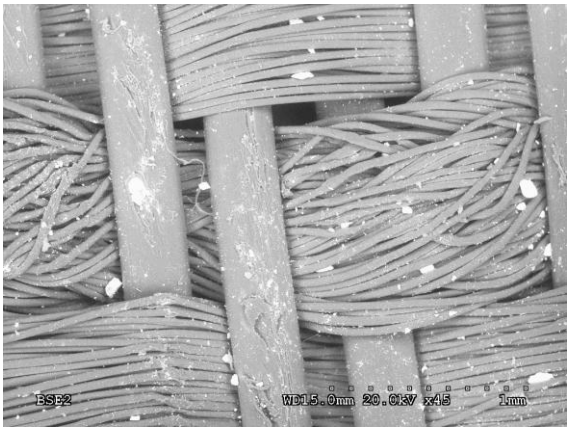

(b)

Figure 4.13 SEM images of woven geotextiles: a) tested W1 (from D-W1-T6); b) tested W2 (from C-W2-T6)

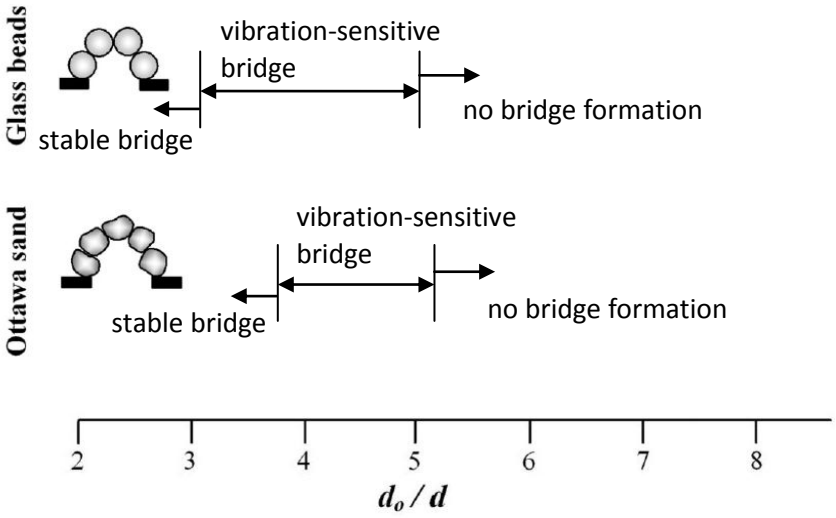

(a)

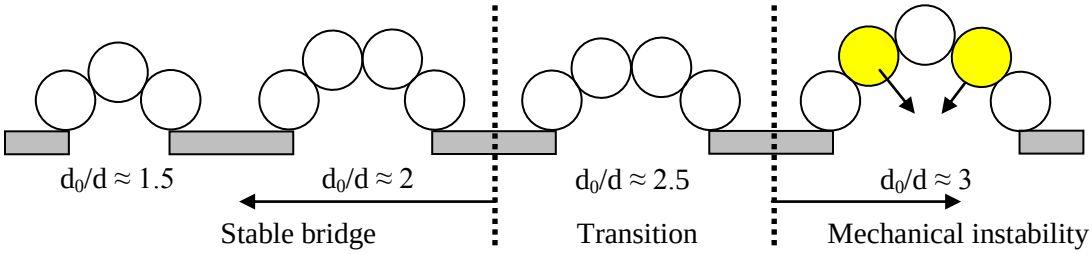

(b)

Figure 4.14 Particle bridging: a) effect of particle shape on vibration-based stability (modified from Valdes and Santamarina, 2008); b) conceptual regime for mechanical instability of spherical particles

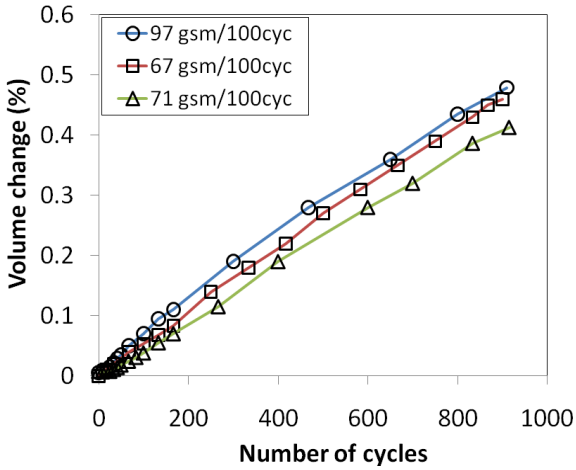

(a)

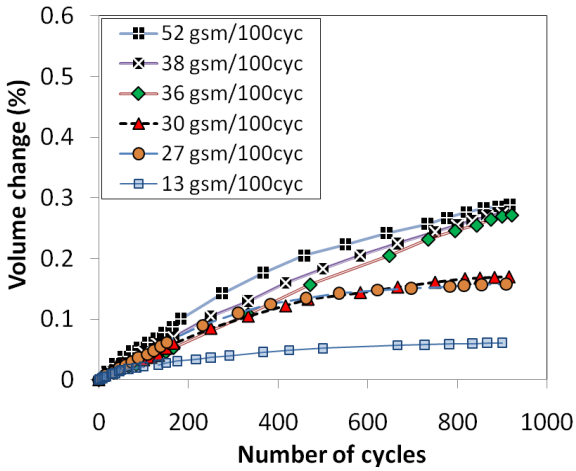

(b)

Figure 4.15 Inspection of retention compatibility (data from tests D-W1-T6, D-W1-T6-R, C-W2-T6 and C-W2-T6-R): a) piping; b) washout

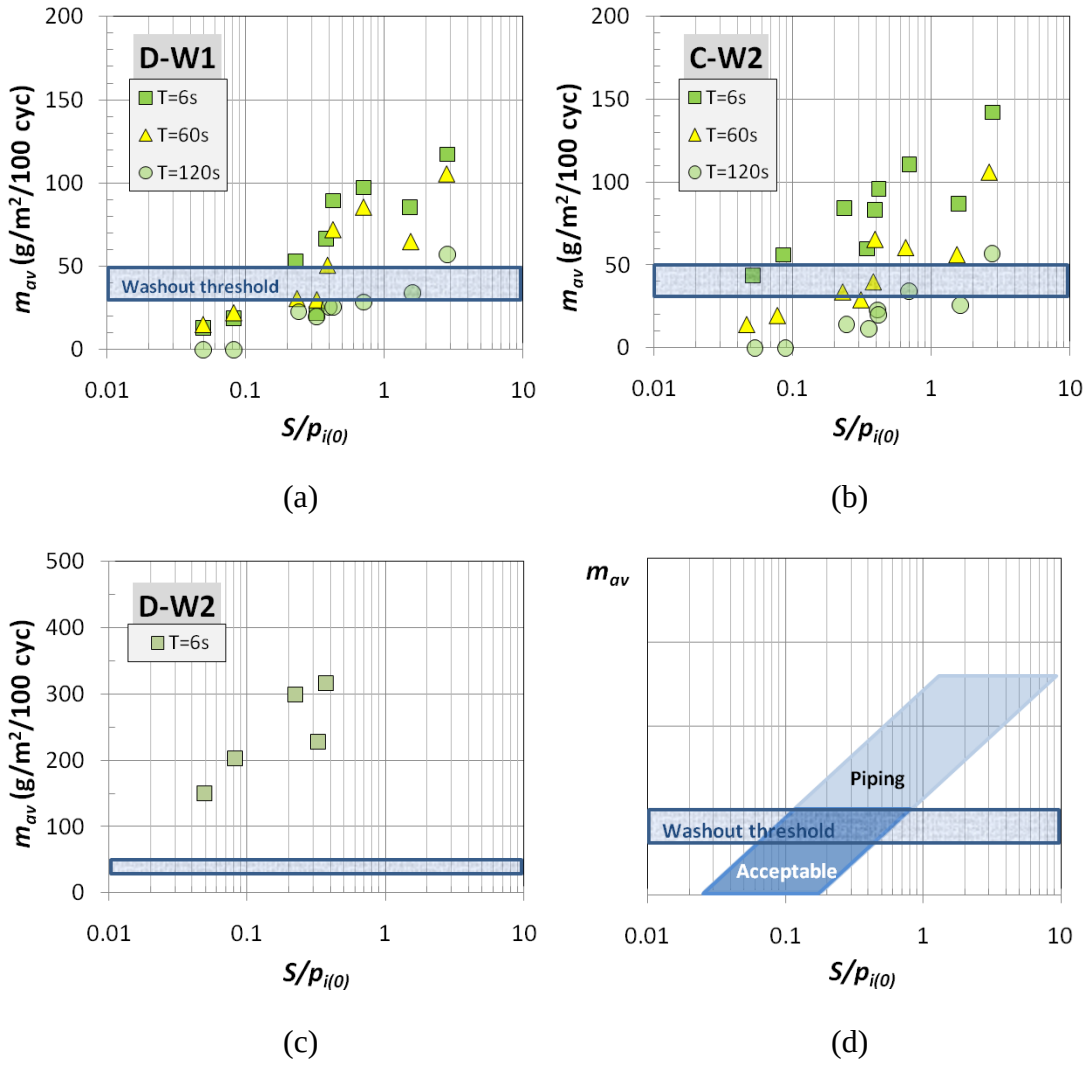

Figure 4.16 Onset of piping: a) soil D - geotextile W1; b) soil C – geotextile W2; c) soil D – geotextile W2; d) concept of hydromechanical stability

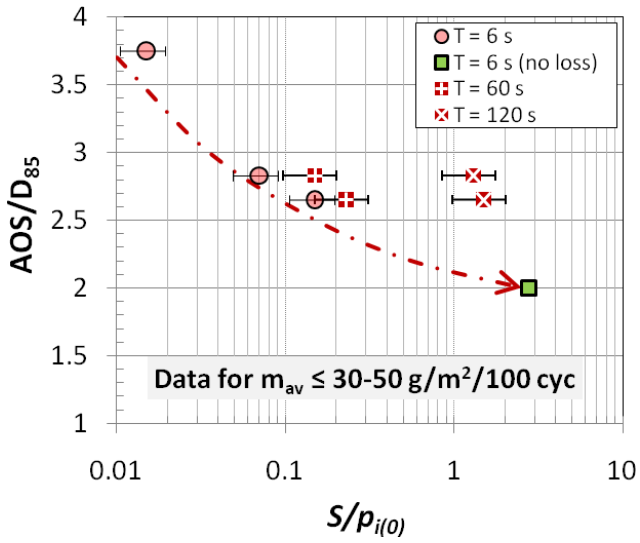

Figure 4.17 Hydromechanical influences on soil retention in cyclic flow for woven geotextiles (data for T = 6 s from Fig. 4.16a, 4.16b, 4.16c and test C-W1-T6)

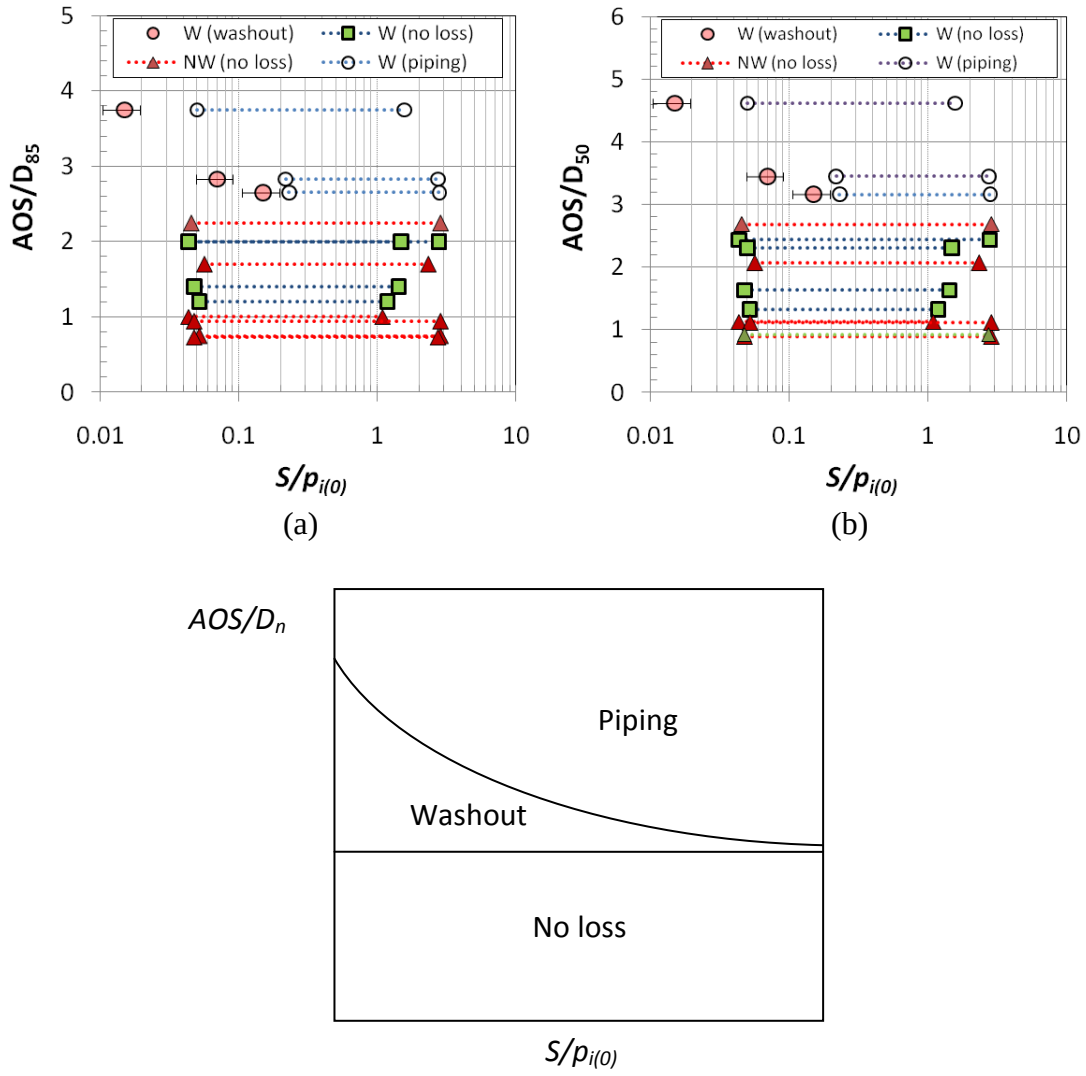

Figure 4.18 Retention compatibility for uniformly-graded soil and wave period T = 6 s: a) AOS/D_{85} and b) AOS/D_{50}; c) characteristic zone of soil retention

4.7 References

Canadian Geotechnical Society (2006). Canadian Foundation Engineering Manual, 4th edition, BiTech Publishers Ltd.

Cazzuffi, D. A., Mazzucato, A., Moraci, N., & Tondello, M. (1999). A new test apparatus for the study of geotextiles behaviour as filters in unsteady flow conditions: relevance and use. *Geotextiles and Geomembranes* **17**, No. 5-6, 313 - 329.

Chew, S. H., Zhao, Z. K., Karunaratne, G. P., Tan, S. A, Delmas, Ph., & Loke, K. H. (2000). Revetment geotextile filter subjected to cyclic wave loading. *Proceedings of Geo-Denver 2000*, Denver, CO, USA, pp. 162 – 175.

Christopher, B.R., and Holtz, R.D. (1985), Geotextile engineering manual, *Report No. FHWA-TS-86/203*, Federal Highway Administration, D.C., USA, 1044 p.

Fannin, R.J. (2007). Chapter 6: The use of geosynthetics as filters. *Geosynthetics in Civil Engineering*. Woodhead Publishing, Cambridge, UK, 295p.

Hameiri, A. (2000). Soil geotextile filtration behavior under dynamic conditions of vibration and cyclic flow. PhD Thesis, University of British Columbia, British Columbia, Canada, 270p.

Hameiri, A. & Fannin, R. J. (2002). A cyclic gradient ratio test device. *ASTM Geotechnical Testing Journal*, **39**, No.2, 266-276.

Hawley, R. (2001). Filtration performance of geotextiles in cyclic flow conditions. MASc Thesis, University of British Columbia, Vancouver, B.C., Canada, 141p.

Heerten, G. (1982). Dimensioning the filtration properties of geotextiles considering long-term conditions. *Proceedings of 2nd international conference on geotextiles*, Las Vegas, NV, USA, pp. 115 – 20

Holtz, R.D, Christopher, B.R., and Berg, R.R. (1997). *Geosynthetic Engineering*. BiTech Publishers, Richmond, BC, Canada, 452 p.

Indraratna, B & Vafai, F (1997). Analytical model for particle migration within base soil-filter system, *Journal of Geotechnical and Geoenvironmental Engineering*, **123**, No. 2, 100-109.

Indraratna, B & Radampola, S. (2002). Analysis of Critical Hydraulic Gradient for Particle Movement in Filtration. *Journal of Geotechnical and Geoenvironmental Engineering*, **128**, No. 4, 347-350.

Luettich, S.M., Giroud, J.P., and Bachus, R.C. (1992). Geotextile filter design guide. *Geotextiles and Geomembranes*, ***11***, 355 - 370.

Pilarczyk, K. W. (2000). Geosynthetics and geosystem in hydraulic and coastal engineering. A.A. Balkema, Rotterdam, The Netherlands, 913 p.

Reddi, L. N. (2003). Seepage in soils principles and applications. John Wiley & Sons, NJ, USA, 402 p.

Shukla, S. K., Yin, J-H. (2006). *Fundamentals of geosynthetic engineering*. Taylor & Francis/Balkema, Natherlands, 410 p.

Srikongsri, A. and Fannin, R.J. (2009). Retention capacity of geotextile filters in cyclic flow. *Proceedings of Geosynthetics 2009*, Salt Lake City, UT, USA, pp. 498-508.

Srikongsri, A. and Fannin, R.J. (2010a). Soil-geotextile compatibility testing in cyclic flow. *Manuscript draft*, see Chapter 2.

Srikongsri, A. and Fannin, R.J. (2010b). Influences of testing methodology on soil-geotextile compatibility in cyclic flow using rigid-wall permeameters. *Manuscript draft*, see Chapter 3.

Valdes, J. R. and Satamarina, J. C. (2008). Clogging: bridge formation and vibration-based destabilization. *Canadian Geotechnical Journal*. **45**, No. 2, 177-184.

5 Retention Criteria for Geotextile Filter in Cyclic Flow[4]

5.1 Outline

A hydromechanical framework, for retention compatibility of soil-geotextile filters in cyclic flow, is evaluated through comparison with (i) laboratory test data from three independent studies and (ii) field performance data from four bank and coastal protection sites. The framework is found to distinguish between filter compatibility, and conditions leading to onset of a piping action through the geotextile. The AOS/D_{85} filter ratio appears more suitable than AOS/D_{50} as an indicative particle size for design. For a woven geotextile, the onset of piping occurs at $2 \leq AOS/D_{85} \leq 2.5$. In design for soil retention involving cyclic or dynamic flow, it is recommended that $AOS \leq D_{85}$ in order to achieve an adequate margin of safety. The recommendation is empirical, and appropriate for a uniformly-graded non-plastic base soil that is internally stable.

[4] A version of this chapter will be submitted for publication. Srikongsri, A., Fannin, R. J. (2010). Retention criteria for geotextile filter in cyclic flow.

5.2 Introduction

The nature of dynamic flow, especially cyclic flow reversal, is believed to reduce the inherent margin of safety that is provided by retention criteria intended for applications of unidirectional flow. For example, if a criterion for unidirectional flow requires $O_F < BD_i$, where O_F is a characteristic pore size opening of the geotextile, B is a constant (normally $\approx 1 - 2$) and D_i is an indicative particle size of the base soil, then the criterion for cyclic flow may simply take the form of $O_F < 0.5BD_i$. Accordingly, Luettich et al. (1992) suggests $(O_F = O_{95})/(D_i = D_{50}) < 1$ and Holtz et al. (1997) suggests $(O_F = O_{95})/(D_i = D_{85}) < 0.5$. These criteria are currently used in the USA and the latter criterion is also adopted for recommendation in the current edition of the Canadian Foundation Engineering Manual. In applying this concept, the belief is that O_F retains D_i and, if D_i retains the remainder of particles in the gradation curve, then filtration compatibility is achieved. Undoubtedly, the concept works for a certain range of soil gradations with relatively coarse grains. However, when the base soil to be protected has a relatively small D_i, for example a fine sand or silt, then a geotextile may simply be disqualified as a candidate filter medium because the smallest available O_F cannot satisfy the design filter ratio O_F/D_i (Klein Breteler and Verhey, 1990; Klein Breteler et al. 1994). In contrast, Dutch experience with geotextiles in filtration applications for coastal defense structures using an open filter (i.e. $O_F/D_i > 1$), yields a different approach for conditions of cyclic flow wherein $(O_F = O_{98})/(D_i = D_{85}) < 1$ to 2,

for cohesionless soil with C_u < 6 to 10 (Pilarczyk, 2000). In addition, the current Dutch design practice also recommends the criterion $(O_F = O_{90})/(D_i = D_{90}) \leq 1$, for an internally stable base soil with D_{40} > 60 μm (modified from Heerten, 1982 as reported by Pilarczyk, 2000). Note that the findings of Heerten (1982) have been briefly mentioned in Srikongsri and Fannin (2010b: see chapter 4). These two criteria are provided in a revetment design manual, which can be found at the website of the Expertise Network for Flood Protection (Expertise Netwerk Waterveiligheid, ENW) using the link:

http://www.tawinfo.nl/engels/downloads/DesignRevetments.pdf.

A hydromechanical framework has been proposed for retention compatibility. It relates filter ratio (AOS/D_{50} or AOS/D_{85}) and normalized seepage pressure ($S/p_{i(0)}$), based on laboratory test data from a systematic study of soil-geotextile compatibility in cyclic flow (Srikongsri and Fannin, (2010b: see chapter 4). Seepage pressure (S) is calculated from:

$$S = i_{av}\gamma_w Z \tag{1}$$

where i_{av} is average hydraulic gradient across the soil specimen, γ_w is unit weight of water and Z is specimen length. In a rigid-wall permeameter, the initial mean effective

stress ($p_{i(0)}$) or "confining stress" is deduced from the vertical effective stress applied to the top of the specimen (Srikongsri and Fannin, (2010a: see chapter 3), which is calculated as:

$$p_{i(0)} = \sigma'_{vb(0)} (1+2K_0)/3 \quad (2)$$

where $\sigma'_{vb(0)}$ is vertical effective stress at the geotextile and K_0 is an at-rest coefficient of lateral stress.

A schematic illustration of the hydromechanical framework (see Fig. 5.1) depicts the general experimental finding that onset of retention instability in a woven geotextile occurs at $2.4 < AOS/D_{50}$ or $2 < AOS/D_{85}$. The fact that needle-punched nonwoven geotextiles were found retention compatible at $AOS/D_{50} \leq 2.7$ or $AOS/D_{85} \leq 2.3$ in the same experiments lends additional confidence to the finding. Consider now the criteria of Luettich et al. (1992) in Fig. 5.1a and Holtz et al. (1997) in Fig. 5.1b, which both locate in the lower part of the "no loss" zone in the hydromechanical framework and are likely overly conservative. Consider also the more general Dutch approach represented in Fig. 5.1b, assuming $O_{98} \approx AOS$. Again, the hydromechanical framework appears reasonably supportive of this approach at relatively low values of normalized seepage pressure. At higher values of $S/p_{i(0)}$, for example at $S/p_{i(0)} \geq 1$ (see Fig. 5.1b), the upper threshold of $(O_{98} \approx AOS)/D_{85} < 2$ provides for a little or no margin of safety. Therefore, it seems prudent to undertake an independent evaluation

of the proposed hydromechanical framework for retention compatibility in cyclic flow through comparison with (i) other published laboratory test data and (ii) field performance data reported in the literature.

Notable laboratory studies on the nature of soil-geotextile compatibility in cyclic flow are reported by Cazzuffi et al. (1999), Chew et al. (2000) and Hawley (2001). Given the limited test data used in support of the findings of Srikongsri and Fannin (2010b: chapter 4), a comparison with test data from three additional laboratory studies is of tremendous benefit. In addition, field performance data reported by Mannsbart and Christopher (1997) from four bank and coastal protection sites enable further evaluation of the hydromechanical framework, and address the confidence with which it can be considered for use in engineering practice.

5.3 Select laboratory test data

Grain size distribution curves of five soils from three experimental studies are shown in Figure 5.2. Three soils, namely Fraser River Sand (FS), Mine Waste Tailings (MT) and Port Coquitlam Sand (PC) are examined by Hawley (2001): they were used in laboratory testing at UBC, in work to evaluate filtration compatibility of two needle-punched nonwoven geotextiles and five woven geotextiles, in an investigation that preceded the current study. One soil, Beach sand (BS), was tested against a nonwoven

and a woven geotextile, in work to examine the influence of hydraulic gradient and effective stress in an investigation by Cazzuffi et al. (1999). Finally, tests on sand used for reclamation purposes (RS) are reported from an investigation by Chew et al. (2000), involving one nonwoven geotextile and one woven geotextile. Notwithstanding the fact that all three test programs invoked different test methods, the results are still useful for purposes of evaluating the proposed hydromechanical framework. All five gradation curves from the three separate investigations are narrowly graded ($Cu \leq 6$), and deemed internally stable soil according to the method of Kenney and Lau (1985 and 1986) and Li and Fannin (2008). Properties of the soils are summarized in Table 5.1.

The characteristic pore size opening of a geotextile may be established by a dry sieving technique (Apparent Opening Size (AOS), according to ASTM D-4751). However, there are also a number of different standardized methods used in various countries that involve techniques of wet, or alternatively hydrodynamic sieving, that define a similar, but not identical, value of O_{95} (see Table 5.2). For a woven geotextile, the index values of opening size are believed reasonably comparable. In contrast, they can be significantly different for a nonwoven geotextile. Typically, the AOS value is found to be larger than those obtained from wet or hydrodynamic sieving (Bathia et al. 1996).

5.3.1 Hawley (2001)

The study was undertaken at UBC in the same cyclic gradient ratio test device used by Srikongsri and Fannin (2010a: see chapter 3), to examine the filtration compatibility of three sands and seven geotextiles. The resulting database comprises twenty one test combinations examining a filter ratio in the range $0.8 < AOS/D_{50} < 3.4$ and $0.6 < AOS/D_{85} < 2.8$, for two needle-punched nonwoven and five woven geotextiles. Tests were conducted at only one average hydraulic gradient (i_{av}) of approximately 4. Test variables examined comprise vertical effective stress on the top surface of the soil specimen (σ_{vt} = 25 and 0 kPa, namely unloaded), and the wave period of cyclic flow reversal (T = 50 or 10 s). The test sequence involved a relatively long stage of cyclic flow at T = 50 s (1080 cycles) that was followed by a shorter stage at T = 10 s (260 cycles), whereupon the normal stress was reduced from 25 kPa to zero, and the shorter stage at T = 10 s then repeated (260 cycles). Each cyclic stage was preceded and followed by a stage of unidirectional flow.

Interpreting data in the hydromechanical framework requires the applied top stress and the imposed hydraulic gradient to be expressed as a value of $S/p_{i(0)}$. Srikongsri and Fannin (2010b: see chapter 4) established a relation between σ_{vt} and $p_{i(0)}$ for a uniformly-graded fine sand: this relation is assumed, for purposes of analysis, to apply for soils FR, MT and PC. Accordingly, the combinations of $i_{av} \approx 4$ at σ_{vt} = 25 kPa and 0 kPa yield values of $S/p_{i(0)}$ = 0.37 and 4.2, respectively.

The combination of soil type FS and seven geotextiles in the range $1 < AOS/D_{50} < 2.2$ or $0.6 < AOS/D_{85} < 1.8$ was reported as retention compatible with essentially no soil loss through the geotextile (Hawley, 2001). Soil MT is also reported compatible with no loss in the range $AOS/D_{50} < 2.4$ or $AOS/D_{85} < 1.5$, but evidence of some mass loss was reported in the range $2.4 \leq AOS/D_{50} \leq 3.4$ or $1.5 \leq AOS/D_{85} \leq 2.1$ (see Table 5.3). In the latter case, the losses were deemed necessary for development of filter stability and are not believed to represent retention incompatibility of the soil-geotextile combination: it was concluded that all of these test combinations were also stable. A companion analysis of the data is made using AOS/D_{50} (see Fig. 5.3a) and AOS/D_{85} (see Fig. 5.3b), which enables comparison with the hydromechanical framework developed in this study. Given the observed filtration compatibility that was common to all test combinations, the trend appears to be better explained by the AOS/D_{85} value rather than the AOS/D_{50} value. The filter ratio $AOS/D_{85} = 2.1$ (test MT-G60W, Table 5.3) at which washout occurred appears to agree very well with that anticipated by the hydromechanical framework (see Fig. 5.3b and Fig. 5.1b).

Soil PC was reported stable for a filter ratio $AOS/D_{50} \leq 1.7$ or $AOS/D_{85} \leq 1.4$. However, results of tests on two woven geotextiles at $AOS/D_{50} = 2.4$ or $AOS/D_{85} = 2.0$ (tests PC-G43aW and PC-G43bW) exhibited washout at the stage with σ_{vt} = 25 kPa at T = 10 s and subsequently exhibited a piping failure that involved excessive amounts of mass loss (see Table 5.3) in the test stage with σ_{vt} = 0 kPa, for which

$S/p_{i(0)}$ = 4.2 (see Fig. 5.4). Additionally, one planned test involving a woven geotextile at AOS/D_{50} = 3.3 or AOS/D_{85} = 2.8 exhibited an excessive soil loss through the geotextile during reconstitution of the soil specimen by water pluviation against the geotextile, which it is clearly a case of retention incompatible. For plotting purposes, the data point for this latter soil-geotextile combination is nominally located at $S/p_{i(0)}$ = 0.01, which places it in the washout zone of the framework (see Fig. 5.4). Generally, the piping response with soil PC is found at AOS/D_{50} and AOS/D_{85} values that plot at or below the curve-linear relation postulated from the current study, which is based on testing soil of uniform gradation. The response is attributed to the relatively broad gradation curve of the PC soil compared to the others (see Table 1) yielding a different bridging structure at the soil-geotextile interface, and one that may be more susceptible to disturbance by cyclic flow. The grain size distribution reported for soil passing through the G43aW and G43bW geotextile (AOS = 425 μm, see Table 5.2) was predominantly of fines fraction less than 70 μm (see Fig. 5.5).

5.3.2 Cazzuffi et al. (1999)

The data of Cazzuffi et al. (1999) described results from cyclic flow tests on one soil, a uniform fine sand (D_{85} = 0.2 mm and D_{50} = 0.14 mm, C_u = 1.4 and no presence of fines, see Fig. 5.2), in combination with two types of geotextile, a nonwoven (O_{95} = 0.16 mm) or a woven (O_{95} = 0.44 mm) geotextile. The laboratory tests were performed in a bi-directional flow apparatus, with a permeameter that accommodates a

cylindrical specimen 300 mm in diameter and 400 mm long. In testing, the influence of vertical effective stress at the soil-geotextile interface was examined the range 4 to 154 kPa, for a hydraulic gradient in the range 3 to 16, and an unspecified wave period in the range 2 to 20 s, for a test duration of typically 1500 cycles.

At a filter ratio O_{95}/D_{50} = 1.1 or O_{95}/D_{85} = 0.8, for the nonwoven geotextile, a negligible washout less than 10 g/m^2/100 cycles was reported and the combination was deemed retention compatible (see Table 5.4). At a filter ratio O_{95}/D_{50} = 3.1 or O_{95}/D_{85} = 2.2, for the woven geotextile, the response was more subtle: mass loss for this BS-G44W test was negligible at σ_{vt} ≈ 50 kPa, but was reported to increase dramatically when the top stress was reduced to zero (only self weight applies to the geeotextile) yielding an approximate $p_{i(0} = 2.4$ kPa (see Table 5.4, for an assumed $K_0 = 0.42$).

More specifically, consider the mass loss of less than 30 - 50 g/m^2/100 cycles at S = 11.7 kPa and $p_{i(0)} = 2.4$ kPa, that increased to a mass loss of 323 g/m^2/100 cycles when S was increased to 19.6 kPa. The finding suggests the onset of retention incompatibility was triggered at $4.9 < S/p_{i(0)} < 8.2$ (see Table 5.4). A separate presentation of the data is made using AOS/D_{50} (see Fig. 5.6a) and AOS/D_{85} (see Fig. 5.6b), which enables comparison with the hydromechanical framework developed in the current study. Given the filtration compatibility that was common to all tests except one, once again the trend appears to be moderately better explained by the AOS/D_{85} value rather than the AOS/D_{50} value.

5.3.3 Chew et al. (2000)

The testing of Chew et al. (2000) was performed using a slightly modified version of the apparatus developed by Cazzuffi et al. (1999). The primary objective of the work was to observe the influence of wave period in the range T = 2 to 15 s. The tests were performed at σ_{vt} = 113 kPa and a maximum hydraulic gradient of 26, for a typical test duration of 2000 to 2500 flow cycles. The data describe results from cyclic flow tests on one soil, a coarse sand (D_{85} = 2 mm and D_{50} = 0.9 mm, C_u = 3.3 and fines < 2%, see Fig. 5.2), in combination with two types of geotextile, a nonwoven (O_{95} = 0.1 mm) or a woven (O_{95} = 0.47 mm) geotextile. At a filter ratio O_{95}/D_{50} = 0.1 or O_{95}/D_{85} = 0.05, for the nonwoven geotextile (see Fig. 5.6), a negligible washout was reported and the combination was deemed retention compatible. Likewise, the same conclusion was drawn for the woven geotextile (see Fig. 5.6b), at filter ratio O_{95}/D_{50} = 0.52 or O_{95}/D_{85} = 0.24.

The values of filter ratio AOS/D_{50} and AOS/D_{85} examined by Chew et al. (2000) are the lowest of all test data compared to evaluate the proposed hydromechanical framework, and are found to be in good agreement with it.

5.4 Field data

Mannsbart and Christopher (1997) report on the long-term field performance of geotextiles used as a filter in coastal and bank protection applications. They provide schematic drawings, together with information on the grain size distribution curve of each base soil, material properties of each geotextile and describe, albeit in very general terms, the severity of the hydraulic action at each site location. Filtration compatibility was considered satisfied at all sites, based on the fact that no evidence was found to indicate concern either for clogging or piping activity over the service life of the installation at that time. Taken collectively, it yields a sufficiently comprehensive record to allow for comparison with the proposed hydromechanical framework. All of the geotextiles were needle-punched nonwoven fabrics, samples of which were exhumed for forensic analysis. Pore size of the fabric was reported with reference to values of O_{90}, based on a wet sieving technique, and therefore values of AOS were sourced from the manufacturer's technical database for the purposes of this study (see Table 5.5a), enabling determination of the corresponding filter ratio AOS/D_{50} and AOS/D_{85}.

From the drawings provided for each site (see, for example, Fig. 5.7), an approximate value of initial confining stress ($p_{i(0)}$) at the soil-geotextile interface was calculated based on thickness of the overlying armor layer (assuming a unit weight of 15 kN/m^3,

and K_0 = 0.42). An approximate value of seepage pressure at the soil-geotextile interface was established indirectly. Wave-generated pressure on the armor layer is a function of wave characteristic and geometry of the slope. It is a stochastic phenomenon. This value may be assumed equal to a seepage pressure (S) for the purpose of defining $S/p_{i(0)}$ at particular field location. Pilarczyk (2000) proposed a simplified relation between the maximum value (P_{max}) of wave-generated pressure and a significant wave height (H_s):

$$S = P_{\max} = A_0 \gamma_w H_s \tag{3}$$

where A_0 is an empirical factor which may be obtained by experiments, γ_w is the unit weight of water, and H_s is the significant wave height or design value of wave height.

The value of A_0 is a function of wave characteristic that accounts for the influence of both hydrostatic and hydrodynamic components of wave energy. Pilarczyk (2000) suggested, for calculation purposes, that the value of A_0 can be assumed equal to 2 as an approximation for a value of P_{max} within the armor stone; in a filter layer (the soil-geotextile interface), the wave impact will be partly damped by the armor stone, in which case a value of $A_0/2$ is suggested.

A value of H_s is not reported for each site in the work of Mannsbart and Christopher (1997). However, it is possible to obtain an approximate value of H_s by indirect means, knowing the characteristic size (or mass) of the armor stone. The Hudson formula (USACoE, 1984) relates H_s to mass of the median rock size (W_{50}):

$$W_{50} = \frac{w_r H_s^{\,3}}{K_D (G_r - 1) \cot\theta} \tag{4}$$

Where K_D is the stability coefficient, w_r is the density of rock mass, G_r is the specific gravity of rock, and θ is the slope of the rip-rap.

The value of K_D varies significantly with type and shape of armor materials, whether the wave is non-breaking or breaking, and method of armor placement. Breaking waves may result in large pressure variation. At all sites reported herein, inspection of the drawings indicates the stones are angular in shape, and randomly placed. Assuming a condition of breaking wave leads to K_D of approximately 2.2 (USACoE, 1984). Values of w_r = 2650 kg/m^3 and G_r = 2.65 were assumed for all four sites. Establishing W_{50}, again from inspection of the drawings, allows for a back-calculation of H_s (Eq. 4). Knowing H_s, a value of P_{max} is then back-calculated (Eq. 3), and used to determined the ratio $S/p_{i(0)}$ (see Table 5.5b).

Each site is reported with reference to the ratio AOS/D_{50} and AOS/D_{85}, and for purposes of comparison, O_{90}/D_{50} and O_{90}/D_{85} (see Fig. 5.8). Therefore, each site yields a total of four data points. The range of $S/p_{i(0)}$ depicted for each point (horizontal error bar) results from the constant of A_0 having a lower bound A_0 =1 and upper bound of A_0 = 2, which is believed appropriate given the uncertainty in determination of normalized seepage pressure.

It is not feasible to provide a companion error bar for the AOS/D_n values. By definition 95% of pore size openings are smaller than the AOS value, but the range is unknown. Furthermore, the spatial variations in grain size of the base soil are unknown. Accordingly, it is not possible to assign a range of AOS/D_n, as was done for $S/p_{i(0)}$.

All four sites yields a value of $S/p_{i(0)} \approx 1$ (see Table 5.5b), which implies a seepage pressure that likely results in very low effective stress in the base soil adjacent to the geotextile. Three of the four sites exhibit a relatively low $AOS/D_{85} \leq 0.5$ (and $AOS/D_{50} \leq 1$) and one, at Sungai Buntu, a relatively large value of $AOS/D_{85} \approx 1.5$ (and $AOS/D_{50} \approx 5$). Recall all four sites are deemed filtration compatible, based on field observations (Mannsbart and Christopher, 1997). From comparison of the AOS/D_{50} (see Fig. 5.8a) and AOS/D_{85} (see Fig. 5.8b) filter ratio, and the postulated curve-linear threshold to onset of piping (shown dashed) it appears, once again, that the AOS/D_{85} values provide a better agreement to the proposed hydromechanical framework.

5.5 A recommended criterion for soil retention

Verification of the hydromechanical framework with the selected additional laboratory and field studies implies that AOS/D_{85} is more suitable than AOS/D_{50} as an indicative filter ratio for design. The finding is consistent with the observation of Watson and John (1999) who established, from statistical analysis, that particles in the size range D_{70} to D_{90} govern the formation of a soil bridge at the openings of a filter. Therefore, all laboratory test data, including test data of the current study by Srikongsri and Fannin (2010b: see chapter 4), and the field data (section 5.4) are reproduced in Figure 5.9, with reference to an AOS/D_{85} filter ratio.

Recall the Holtz et al. (1997) criterion of (O_{95} or AOS)/$D_{85} \leq 0.5$ that was modified from earlier work reported by Christopher and Holtz (1985): its development was not supported by any systematic mechanics-based study of soil-geotextile behaviour in dynamic, pulsating or cyclic flow. The unified plot of AOS/D_{85} versus $S/p_{i(0)}$ confirms that the current design guidance used in North America is conservative for these uniformly-graded soils. Comparison of the database and the empirical criteria suggests there is sufficient conservatism to warrant a revision to the criterion.

Recall the Dutch approach that a filter ratio, $O_{98}/D_{85} < 1$ to 2 be used for cohesionless soil with $C_u < 6$ to 10. Although, the upper bound value of 2 appears to provide a broader choice for selecting a candidate geotextile, it is deemed too close to the zone of soil piping for $S/p_{i(0)} \geq 1$. Over the service life of a rip-rap revetment, the filter is expected to occasionally experience a very large $S/p_{i(0)}$. Hence, the lower bound $O_{98}/D_{85} < 1$ is considered more appropriate as it provides an adequate margin of safety for the uncertainty in hydraulic loads (see Fig. 5.9).

In summary, the newly proposed hydromechanical framework of AOS/D_{85} (a geometric index of capacity) versus $S/p_{i(0)}$ (a hydromechanical index of demand) both demonstrates and explains the nature of conservatism in empirical criteria for soil retention in cyclic flow, with reference to a qualitative margin of safety against onset of piping. In addition, with the assumption that $AOS \approx O_{98}$, it enables a comparison with experience reported from practice in the Netherlands, which likewise has not been developed with reference to any systematic mechanics-based study of soil-geotextile behaviour in dynamic, pulsating or cyclic flow.

Accordingly, and with recognition of the Holtz et al. (1997) and Pilarczyk (2000) guidance, it is proposed that the criterion O_{95} or $AOS/D_{85} \leq 0.5$ be relaxed to yield a recommended criterion of $AOS \leq D_{85}$. The recommended criterion is appropriate for a

uniformly-graded ($C_u \leq 6$) non-plastic base soil that is internally stable. It provides a significant margin of safety against piping failure, given the difference between $AOS/D_{85} = 1$ and the filter ratio $AOS/D_{85} \approx 2$ at which retention incompatibility is found to initiate for a woven geotextile (see Fig. 5.9). The relative margin of safety is believed greater for a nonwoven geotextile, and attributed to the more tortuous nature of the pore size distributions and related constrictions.

In all likelihood, entrapment of soil particles may occur with time over the service life of the geotextile filter, particularly as a result of wave loading and episodic fluidization of the soil immediately adjacent to the fabric, where the contact is not intimate. It is believed that any such entrapment of soil particles makes the retention criterion yet more conservative.

Use of the recommended criterion, and indeed any criterion for soil retention, is made on the basis that adequate site supervision during handling and installation of the geotextile eliminates the possibility of mechanical damage yielding any significant increase in the characteristic pore size opening.

5.6 Conclusions

Analysis of laboratory test data from three studies, and select field data from four project sites, is made with reference to attributes of the base soil (D_{50} and D_{85}), the pore size opening of the geotextile (AOS), an estimate of likely seepage pressure (S) from cyclic flow, and initial mean effective stress ($p_{i(0)}$) in the base soil. The three laboratory studies involve both woven and needle-punched nonwoven geotextiles, in filtration applications that include both compatible and incompatible soil-geotextile combinations. The four field applications involve needle-punched nonwoven geotextiles that are compatible soil-geotextile combination. Accordingly, the database provides opportunity to critically evaluate the merits of a proposed hydromechanical framework, for retention compatibility in cyclic flow, based on a relation between filter ratio (AOS/D_{85}, and AOS/D_{50}) and normalized seepage pressure ($S/p_{i(0)}$).

Generally good agreement is found between the proposed framework and the database of independent laboratory and field experience. The framework is found to distinguish between filter compatibility with some washout, and filter incompatibility in the form of a piping action through the geotextile. Inspection of the data suggests that, AOS/D_{85} is generally more suitable than AOS/D_{50} as an indicative filter ratio for design.

More specifically, and with reference to AOS/D_{85} filter ratio, analysis of the laboratory test data suggests:

- For narrowly-graded non-plastic soils ($C_u \leq 6$) in combination with a woven geotextile, a transition occurs from filter compatibility to onset of piping action at a filter ratio $2 \leq AOS/D_{85} \leq 2.5$.

Analysis of the laboratory and field data also suggests:

- For narrowly-graded non-plastic soils ($C_u \leq 6$) in combination with a needle-punched nonwoven geotextile, retention compatibility is satisfied at $AOS/D_{85} \approx 1.5$.

The findings are consistent with Srikongsri and Fannin (2010b: see chapter 4) reporting onset of piping for woven geotextiles at $2.0 \leq AOS/D_{85}$, and retention compatibility for needle-punched nonwoven geotextiles at $2.3 \leq AOS/D_{85}$. The concept of a unified plot of AOS/D_{85} versus $S/p_{i(0)}$ yields a hydromechanical framework that describes the relation between geometric index of capacity and hydromechanical index of demand.

This novel framework is used to illustrate the unspecified margin of safety associated with criteria for soil retention, and thereby improve confidence in their application to engineering practice. Accordingly, the following empirical criterion is recommended for cyclic or dynamic flow conditions:

- O_{95} or AOS $\leq D_{85}$

The criterion is verified from inspection of a database comprising 50 values of filter ratio (AOS/D_{85}) and normalized seepage pressure ($S/p_{i(0)}$), 46 of which are established from laboratory studies and 4 of which are derived from field observations. Given the nature of the soils examined in the tests and in the field, it is appropriate for a uniformly-graded ($C_u \leq 6$) non-plastic base soil that is internally stable. The form of the empirical relation is consistent with the lower bound suggested by Pilarczyk (2000), which was developed with reference to practical experience but not supported by any systematic laboratory study. It provides a significant margin of safety against piping failure for woven geotextile. The relative margin of safety is believed greater for a nonwoven geotextile, and attributed to the more tortuous nature of the pore size distributions and related constrictions.

Table 5.1 Properties of soils

Author	Soil code	D_{85} (mm)	D_{50} (mm)	D < 75μ (%)	C_u	Internal stability (Kenney & Lau)
Hawley	FR	0.33	0.26	< 3	1.8	Stable
	MT	0.29	0.18	10	3.3	Stable
	PC	0.21	0.18	15	5.8	Stable
Cazzuffi et al.	BS	0.20	0.14	< 2	1.5	Stable
Chew et al.	RS	2.20	0.90	< 2	3.3	Stable

Table 5.2 Properties of geotextiles

Author	Geotextile code	Fabric structure	AOS or O_{95} (μm)	POA (%)	Thickness (mm)	Unit mass (g/m^2)
Hawley	G21aN	NW-NP	212	N/A	1.0	163
	G21bN	NW-NP	212	N/A	1.7	220
	G21W	W-M	212	4-6	N/A	190
	G30W	W-M	300	4	N/A	170
	G43aW	W-M	425	<5	N/A	282
	G43bW	W-M	425	10	N/A	304
	G60W	W-MT	600	N/A	N/A	490
Cazzuffi et al.	G16N	NW-NP	160†	N/A	3.0	300
	G44W	W	440†	N/A	0.8	250
Chew et al.	G10N	NW	100	N/A	3.5	400
	G47W	W	470††	N/A	1.6	400

NW - NP denotes needle-punched nonwoven
W denotes woven (M = Monofilament and MT = Multifilament)
POA is percent open area
N/A denotes no data available
† = hydrodynamic sieving, and †† = wet sieving

Table 5.3 Mass washout and mass piping (after Hawley 2001)

Test combination	Filter ratio		m_{av} (g/m^2/100 cyc) for $i_{av} \approx 4$ (S = 3.9 kPa)		
	AOS/D_{85}	AOS/D_{50}	T = 50 s $p_{i(0)} \approx 10$ kPa	T = 10 s $p_{i(0)} \approx 10$ kPa	T = 10 s $p_{i(0)} \approx 1.5$ kPa
FR-G21aN	0.6	0.8	≈ 0	≈ 0	≈ 0
FR-G21bN	0.6	0.8	≈ 0	≈ 0	≈ 0
FR-G21W	0.6	0.8	≈ 0	≈ 0	≈ 0
FR-G30W	0.9	1.2	≈ 0	≈ 0	≈ 0
FR-G43aW	1.3	1.6	≈ 0	≈ 0	≈ 0
FR-G43bW	1.3	1.6	1	≈ 0	≈ 0
FR-G60W	1.8	2.3	4	≈ 0	≈ 0
MT-G21aN	0.7	1.2	2	≈ 0	≈ 0
MT-G21bN	0.7	1.2	1	≈ 0	≈ 0
MT-G21W	0.7	1.2	≈ 0	≈ 0	≈ 0
MT-G30W	1.0	1.7	6	≈ 0	≈ 0
MT-G43aW	1.5	2.4	29	44	49
MT-G43bW	1.5	2.4	15	7	20
MT-G60W	2.1	3.4	115	≈ 0	34
PC-G21aN	1.0	1.2	3	≈ 0	15
PC-G21bN	1.0	1.2	4	≈ 0	≈ 0
PC-G21W	1.0	1.2	5	≈ 0	11
PC-G30W	1.4	1.7	5	≈ 0	20
PC-G43aW	2.0	2.4	9	≈ 0	1673†
PC-G43bW	2.0	2.4	22	63	1905†

† denotes mass piping

Table 5.4 Mass loss (after Cazzuffi et al. 1999 and Chew et al. 2000)

Test combination	i_{av} and [S in kPa]	Filter ratio		m_{av} (g/m^2/100 cyc), for σ'_{vt} and [approximate $p_{i(0)}$value]			
		AOS/D_{85}	AOS/D_{50}	154 [93] (kPa)	113 [67] (kPa)	54 [33] (kPa)	4 [2.4] (kPa)
BS-G16N[(a)]	12 [47 kPa]	0.8	1.1	1	-	2	8
BS-G44W[(a)]	3 [11.7 kPa]	2.2	3.1	3	-	4	21.9
	5 [19.6 kPa]	2.2	3.1	5	-	8	323[(c)]
	16 [62.7 kPa]	2.2	3.1	7	-	10	426[(c)]
RS-G-10N[(b)]	26 [76.4 kPa]	0.05	0.1	-	20	-	-
RS-G47W[(b)]	26 [76.4 kPa]	0.12	0.3	-	30	-	-

a) T varies from 2 s – 20 s and m_{av} values deduced from a duration of 1500 cycles

b) T = 2 s and m_{av} values deduced from a duration of 2000 cycles

c) Unacceptable mass loss

Table 5.5 Field performance evaluation data (after G. Mannsbart & B.R. Christopher, 1997)

Table 5.5a Key summary of material properties and performence evaluation

Project title and year of construction	Type of protection	NP-NW Geotextile opening size† (mm)		Soil indicative particle size (mm)			Evaluation	
		AOS	O_{90w}	D_{85}	D_{50}	C_u	Piping	Clogging
Lacanau, France (1984)	Rip-rap Coastal	0.15	0.10	0.8	0.35	2	No	No
Pantai Murni, Malaysia (1986)	Rip-rap Coastal	0.21	0.11	2.5	0.4	15	No	No
Greifenstein, Austria (1981)	Rip-rap River bank	0.21	0.10	7.5†	0.2	4	No	No
Sungai Buntu, Malaysia (1986)	Rip-rap Coastal	0.25	0.15	0.16	0.05	5	No	No

† Gap-graded gravelly sand

Table 5.5b Approximate hydromechanical loading regime

Project title	Armor layer thickness (m)	slope	K_0	$p_{i(0)}$ (kPa)	W_{50} (kg)	Significant wave height, H_s (m)	S (kPa)	$S/p_{i(0)}$
Lacanau	3	1:2.0	0.42	27.6	1500	2.24	22.0	0.8
Pantai Murni	1.6	1:3.0	0.42	14.7	430	1.69	16.6	1.13
Greifenstein	1	1:1.5	0.42	9.2	125	0.89	8.7	0.95
Sungai, Buntu	1.6	3.00	0.42	14.7	200	1.31	12.8	0.87

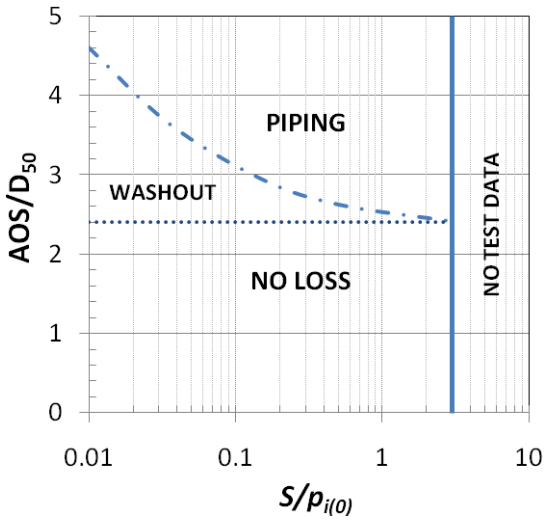

(a)

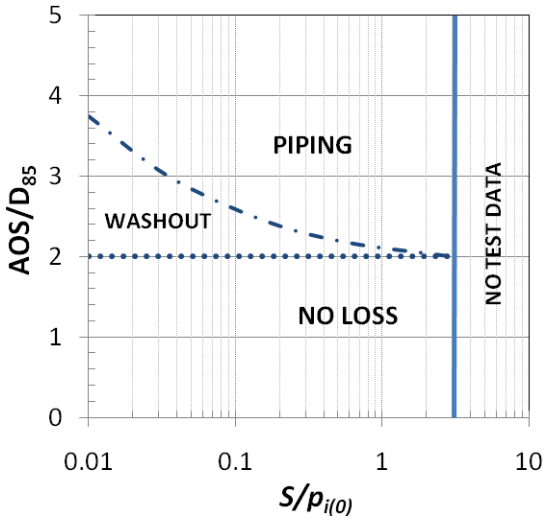

(b)

Figure 5.1 Geotextile-soil retention: a) AOS/D_{50}; b) AOS/D_{85}

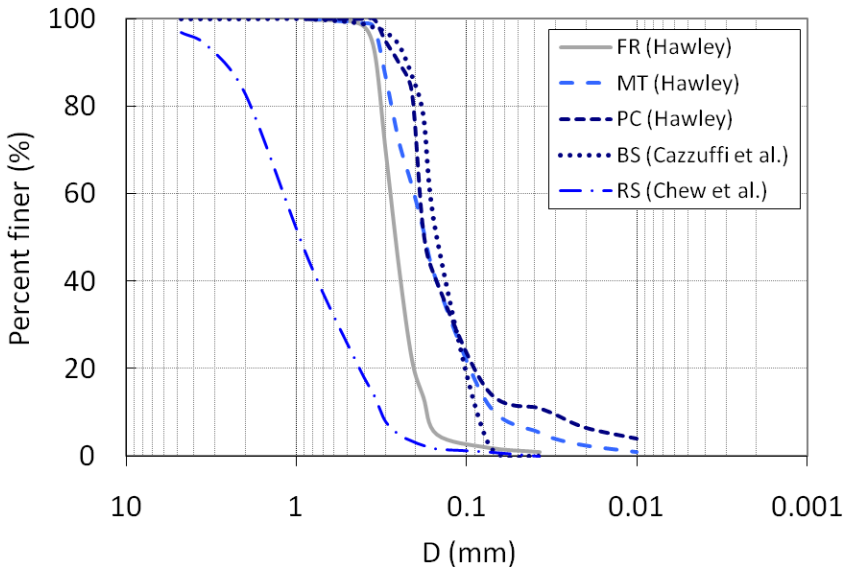

Figure 5.2 Grain size distribution curves

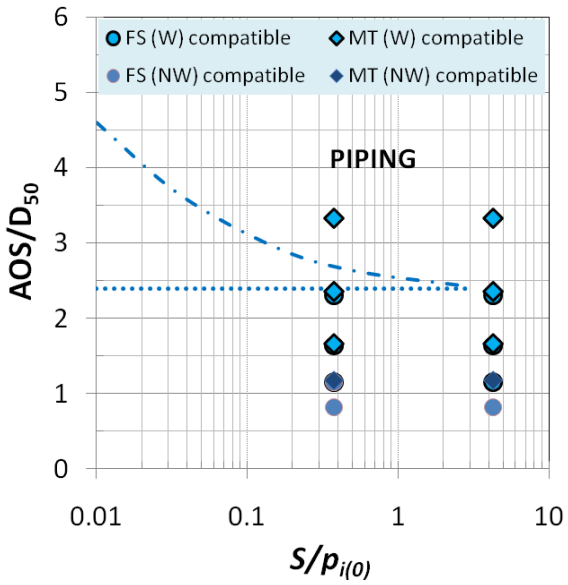

(a)

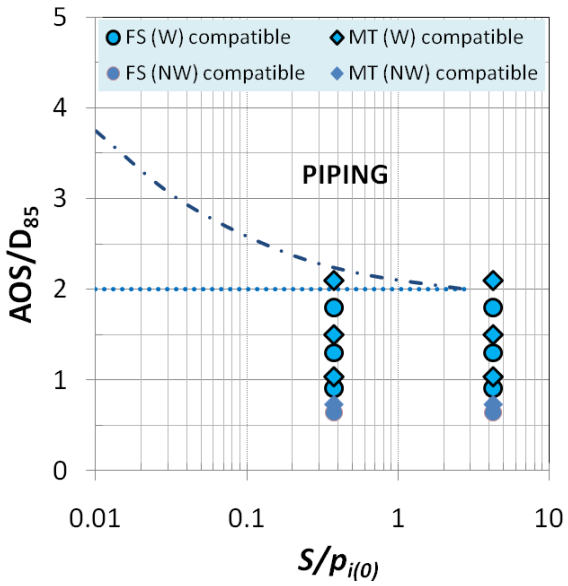

(b)

Figure 5.3 Comparison of Hawley (2000) test data for the FR and MT soil

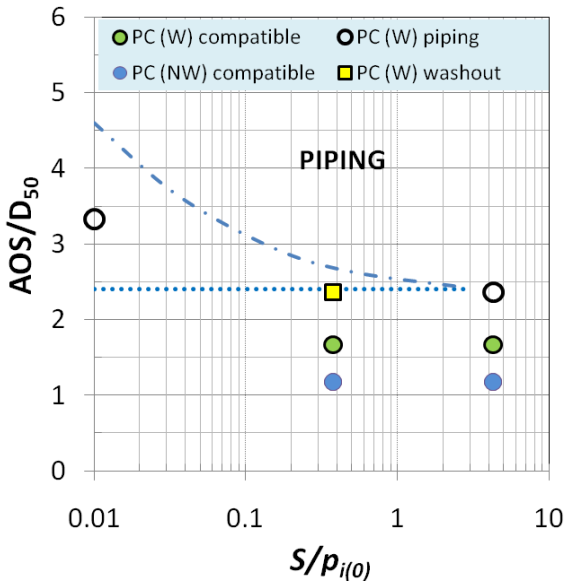

(a)

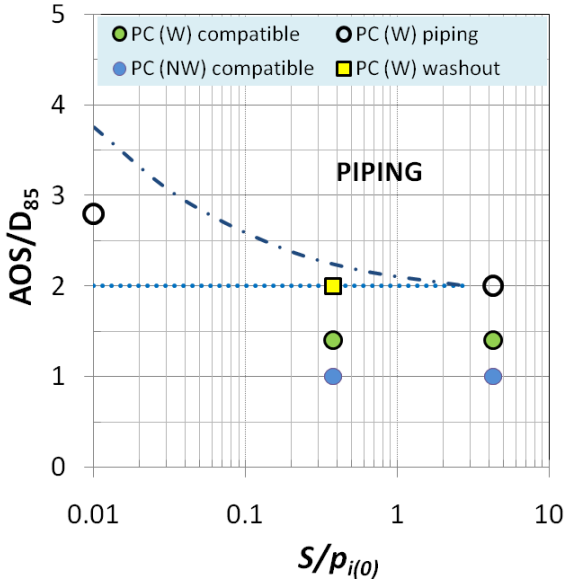

(b)

Figure 5.4 Comparison of Hawley (2000) test data for the PC soil

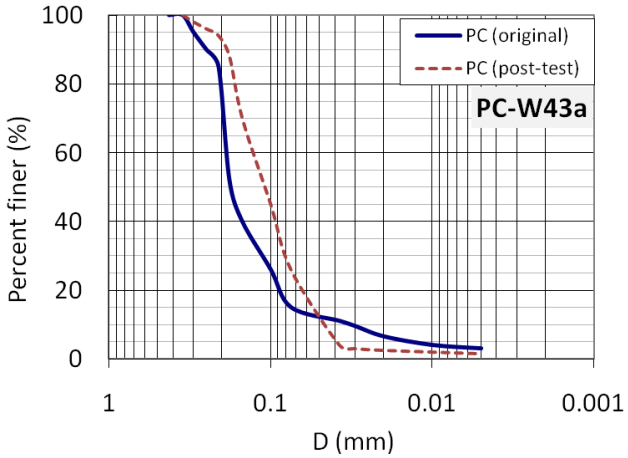

(a)

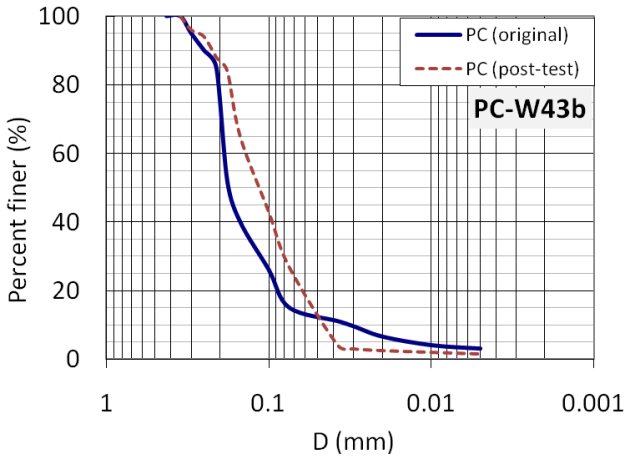

(b)

Figure 5.5 Original and post-test soil gradation curves: a) test PC-W43a; b) test PC-W43b

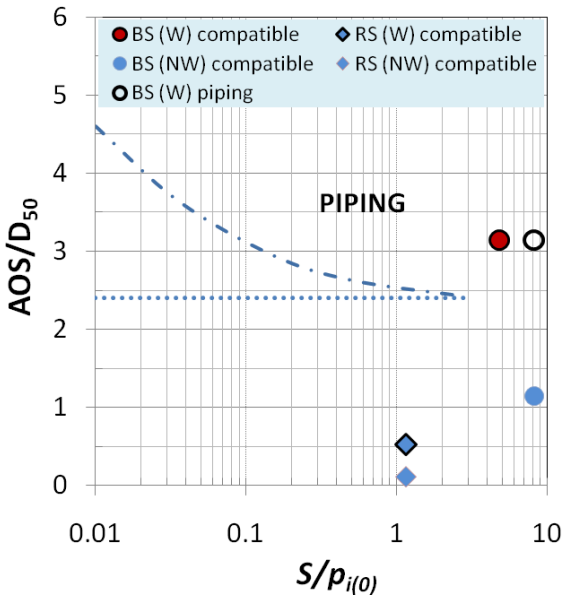

(a)

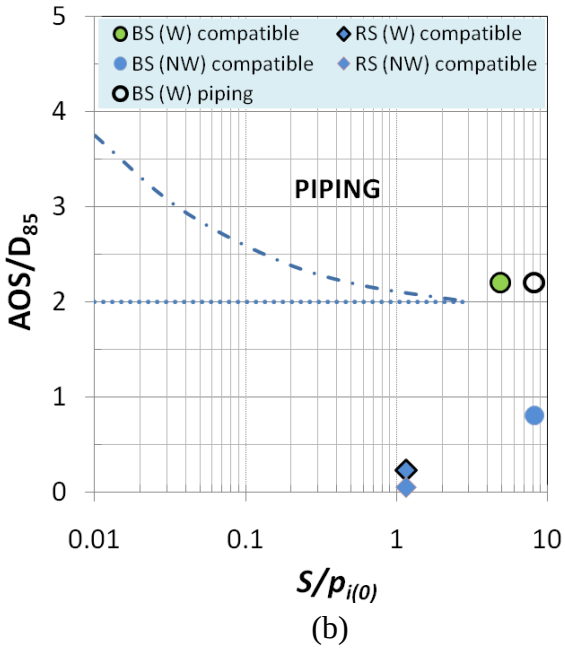

(b)

Figure 5.6 Comparison of Cazzuffi et al. (1999) and Chew et al. (2000) test data for the BS and RS soil

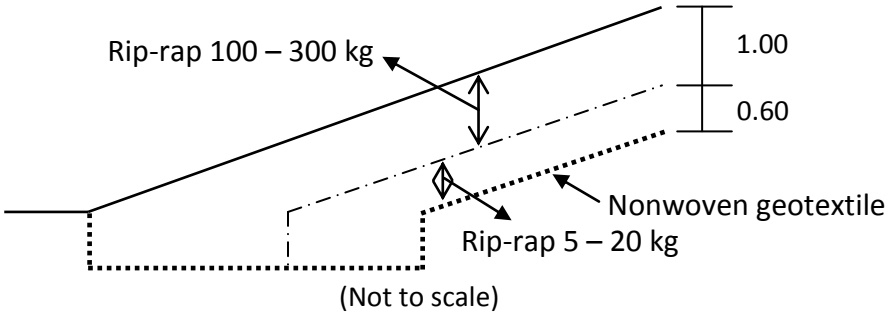

Figure 5.7 Cross-section of Sungai Buntu

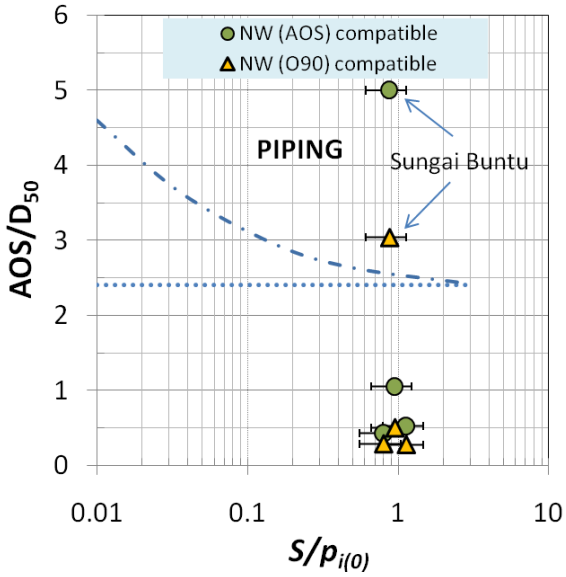

(a)

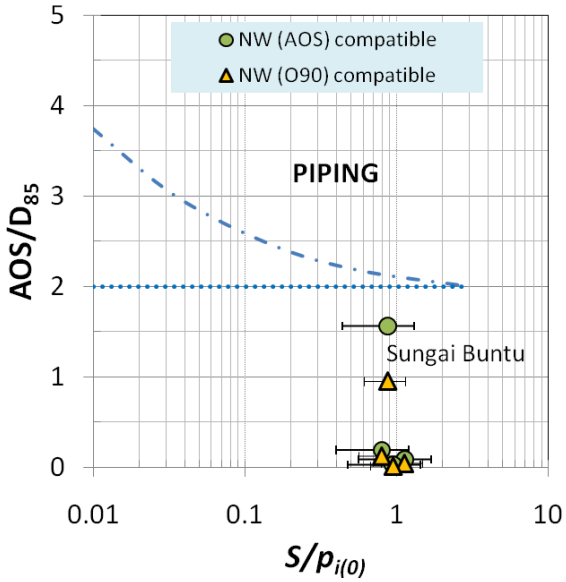

(b)

Figure 5.8 Comparison of Mannsbart and Christopher field observations

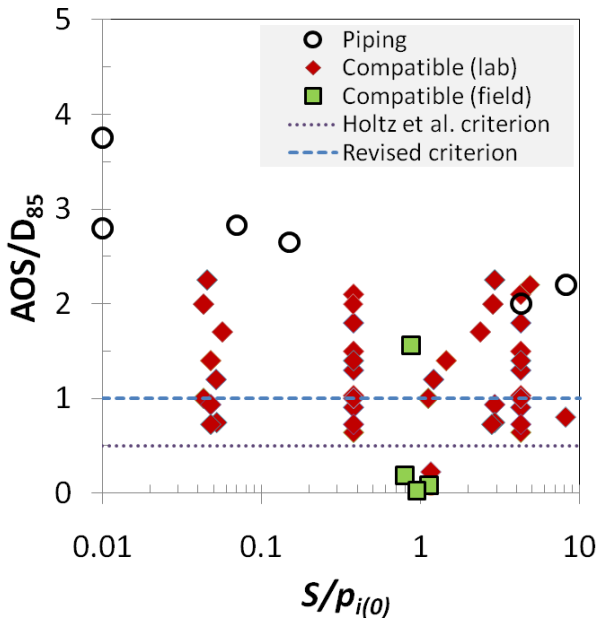

Figure 5.9 Combined database for wave period in the range 2 s ≤ T ≤ 20 s

5.7 References

ASTM D 4751, Standard Test Method for Determining Apparent Opening Size of a Geotextile. American Society foe Testing and Materials, West Conshohocken, PA, USA.

Bathia, S. K., Smith, J. L. and Christopher, B. R. (1996). Characterization and pore-Size distribution: part III: comparison of methods and application to design", *Geosynthetics International*, **3**, No. 3, 301-328.

Cazzuffi, D. A., Mazzucato, A., Moraci, N., & Tondello, M. (1999). A new test apparatus for the study of geotextiles behaviour as filters in unsteady flow conditions: relevance and use. *Geotextiles and Geomembranes*, **17**, No. 5-6, 313 - 329.

Chew, S. H., Zhao, Z. K., Karunaratne, G. P., Tan, S. A, Delmas, Ph., & Loke, K. H. (2000). Revetment geotextile filter subjected to cyclic wave loading. *Proceedings of Geo-Denver 2000*, Denver, CO, USA, pp 162 – 175.

Hawley, R. (2001). Filtration performance of geotextiles in cyclic flow conditions. MASc Thesis, University of British Columbia, Vancouver, B.C., Canada, 141p.

Kenney, T. C. and Lau, D. (1985). Internal stability of granular filters. *Canadian Geotechnical Journal*, **22**, No. 2, 215-225

Kenney, T. C. and Lau, D. (1986). Internal stability of granular filters: Reply. *Canadian Geotechnical Journal*, **23**, No. 3, 420-423

Klein Breteler, M., Pilarczyk, K. W. and Smith, G. M. (1995). Geotextiles in bed and bank protection structures. *Publication No. 488*, Delft hydraulics laboratory, Delft, The Netherlands.

Klein Breteler, M. and Verhey, H. J. (1990). Erosion control by hydrodynamically sandtight geotextiles. *Proceedings of 4th International conference on geotextiles, geomembranes and related products*, Hague, The Natherlands, Vol. 1, pp. 385 – 390

Li, M. and Fannin, R.J. (2008). A comparison of two criteria for internal stability of granular soil. *Canadian Geotechnical Journal*, 45, No. 9, 1303-1309.

Mannsbart, G. and Christopher, B.R. (1997). Long-term performance of nonwoven geotextile filters in five coastal and bank protection projects, *Geotextiles and Geomembranes*, **15**, 207 – 221.

Pilarczyk, K. W. (2000). *Geosynthetics and geosystem in hydraulic and coastal engineering*. A.A. Balkema, Rotterdam, The Netherlands, 913 p.

Srikongsri, A. and Fannin, R.J. (2010a). Influences of testing methodology on soil-geotextile compatibility in cyclic flow using rigid-wall permeameters. *Manuscript draft*, see Chapter 3.

Srikongsri, A. and Fannin, R.J. (2010b). Geotextile-soil retention in cyclic flow. *Manuscript draft*, see Chapter 4.

U.S. Army Corps of Engineers (1984). *Shore Protection Manual*. Coastal Engineering Research Center, Washington, DC, USA.

Watson, P. D. J., and John, N. W. M. (1999). Geotextile filter design and simulated bridge formation at the soil-geotextile interface. *Geotextiles and Geomembranes*, **17**, 265 - 280

6 Conclusions and Recommendations

The research study has two main objectives. First, to develop the concept of a hydromechanics-based framework that accounts for (i) capacity of the soil-geotextile filter, by means of a filter ratio or geometric constraint to the onset of retention incompatibility in cyclic flow, and also accounts for (ii) the transient demand on the soil-geotextile filter, by means of seepage-induced change in effective stress. Second, to characterize the unspecified margin of safety that exists in current design guidance for a geotextile filter in applications of cyclic flow, using the empirical rules of Luettich et al. (1992), Holtz et al. (1997) and Pilarczyk (2000), and if appropriate, to recommend changes to address conservatism in those rules.

6.1 Conclusions

The filtration compatibility of a geotextile, for soil retention in cyclic flow, has been systematically investigated in a program of laboratory permeameter testing. Onset of retention incompatibility is governed by: (i) grain size distribution of the base soil, (ii) opening size of the geotextile, (iii) a combination of effective stress and hydraulic gradient, and (iv) wave period of flow reversal. A conceptual hydromechanical framework is proposed that unifies these governing factors. The framework relates

filter ratio (AOS/D_n) to a value of normalized seepage pressure ($S/p_{i(0)}$) associated with quantities of soil loss by "washout" that do not exceed a threshold value ($g/m^2/100$ cycles) considered representative of piping through the geotextile: the threshold value of soil loss is defined empirically by the rate of loss-induced volume change. A soil-geotextile combination is deemed retention compatible if the rate diminishes with number of cycles, and hence time; in contrast, a rate that was constant or increased during the test was indicative of a piping action.

Using the proposed concept, conservatism of select current design guidance is examined with regard to the filter ratios AOS/D_{50} and AOS/D_{85}. Verification of the concept through comparison with other laboratory studies, and also with field observations, then leads to a recommendation for current design guidance. The following summary of findings from the study addresses (i) insights to important factors governing soil-geotextile compatibility and the need for a systematic study of cyclic flow conditions, (ii) the influence of test method, scale effect in a small and large permeameter, and stress distribution in a rigid-wall permeameter, (iii) a novel hydromechanical-based approach to interpretation of retention incompatibility and, (iv) evidence of undue conservatism in current design guidance, and a proposed revision to an empirical criterion for soil retention in cyclic flow.

6.1.1 Previous study

Analysis of data on soil-geotextile compatibility using the small permeameter, from a study (Hawley, 2001) that preceded the current research, examines filtration combinations of three cohesionless soils and seven geotextiles (5 woven geotextiles, and 2 needle-punched nonwoven geotextiles). Uncertainty surrounding inherent margins of safety in design guidance is addressed through re-interpretation of the data. Specifically, based on characterization of the soil (D_{85}), geotextile (AOS), soil-geotextile compatibility (GR_8) and mass of soil passing per unit area (m_p), the findings suggest:

- mass loss per unit area provides a very useful index of filtration compatibility for soil-geotextile combinations that exhibit piping, and should be reported to assist with test interpretation;
- mass loss per unit area increases with larger AOS/D_{85};
- the empirical design criterion of $AOS/D_{85} \leq 0.5$ for soil retention in cyclic flow is unduly conservative;
- wave period and confining stress influence the filtration compatibility of a soil-geotextile combination, and those two parameters, in combination with hydraulic gradient, require systematic study in order to properly understand the margin of safety in empirical design criteria.

6.1.2 Influence of test method

Newly-acquired data from the small (100 mm diameter) permeameter, and a large permeameter (280 mm diameter) test device, for a uniformly-graded sand and two woven geotextiles were used to evaluate the influence of test method, with emphasis on matters of scale effect in the test equipment, test procedure and the test device itself on hydromechanical conditions at the soil-geotextile interface. In the absence of a standard test device and procedure, the objective was to develop and validate a suitable laboratory technique for systematic study of soil-geotextile compatibility in cyclic flow. The following conclusions are drawn:

- measurement of axial load in the large permeameter indicates a reduction of 20% to 40% in effective stress along the specimen length that is attributed to interface friction, a finding that implies any stress-based interpretation of soil-geotextile compatibility in a rigid-wall permeameter must address the phenomenon of sidewall friction;
- inspection of mass loss-volume change in the large and small permeameter indicates no scale effect in the two permeameters. The difference of results (mass loss) is attributed to spatial variation of the pore opening size of the geotextile, hence it is recommended to repeat a test in the small permeameter

where it is believed the soil and geotextile exhibit filtration incompatibility, and report an average of the experimental findings for purposes of analysis.

Findings in the small permeameter appropriate for a systematic study of test variables, the experimental data and a companion theoretical analysis show that:

- a multi-stage test method involving reduction of axial stress, and the corresponding variation of lateral stress in the rigid wall permeameter, suggest mean effective stress at the soil-geotextile interface (p_i) is a better parameter for interpretation of test performance than vertical stress; and
- soil retention is very sensitive to the upward component of cyclic flow that yields a reduction in mean effective stress and, it is postulated, thereby acts to destabilize arching in soil particles at the openings of the woven geotextile.

Finally, for the range of variables examined in testing, mass loss is found negligible in cyclic flow at a filter ratio $AOS/D_{85} \approx 2$, but very significant at $AOS/D_{85} \approx 2.8$, where soil-geotextile retention incompatibility is triggered by loading conditions governed by a combination of wave period, hydraulic gradient and confining stress. The findings suggest that mass loss may be used to distinguish between a soil-combination that is compatible, versus incompatible in cyclic flow. The results are sufficiently encouraging that more data, also including tests on nonwoven geotextiles, are required

to characterize a greater range of AOS/D_{85} to enable development of an empirical rule for soil-geotextile retention compatibility in cyclic flow based on principles of mechanics.

6.1.3 A hydromechanical framework (for onset of retention incompatibility)

The main experimental program of the current study was performed on combinations of four uniformly-graded base soils (two fine sands, a silty sand and a coarse sandy silt), five needle-punched nonwoven geotextiles and two woven geotextiles. The utility of an empirical filter ratio, expressed as AOS/D_{50} and AOS/D_{85}, is evaluated. The potential for a relation between filter ratio and normalized seepage pressure ($S/p_{i(0)}$) to explain the onset of retention incompatibility in cyclic flow is explored, leading to a conceptual hydromechanical framework for interpretation of the test data. With reference to a characteristic opening size AOS and an indicative particle size D_n, the following conclusions are drawn:

- For unidirectional flow at $i_{av} < 10$, no unacceptable mass loss was observed for nonwoven geotextiles at $0.7 \leq AOS/D_{85} \leq 2.3$ ($0.9 \leq AOS/D_{50} \leq 2.7$), and woven geotextiles at $1.2 \leq AOS/D_{85} \leq 3.7$ ($1.3 \leq AOS/D_{50} \leq 4.6$). The finding implies retention compatibility;
- For cyclic flow at $i_{av} < 10$, with nonwoven geotextiles at $0.7 \leq AOS/D_{85} \leq 2.3$ ($0.9 \leq AOS/D_{50} \leq 2.7$), and with woven geotextiles examined at $1.2 \leq AOS/D_{85}$

$\leq$ 2.0 ($1.3 \leq AOS/D_{50} \leq 2.5$), there was again no unacceptable mass loss observed, which also implies retention compatibility.

However for woven geotextiles at $AOS/D_{85} > 2.0$, mass loss (m_{av}, g/m^2/100 cycles) was observed under cyclic loading conditions. From interpretation of specimen volume change, the following conclusions are made:

- a value $30 \leq m_{av} \leq 50$ g/m^2/100 cycles defines a threshold for soil arching at openings of the geotextile that describes the boundary between washout and onset of retention incompatibility;
- At $2.0 < AOS/D_{85} \leq 2.5$ ($2.5 \leq AOS/D_{50} \leq 3.0$), a transition occurs from retention compatible to retention sensitivity;
- At $2.5 < AOS/D_{85} \leq 3.7$ ($3.0 \leq AOS/D_{50} \leq 4.6$), soil retention is found very sensitive to loading conditions that are governed by hydraulic gradient, stress and wave period.

A hydromechanics-based interpretation is proposed to account for the combined influence of hydraulic gradient and effective stress. A normalized value of seepage pressure at the soil-geotextile interface ($S/p_{i(0)}$) appears to explain the nature of mass loss through pore size openings of the geotextile. For woven geotextiles, the finding implies that T = 6 s governs the filtration compatibility, for the range 6 s $\leq$ T $\leq$ 120 s.

The fundamental mechanism of soil retention, from interpretation based on the range of m_{av} and analysis of the test data at T = 6 s, suggests:

- A threshold boundary between no loss and washout is governed by AOS/D_n;
- A threshold boundary between washout and piping is governed by AOS/D_n and $S/p_{i(0)}$;
- Transition from no loss to piping is very sensitive to a change of AOS/D_n when seepage pressure exceeds the initial mean effective stress ($S/p_{i(0)} > 1$).

Overall, the findings of the laboratory experimental program on uniformly-graded soils indicate filtration compatibility in cyclic flow reversal for a nonwoven geotextile at $AOS/D_{50} \leq 2.7$ or $AOS/D_{85} \leq 2.3$, and the onset of retention incompatibility for a woven geotextile at 2.5 □ AOS/D_{50} or 2 □ AOS/D_{85}. Accordingly, the design criterion $AOS/D_{50} \leq 1$ (Luettich et al., 1992), or alternatively $AOS/D_{85} \leq 0.5$ (Holtz et al., 1997; CFEM, 2006), appear to provide a generous margin of safety for applications involving filtration of a uniformly-graded base soil. Indeed, it is considered unduly conservative, because it has potential to eliminate the use of a geotextile with base soil of fine sand - yet results of the current laboratory test program, supported by insights from the proposed hydromechanical framework, demonstrate the combinations to yield a retention compatible filter.

6.1.4 A recommended criterion for soil retention

In order to more thoroughly examine this concern for undue conservatism in design guidance for cyclic flow, arising from interpretation of the newly acquired laboratory permeameter data, the study evolved to re-analyze test data from three other laboratory studies published in the literature, and select field data reported from four project sites. The re-analysis is undertaken with reference to attributes of the base soil (D_{50} and D_{85}), the pore size opening of the geotextile (AOS), an estimate of likely seepage pressure (S) from cyclic flow, and an estimate of initial mean effective stress ($p_{i(0)}$) in the base soil. The laboratory and field applications involve both woven and needle-punched nonwoven geotextiles, in filtration applications that include both compatible and incompatible soil-geotextile combinations. Accordingly, the database provides opportunity to critically evaluate the merits of a proposed hydromechanical framework, for retention compatibility in cyclic flow, based on a relation between filter ratio (AOS/D_{85}, and AOS/D_{50}) and normalized seepage pressure ($S/p_{i(0)}$).

Generally good agreement is found between the proposed framework and the database of independent laboratory and field experience. The framework is found to distinguish between filter compatibility, and incompatibility in the form of a piping action through the geotextile. It appears that AOS/D_{85} is more suitable than AOS/D_{50} as an indicative filter ratio for design. The finding is consistent with the observation of Watson and

John (1999) who established, from statistical analysis, that the particles in the size range D_{70} to D_{90} govern the formation of a soil bridge at the openings of a filter.

More specifically, analysis of the laboratory test data suggests:

- For narrowly-graded non-plastic soils ($C_u \leq 6$) in combination with a woven geotextile, a transition occurs from filter compatibility to onset of piping action at a filter ratio $2 \leq AOS/D_{85} \leq 2.5$.

Analysis of the laboratory and field data also suggests:

- For narrowly-graded non-plastic soils ($C_u \leq 6$) in combination with a needle-punched nonwoven geotextile, retention compatibility is satisfied at $AOS/D_{85} \approx 1.5$.

Recall the experimental findings, reported in section 6.1.3, that onset of piping for woven geotextiles is found at $2.0 \leq AOS/D_{85}$, and retention compatibility for needle-punched nonwoven geotextiles is found at $2.3 \leq AOS/D_{85}$. The proposed novel hydromechanical framework of AOS/D_{85} versus $S/P_{i(0)}$ proves useful to illustrate the unspecified margin of safety associated with criteria for soil retention, and thereby improve confidence in their application to engineering practice. Accordingly, and in

order to address undue conservatism, it is proposed the current empirical criterion of $AOS \leq 0.5\ D_{85}$ for soil retention cyclic or dynamic flow conditions be revised to:

- O_{95} or $AOS \leq D_{85}$

The recommended criterion is appropriate for a uniformly-graded ($C_u \leq 6$) non-plastic base soil that is internally stable, and in agreement with the lower bound (but not the upper bound) to design guidance in the Netherlands. It provides a significant margin of safety against piping failure, given the difference between $AOS/D_{85} = 1$ and the filter ratio $AOS/D_{85} \approx 2$ at which retention incompatibility is found to initiate for a woven geotextile. The relative margin of safety is believed greater for a nonwoven geotextile, and attributed to the more tortuous nature of the pore size distributions and related inter-fiber constrictions.

6.2 Recommendations for further study

It has been postulated, and then proven, that a relation between hydromechanical demand and geometric constraint determines the onset of retention incompatibility in a geotextile in combination with a uniformly-graded non-plastic base soil in cyclic flow. Many existing retention criteria for unidirectional flow involve a value of C_u (= D_{60}/D_{10}) to address the influence of shape of the grain size distribution curve (see, for

example, Geotechnical Engineering Office, 1993; Pilarczyk, 2000; Fannin, 2007). In general, the recommended filter ratio is reduced for a broader soil gradation. It is also reduced if the base soil is internally unstable and therefore susceptible to seepage-induced migration of the finer fraction (Lafleur 1999; Mylnarek 2000). This gives recognition to the fact that, in broadly-graded and internally unstable soil, a stable bridging network of particles may not easily develop at the pore size openings of the geotextile (Bhatia and Huang 1995). Furthermore, fines content also appears to influence retention compatibility (Hawley, 2001). Clogging potential or long-term permeability in dynamic or cyclic flow is not yet supported by an extensive body of experimental data and supporting theoretical concepts, and therefore not yet properly addressed in design criteria. Accordingly, the following recommendations are made for further study:

- a systematic study of broadly-graded soils and internally unstable soils; and
- a systematic study of fines content;

both of which have potential to challenge empirical criteria not only for soil retention, but also physical clogging. In addition, influence of pore size distribution should be investigated in order to provide a better recommendation for design guidance that may distinguish between a woven and a nonwoven style of geotextile.

The study has been undertaken in the absence of a standard test method for cyclic flow, and very limited well-documented laboratory and field data. A novel concept is proposed that links geometric constraint (O_{95}/D_n, in the form of AOS/D_{85}) to normalized seepage pressure ($S/p_{i(0)}$). A comparison of experience between different research studies would benefit greatly from a standardized method of testing, and it is recommended that efforts be placed in developing such a method. This will require a standard form of permeameter, for which the choice rests between: (i) rigid-wall without sidewall lubrication (used in the current study); (ii) rigid-wall with sidewall lubrication (for example, Chen et al. 2008) and (iii) a flexible-wall permeameter (for example, Harney and Holtz, 2001). The first option requires a correction for the influence of sidewall friction in order to obtain a value of $S/p_{i(0)}$, and the third option eliminates sidewall friction. It is recommended that a comparative study be made to establish the merits of each approach. It is also recommended that greater emphasis be placed in characterizing effective stress at the soil-geotextile interface, in fundamental studies involving cyclic flow. However, a proper interpretation of retention incompatibility requires a confident distinction between acceptable washout and unacceptable piping actions. This distinction is likely more important to address than greater precision of soil-geotextile interface stress.

Finally, any confidence derived from analysis and interpretation of laboratory studies will be greatly enhanced by corroboration through comparison with field performance

data. Construction applications in dynamic flow conditions may involve flow in many directions: issues of cyclic flow parallel to the plane of filter, as well as normal to it, may have implications for the proposed hydromechanical interpretation of soil retention. The careful reporting of such field performance data, and long-term monitoring of field test sites, will only serve to enhance confidence in the applicability of design guidance to engineering practice.

6.3 References

Bhatia, S.K. and Huang, Q. (1995). Geotextile Filters for Internally Stable/Unstable Soils. *Geosynthetics International*, **2**, No. 3, 537-565.

Canadian Geotechnical Society. Canadian Foundation Engineering Manual, 4th edition, BiTech Publishers Ltd.

Chen, R.-H., Ho, C.-C. & Hsu, C.-Y. (2008). The effect of fine soil content on the filtration characteristics of geotextile under cyclic flows. *Geosynthetics International*, **15**, No. 2, 95–106.

Fannin, R.J. (2007). Chapter 6: The use of geosynthetics as filters. *Geosynthetics in Civil Engineering*. Woodhead Publishing, Cambridge, UK, 295p.

Geotechnical Engineering Office Civil Engineering Department, Hong Kong (1993), Review of Granular and Geotextile Filters, *Geo Publication No. 1/93*, The Government Printer, Hong Kong

Harney, D. H. and Holtz, R. D. (2001). A flexible gradient ratio test. *Proceedings of geosynthetics conference 2001*, Portland, Oregon, USA, pp. 409 – 422.

Hawley, R. (2001). Filtration performance of geotextiles in cyclic flow conditions. MASc Thesis, University of British Columbia, Vancouver, B.C., Canada, 141p.

Holtz, R.D, Christopher, B.R., and Berg, R.R. (1997). *Geosynthetic Engineering*. BiTech Publishers, Richmond, BC, Canada, 452 p.

Lafleur, J. (1999). Selection of geotextiles to filter broadly graded cohesionless soils. *Geotextiles and Geomembranes*, **17**, 299 - 312

Luettich, S.M., Giroud, J.P., and Bachus, R.C. (1992). Geotextile filter design guide. *Geotextiles and Geomembranes, **11***, 355 - 370.

Mlynarek J. (2000). Geo drains and geo filter-retrospective and future trends. *Filters and Drainage in Geotechnical and Geoenvironmental Engineering*, Balkema, Rotterdam, The Netherlands, pp. 27 - 47.

Pilarczyk, K. W. (2000). Geosynthetics and geosystem in hydraulic and coastal engineering. A.A. Balkema, Rotterdam, The Netherlands, 913 p.

Watson, P. D. J., and John, N. W. M. (1999). Geotextile filter design and simulated bridge formation at the soil-geotextile interface. *Geotextiles and Geomembranes*, **17**, 265 – 280

Appendix A Mobilization of sidewall friction

Consider a rigid-wall permeameter in which a test specimen rests on a rigid, zero displacement ($d_s = 0$) at lower boundary. It is postulated that application of an axial load on the top surface of the test specimen develops a maximum value of soil-wall relative displacement at the top of the specimen (d_{st}), which decreases to zero at the base of the specimen. Accordingly, there is a constraint to full mobilization of sidewall friction along the entire specimen length (see Fig. A1a). Hence, the coefficient of side-wall friction for a cohesionless soil may be expressed as:

$$f < \tan\delta \qquad \text{(A1)}$$

where f is a coefficient of sidewall friction and δ is the soil-wall interface friction angle.

For purposes of analysis, a simplified linear elastic-perfectly plastic is adopted (Fig. A1b). The value of f is influenced by stress magnitude and compressibility of the soil. Hence, the magnitude of f may be categorized according to two simple cases. First, the relative displacement at the top of the specimen is less than or equal to the value of relative displacement at mobilization of full interface friction; ($d_{st} \leq d_{sp}$, see Fig. A1c and Fig. A1e), for which:

$$f = \left(\frac{area\ OAB}{area\ OACE} \right) \tan\delta \le 0.5 \tan\delta \qquad \text{(A2)}$$

Second, the relative displacement at the top of the specimen exceeds the value of relative displacement at mobilization of full friction; $d_{st} > d_{sp}$, see Fig. A1d and Fig. A1e).

$$0.5 \tan\delta < f = \left(\frac{area\ OACD}{area\ OACE} \right) \tan\delta < \tan\delta \qquad \text{(A3)}$$

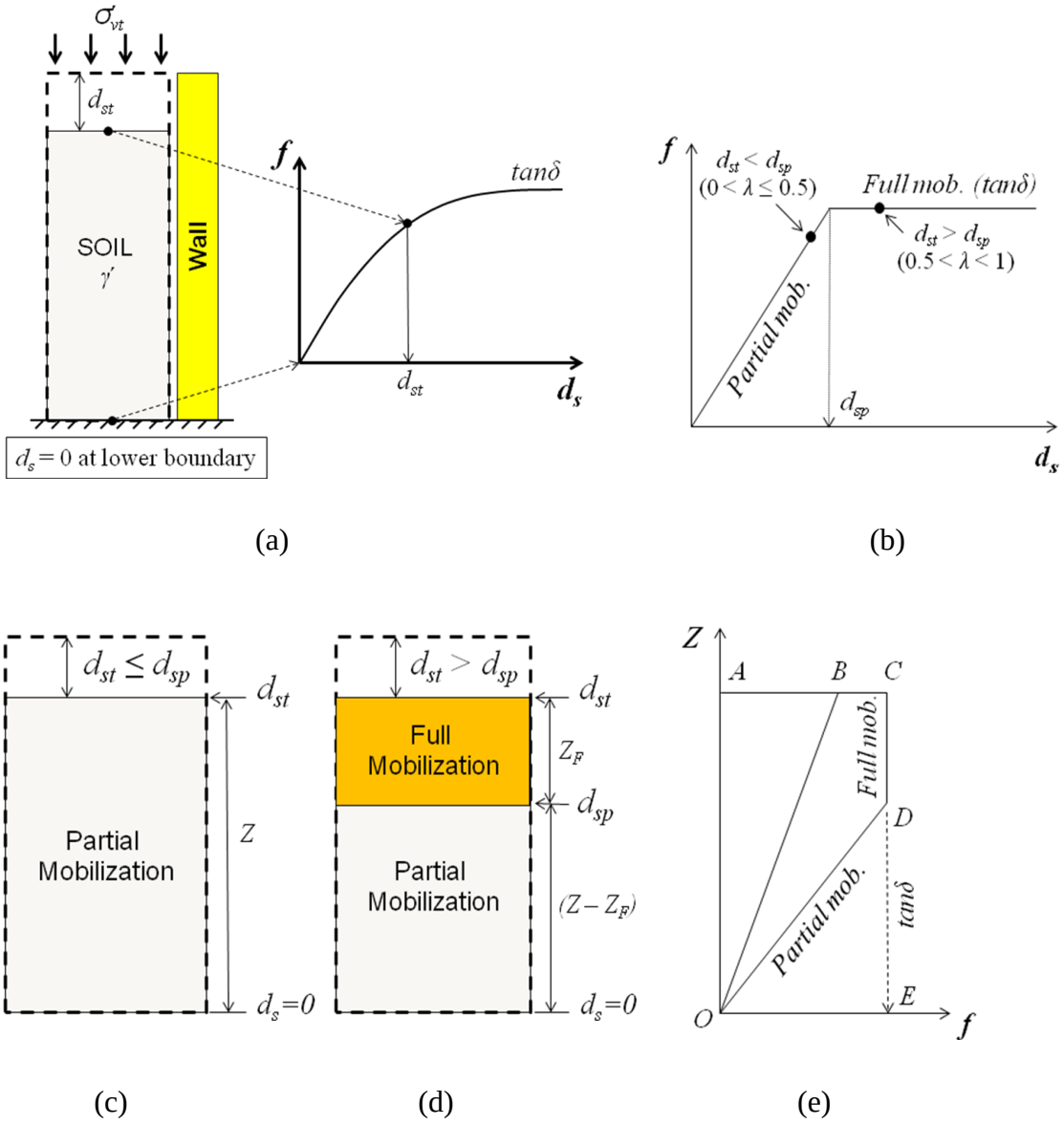

Figure A1 Mobilization of sidewall friction in the rigid-wall permeameter

Appendix B Example stress calculation for section 3.6.4.2

For stage CYC1 during downward flow: σ'_{vt} = 66 kPa, $\Delta\sigma'_{v(0)}$ = 25.9 kPa, S = 8.8 kPa, f = 0.35 (from Fig. 3.14a), γ' = 8 kN/m^3, Z = D = 0.1 m, OCR = 1 and $\varphi = 38^\circ$

$K_0 = (1\text{-}\sin 38^\circ) = 0.384$

$$\sigma'_{vm} = \frac{\sigma'_{vt} + 0.5(\gamma' Z \pm S)}{\left(1 + \frac{2K_0 f Z}{D}\right)} = \sigma'_{vm,\max} = \frac{66 + 0.5(8(0.1) + 8.8)}{\left(1 + \frac{2(0.384)(0.35)(0.1)}{(0.1)}\right)} = 55.8 \text{ kPa}$$

For stage CYC3 during downward flow: σ'_{vt} = 33 kPa, $\sigma'_{vm(0)}$ = 26 kPa, $\Delta\sigma'_{v(0)}$ = 15.0 kPa, S = 8.8 kPa, f = 0.29 (from Fig. 3.14a), γ' = 8 kN/m^3, Z = D = 0.1 m and $\varphi = 40^\circ$

$$\text{Trial } OCR \approx \frac{\sigma_{vm,\max}}{(\sigma_{vm(0)} \pm 0.5S)} = \frac{55.8}{(26 \pm 0.5(8.8))} = 1.83$$

$$K_0 = (1 - \sin 40)1.83^{\sin 40} = 0.53$$

$$\sigma'_{vm} = \frac{\sigma'_{vt} + 0.5(\gamma' Z \pm S)}{\left(1 + \frac{2K_0 f Z}{D}\right)} = \frac{33 + 0.5(8(0.1) + 8.8)}{\left(1 + \frac{2(0.53)(0.29)(0.1)}{(0.1)}\right)} = 29.0 \text{ kPa}$$

$$\text{Check } OCR = \frac{\sigma'_{vm,\max}}{\sigma'_{vm}} = \frac{55.8}{29} = 1.93 \approx \text{the trial value} - \text{OK}$$

$$\Delta\sigma'_v = \frac{4Z}{D}\sigma'_{vm} K_0 f = 4(29)(0.53)(0.29) = 17.7 \text{ kPa}$$

$$\sigma'_{vb} = \sigma'_{vt} + \gamma' Z - \Delta\sigma'_v \pm S = 33 + (8)(0.1) - 17.7 + 8.8 = 24.9 \text{ kPa}$$

Appendix C Summary of key results

Small permeameter: test A-NW4-T6

i_{av}	UNI 1a		UNI 1b		UNI 2a		UNI 2b		UNI 3a		UNI 3b		k_{av} (cm/s)
	GR 25	GR 8	GR 25	GR 8	GR 25	GR 8	GR 25	GR 8	GR 25	GR 8	GR 25	GR 8	
1	1.0	0.9	1.0	0.9	1.0	0.9	1.0	0.9	0.9	0.9	1.0	0.9	0.026
5	1.0	1.0	1.0	0.9	1.0	0.9	1.0	0.9	1.0	0.9	1.0	0.9	0.022
9	1.0	0.9	0.9	0.9	0.9	0.9	0.9	0.9	1.0	0.9	0.9	0.9	0.018

Remarks: (a) NO MASS LOSS was observed in all UNI and CYC stages.
(b) ZERO volume change.

Small permeameter: test A-W1-T6

i_{av}	UNI 1a		UNI 1b		UNI 2a		UNI 2b		UNI 3a		UNI 3b		k_{av} (cm/s)
	GR 25	GR 8	GR 25	GR 8	GR 25	GR 8	GR 25	GR 8	GR 25	GR 8	GR 25	GR 8	
1	1.1	1.2	1.1	1.2	1.0	1.1	1.1	1.1	1.1	1.2	1.1	1.1	0.019
5	1.1	1.3	1.0	1.2	1.0	1.2	1.0	1.1	1.0	1.1	1.1	1.2	0.021
9	1.1	1.3	1.1	1.2	1.2	1.3	1.2	1.3	1.2	1.3	1.2	1.2	0.016

Remarks: (a) NO MASS LOSS was observed in all UNI and CYC stages.
(b) ZERO volume change.

Small permeameter: test A-W1-T60

i_{av}	UNI 1a		UNI 1b		UNI 2a		UNI 2b		UNI 3a		UNI 3b		k_{av} (cm/s)
	GR 25	GR 8	GR 25	GR 8	GR 25	GR 8	GR 25	GR 8	GR 25	GR 8	GR 25	GR 8	
1	1.2	1.4	1.2	1.4	1.2	1.3	1.2	1.3	1.2	1.4	1.2	1.4	0.023
5	1.1	1.3	1.0	1.2	1.0	1.2	1.0	1.1	1.0	1.1	1.1	1.2	0.016
9	1.1	1.3	1.1	1.2	1.2	1.3	1.2	1.3	1.2	1.3	1.2	1.2	0.018

Remarks: (a) NO MASS LOSS was observed in all UNI and CYC stages.
(b) ZERO volume change.

Small permeameter: test B-W1-T6

i_{av}	UNI 1a		UNI 1b		UNI 2a		UNI 2b		UNI 3a		UNI 3b		k_{av} (cm/s)
	GR 25	GR 8	GR 25	GR 8	GR 25	GR 8	GR 25	GR 8	GR 25	GR 8	GR 25	GR 8	
1	1.0	1.2	1.0	1.2	1.0	1.2	1.0	1.2	1.0	1.2	1.0	1.2	0.015
5	1.1	1.3	1.1	1.3	1.0	1.3	1.0	1.2	1.0	1.3	1.1	1.2	0.012
9	1.1	1.3	1.1	1.1	1.1	1.1	1.1	1.1	1.0	1.1	1.0	1.1	0.015

Remarks: (a) NO MASS LOSS was observed in all UNI and CYC stages.
(b) ZERO volume change.

Small permeameter: test B-W1-T60

i_{av}	UNI 1a		UNI 1b		UNI 2a		UNI 2b		UNI 3a		UNI 3b		k_{av} (cm/s)
	GR 25	GR 8	GR 25	GR 8	GR 25	GR 8	GR 25	GR 8	GR 25	GR 8	GR 25	GR 8	
1	1.2	1.4	1.2	1.4	1.2	1.3	1.2	1.3	1.2	1.4	1.2	1.4	0.018
5	1.1	1.3	1.0	1.2	1.0	1.3	1.0	1.2	1.0	1.2	1.1	1.3	0.016
9	1.1	1.4	1.1	1.2	1.2	1.3	1.1	1.3	1.1	1.3	1.1	1.3	0.016

Remarks: (a) NO MASS LOSS was observed in all UNI and CYC stages.
(b) ZERO volume change.

Small permeameter: test B-W2-T6

i_{av}	UNI 1a		UNI 1b		UNI 2a		UNI 2b		UNI 3a		UNI 3b		k_{av} (cm/s)
	GR 25	GR 8	GR 25	GR 8	GR 25	GR 8	GR 25	GR 8	GR 25	GR 8	GR 25	GR 8	
1	1.1	1.2	1.1	1.2	1.0	1.1	1.1	1.1	1.1	1.2	1.0	1.1	0.019
5	1.1	1.2	1.0	1.2	1.0	1.2	1.0	1.1	1.0	1.1	1.1	1.1	0.011
9	1.1	1.2	1.1	1.2	1.1	1.2	1.1	1.2	1.2	1.2	1.0	1.1	0.012

Remarks: (a) NO MASS LOSS was observed in all UNI and CYC stages.
(b) ZERO volume change.

Small permeameter: test B-W2-T60

i_{av}	UNI 1a		UNI 1b		UNI 2a		UNI 2b		UNI 3a		UNI 3b		k_{av} (cm/s)
	GR 25	GR 8	GR 25	GR 8	GR 25	GR 8	GR 25	GR 8	GR 25	GR 8	GR 25	GR 8	
1	1.0	1.0	1.0	1.0	1.0	1.1	1.0	1.1	1.0	1.1	1.0	1.1	0.018
5	1.0	1.0	1.0	1.1	1.0	1.1	1.0	1.1	1.0	1.1	1.0	1.0	0.015
9	1.0	1.1	0.9	1.1	0.9	1.1	0.9	1.0	1.0	1.0	1.0	1.1	0.015

Remarks: (a) NO MASS LOSS was observed in all UNI and CYC stages.
(b) ZERO volume change.

Small permeameter: test C-NW3-T6

i_{av}	UNI 1a		UNI 1b		UNI 2a		UNI 2b		UNI 3a		UNI 3b		k_{av} (cm/s)
	GR 25	GR 8	GR 25	GR 8	GR 25	GR 8	GR 25	GR 8	GR 25	GR 8	GR 25	GR 8	
1	1.3	1.6	1.3	1.6	1.2	1.5	1.2	1.7	1.3	1.8	1.4	1.8	0.008
5	1.4	1.8	1.4	1.8	1.4	1.8	1.4	1.7	1.4	1.6	1.4	1.6	0.007
9	1.4	1.7	1.4	1.7	1.4	1.7	1.4	1.6	1.4	1.6	1.4	1.6	0.007

Remarks: (a) NO MASS LOSS was observed in all UNI and CYC stages.
(b) ZERO volume change.

Small permeameter: test C-NW4-T6

i_{av}	UNI 1a		UNI 1b		UNI 2a		UNI 2b		UNI 3a		UNI 3b		k_{av} (cm/s)
	GR 25	GR 8	GR 25	GR 8	GR 25	GR 8	GR 25	GR 8	GR 25	GR 8	GR 25	GR 8	
1	1.0	0.9	1.0	0.9	1.0	0.9	1.0	0.9	1.0	0.9	0.9	0.9	0.009
5	1.0	0.9	1.0	0.9	1.0	0.9	0.9	0.9	0.9	0.9	0.9	0.9	0.008
9	1.0	1.0	1.0	0.9	0.9	0.9	0.9	0.9	0.9	0.9	0.9	0.9	0.008

Remarks: (a) NO MASS LOSS was observed in all UNI and CYC stages.
(b) ZERO volume change.

Small permeameter: test C-NW5-T6

i_{av}	UNI 1a		UNI 1b		UNI 2a		UNI 2b		UNI 3a		UNI 3b		k_{av} (cm/s)
	GR 25	GR 8	GR 25	GR 8	GR 25	GR 8	GR 25	GR 8	GR 25	GR 8	GR 25	GR 8	
1	1.0	0.9	1.0	0.9	1.0	0.9	1.0	1.0	0.9	1.0	1.0	1.0	0.010
5	1.0	1.0	1.0	0.9	1.0	0.9	1.0	0.9	1.0	0.9	1.0	0.9	0.008
9	1.0	0.9	1.0	1.0	1.0	0.9	1.0	0.9	1.0	0.9	1.0	0.9	0.008

Remarks: (a) NO MASS LOSS was observed in all UNI and CYC stages.
(b) ZERO volume change.

Small permeameter: test C-W1-T6

i_{av}	UNI 1a		UNI 1b		UNI 2a		UNI 2b		UNI 3a		UNI 3b		k_{av} (cm/s)
	GR 25	GR 8	GR 25	GR 8	GR 25	GR 8	GR 25	GR 8	GR 25	GR 8	GR 25	GR 8	
1	1.2	1.3	1.1	1.3	1.2	1.3	1.1	1.3	1.2	1.4	1.2	1.3	0.007
5	1.2	1.3	1.1	1.2	1.1	1.2	1.0	1.1	1.0	1.1	1.1	1.2	0.006
9	1.1	1.2	1.1	1.2	1.2	1.3	1.2	1.3	1.1	1.2	1.1	1.2	0.007

Remarks: (a) NO MASS LOSS was observed in all UNI and CYC stages.
(b) ZERO volume change.

Small permeameter: test C-W2-T6

i_{av}	UNI 1a		UNI 1b		UNI 2a		UNI 2b		UNI 3a		UNI 3b		k_{av} (cm/s)
	GR 25	GR 8	GR 25	GR 8	GR 25	GR 8	GR 25	GR 8	GR 25	GR 8	GR 25	GR 8	
1.3	1.1	1.2	1.1	1.2	1.0	1.1	1.1	1.1	1.1	1.2	1.1	1.1	0.006
5.7	1.1	1.1	1.0	1.2	1.0	1.2	1.0	1.1	1.0	1.1	1.0	1.1	0.009
9.5	1.1	1.1	1.1	1.2	1.0	1.2	1.0	1.0	1.0	1.0	1.0	1.1	0.009

Remarks: MASS LOSS (chapter 3 & 4) was observed in all CYC stages, and associated with volume change.

Small permeameter: test C-W2-T6: Change in specimen height (mm)

i_{av}	UNI1a	CYC1	UNI1b	UNI2a	CYC2	UNI2b	UNI3a	CYC3	UNI3b
1.3	0	0.22	0	0	0.09	0	0	0.05	0
5.7	0	0.41	0	0	0.28	0	0	0.45	0
9.5	0	0.41	0	0	0.43	0	0	0.81	0

Small permeameter: test C-W2-T6-R (repeated)

i_{av}	UNI 1a		UNI 1b		UNI 2a		UNI 2b		UNI 3a		UNI 3b		k_{av} (cm/s)
	GR 25	GR 8	GR 25	GR 8	GR 25	GR 8	GR 25	GR 8	GR 25	GR 8	GR 25	GR 8	
1.1	1.0	1.1	1.0	1.1	1.0	1.1	1.0	1.1	1.0	1.1	1.0	1.1	0.007
5.1	1.0	1.1	1.0	1.1	1.0	1.1	1.0	1.1	1.0	1.1	1.0	1.0	0.009
9.1	1.0	1.0	1.0	1.0	1.0	0.9	0.9	0.9	0.9	0.9	0.9	0.9	0.010

Remarks: MASS LOSS (chapter 3 & 4) was observed in all CYC stages, and associated with volume change.

Small permeameter: test C-W2-T6-R (repeated): change in specimen height (mm)

i_{av}	UNI1a	CYC1	UNI1b	UNI2a	CYC2	UNI2b	UNI3a	CYC3	UNI3b
1.1	0	0.28	0	0	0.26	0	0	0.32	0
5.1	0	0.48	0	0	0.44	0	0	0.68	0
9.1	0	0.34	0	0	0.52	0	0	0.94	0

Small permeameter: test C-W2-T60

i_{av}	UNI 1a		UNI 1b		UNI 2a		UNI 2b		UNI 3a		UNI 3b		k_{av} (cm/s)
	GR 25	GR 8	GR 25	GR 8	GR 25	GR 8	GR 25	GR 8	GR 25	GR 8	GR 25	GR 8	
1.1	1.0	1.0	1.0	1.0	1.0	1.0	1.0	0.9	1.0	0.9	1.0	0.9	0.006
5.1	1.0	1.0	1.0	0.9	1.0	0.9	1.0	0.9	1.0	0.9	1.0	0.9	0.008
8.9	0.9	0.9	0.9	0.9	0.9	0.9	1.0	0.9	1.0	0.9	0.9	0.9	0.008

Remarks: MASS LOSS (chapter 3 & 4) was observed in all CYC stages, and associated with volume change.

Small permeameter: test C-W2-T60: change in specimen height (mm)

i_{av}	UNI1a	CYC1	UNI1b	UNI2a	CYC2	UNI2b	UNI3a	CYC3	UNI3b
1.1	0	0.07	0	0	0.01	0	0	0.02	0
5.1	0	0.08	0	0	0.02	0	0	0.16	0
8.9	0	0.02	0	0	0.02	0	0	0.09	0

Small permeameter: test C-W2-T60-R

i_{av}	UNI 1a		UNI 1b		UNI 2a		UNI 2b		UNI 3a		UNI 3b		k_{av} (cm/s)
	GR 25	GR 8	GR 25	GR 8	GR 25	GR 8	GR 25	GR 8	GR 25	GR 8	GR 25	GR 8	
1.0	1.0	1.0	0.9	1.0	1.0	1.0	0.9	1.0	1.0	1.0	1.0	1.0	0.007
5.2	1.0	1.0	1.0	1.0	1.0	1.0	1.0	1.0	1.0	1.0	1.0	1.0	0.006
8.7	0.9	1.0	0.9	1.0	0.9	1.0	0.9	0.9	0.9	0.9	0.9	0.9	0.007

Remarks: MASS LOSS (chapter 3 & 4) was observed in all CYC stages, and associated with volume change.

Small permeameter: test C-W2-T60-R: change in specimen height (mm)

i_{av}	UNI1a	CYC1	UNI1b	UNI2a	CYC2	UNI2b	UNI3a	CYC3	UNI3b
1.0	0	0	0	0	0.03	0	0	0.05	0
5.2	0	0.01	0	0	0.08	0	0	0.03	0
8.7	0	0.02	0	0	0.03	0	0	0.06	0

Small permeameter: test C-W2-T120

i_{av}	UNI 1a		UNI 1b		UNI 2a		UNI 2b		UNI 3a		UNI 3b		k_{av} (cm/s)
	GR 25	GR 8	GR 25	GR 8	GR 25	GR 8	GR 25	GR 8	GR 25	GR 8	GR 25	GR 8	
1.2	1.2	1.4	1.3	1.3	1.3	1.3	1.3	1.4	1.3	1.4	1.3	1.3	0.008
5.5	1.3	1.3	1.3	1.2	1.3	1.2	1.2	1.2	1.2	1.2	1.2	1.2	0.007
9.3	1.2	1.2	1.1	1.1	1.1	1.1	1.1	1.1	1.1	1.1	1.1	1.1	0.006

Remarks: MASS LOSS (chapter 3 & 4) was observed in some CYC stages, and associated with very small volume change.

Small permeameter: test C-W2-T120: change in specimen height (mm)

i_{av}	UNI1a	CYC1	UNI1b	UNI2a	CYC2	UNI2b	UNI3a	CYC3	UNI3b
1.2	0	0	0	0	0	0	0	0	0
5.5	0	0	0	0	0.01	0	0	0.02	0
9.3	0	0.02	0	0	0.02	0	0	0.04	0

Small permeameter: test D-NW1-T6

i_{av}	UNI 1a		UNI 1b		UNI 2a		UNI 2b		UNI 3a		UNI 3b		k_{av} (cm/s)
	GR 25	GR 8	GR 25	GR 8	GR 25	GR 8	GR 25	GR 8	GR 25	GR 8	GR 25	GR 8	
1	1.2	1.4	1.2	1.4	1.2	1.3	1.2	1.3	1.2	1.4	1.2	1.4	0.004
5	1.1	1.3	1.0	1.2	1.0	1.3	1.0	1.2	1.0	1.2	1.1	1.3	0.003
9	1.1	1.4	1.1	1.2	1.2	1.3	1.1	1.3	1.1	1.3	1.1	1.4	0.003

Remarks: (a) NO MASS LOSS was observed in all UNI and CYC stages.
(b) ZERO volume change.

Small permeameter: test D-NW2-T6

i_{av}	UNI 1a		UNI 1b		UNI 2a		UNI 2b		UNI 3a		UNI 3b		k_{av} (cm/s)
	GR 25	GR 8	GR 25	GR 8	GR 25	GR 8	GR 25	GR 8	GR 25	GR 8	GR 25	GR 8	
1	0.9	0.9	0.9	0.8	1.0	0.9	1.0	0.9	0.9	0.8	1.0	0.9	0.005
5	1.0	1.0	1.0	0.9	1.0	0.8	1.0	0.9	1.0	0.9	0.9	0.8	0.005
9	1.0	0.9	0.9	0.8	0.9	0.8	0.9	0.8	1.0	0.9	0.9	0.9	0.004

Remarks: (a) NO MASS LOSS was observed in all UNI and CYC stages.
(b) ZERO volume change.

Small permeameter: test D-NW4-T6

i_{av}	UNI 1a		UNI 1b		UNI 2a		UNI 2b		UNI 3a		UNI 3b		k_{av} (cm/s)
	GR 25	GR 8	GR 25	GR 8	GR 25	GR 8	GR 25	GR 8	GR 25	GR 8	GR 25	GR 8	
1	1.0	1.0	1.0	0.9	1.0	0.9	1.0	1.0	1.0	0.9	1.0	1.0	0.005
5	1.0	1.0	1.0	1.0	1.0	0.9	1.0	1.0	1.0	0.9	1.0	0.9	0.004
9	1.0	0.9	0.9	0.9	1.0	0.9	1.0	0.9	1.0	1.0	1.0	1.0	0.004

Remarks: (a) NO MASS LOSS was observed in all UNI and CYC stages.
(b) ZERO volume change.

Small permeameter: test D-NW4-T60

i_{av}	UNI 1a		UNI 1b		UNI 2a		UNI 2b		UNI 3a		UNI 3b		k_{av} (cm/s)
	GR 25	GR 8	GR 25	GR 8	GR 25	GR 8	GR 25	GR 8	GR 25	GR 8	GR 25	GR 8	
1	1.0	1.0	1.0	0.9	1.0	0.9	1.0	1.0	1.0	0.9	1.0	1.0	0.005
5	1.0	1.0	1.0	1.0	1.0	0.9	1.0	1.0	1.0	0.9	1.0	0.9	0.005
9	1.0	0.9	0.9	0.9	1.0	0.9	1.0	0.9	1.0	1.0	1.0	1.0	0.003

Remarks: (a) NO MASS LOSS was observed in all UNI and CYC stages.
(b) ZERO volume change.

Small permeameter: test D-NW5-T6

i_{av}	UNI 1a		UNI 1b		UNI 2a		UNI 2b		UNI 3a		UNI 3b		k_{av} (cm/s)
	GR 25	GR 8	GR 25	GR 8	GR 25	GR 8	GR 25	GR 8	GR 25	GR 8	GR 25	GR 8	
1	1.2	1.3	1.2	1.3	1.2	1.3	1.2	1.4	1.2	1.4	1.2	1.3	0.006
5	1.2	1.3	1.1	1.3	1.1	1.3	1.2	1.3	1.2	1.3	1.2	1.3	0.005
9	1.2	1.3	1.1	1.3	1.1	1.3	1.1	1.3	1.1	1.3	1.1	1.3	0.005

Remarks: (a) NO MASS LOSS was observed in all UNI and CYC stages.
(b) ZERO volume change.

Small permeameter: test D-W1-T6

i_{av}	UNI 1a		UNI 1b		UNI 2a		UNI 2b		UNI 3a		UNI 3b		k_{av} (cm/s)
	GR 25	GR 8	GR 25	GR 8	GR 25	GR 8	GR 25	GR 8	GR 25	GR 8	GR 25	GR 8	
1.1	1.1	1.2	1.1	1.2	1.0	1.2	1.0	1.2	1.0	1.2	1.1	1.3	0.004
5.2	1.1	1.3	1.1	1.3	1.0	1.3	1.0	1.2	1.0	1.3	1.1	1.2	0.006
9.5	1.1	1.2	1.1	1.1	1.1	1.1	1.1	1.1	1.0	1.1	1.0	1.1	0.007

Remarks: MASS LOSS (chapter 4) was observed in all CYC stages, and associated with volume change.

Small permeameter: test D-W1-T6: change in specimen height (mm)

i_{av}	UNI1a	CYC1	UNI1b	UNI2a	CYC2	UNI2b	UNI3a	CYC3	UNI3b
1.1	0	0.12	0	0	0.04	0	0	0.15	0
5.2	0	0.25	0	0	0.44	0	0	0.83	0
9.5	0	0.37	0	0	0.42	0	0	0.90	0

Small permeameter: test D-W1-T6-R (repeated)

i_{av}	UNI 1a		UNI 1b		UNI 2a		UNI 2b		UNI 3a		UNI 3b		k_{av} (cm/s)
	GR 25	GR 8	GR 25	GR 8	GR 25	GR 8	GR 25	GR 8	GR 25	GR 8	GR 25	GR 8	
1.1	1.1	1.2	1.1	1.2	1.0	1.1	1.1	1.1	1.1	1.2	1.1	1.1	0.005
5.3	1.1	1.1	1.0	1.2	1.0	1.2	1.0	1.1	1.0	1.1	1.0	1.1	0.006
9.7	1.1	1.1	1.1	1.2	1.0	1.2	1.0	1.0	1.0	1.0	1.0	1.1	0.006

Remarks: MASS LOSS (chapter 4) was observed in all CYC stages, and associated with volume change.

Small permeameter: test D-W1-T6-R (repeated): change in specimen height (mm)

i_{av}	UNI1a	CYC1	UNI1b	UNI2a	CYC2	UNI2b	UNI3a	CYC3	UNI3b
1.1	0	0.15	0	0	0.15	0	0	0.18	0
5.3	0	0.26	0	0	0.49	0	0	0.74	0
9.7	0	0.56	0	0	0.61	0	0	1.01	0

Small permeameter: test D-W1-T60

i_{av}	UNI 1a		UNI 1b		UNI 2a		UNI 2b		UNI 3a		UNI 3b		k_{av} (cm/s)
	GR 25	GR 8	GR 25	GR 8	GR 25	GR 8	GR 25	GR 8	GR 25	GR 8	GR 25	GR 8	
1.2	1.2	1.5	1.2	1.5	1.2	1.5	1.2	1.4	1.2	1.4	1.2	1.4	0.004
5.3	1.2	1.4	1.1	1.4	1.1	1.4	1.0	1.3	1.0	1.3	1.1	1.3	0.004
9.4	1.1	1.3	1.1	1.2	1.1	1.3	1.1	1.3	1.1	1.2	1.1	1.2	0.005

Remarks: MASS LOSS (chapter 4) was observed in all CYC stages, and associated with volume change.

Small permeameter: test D-W1-T60: change in specimen height (mm)

i_{av}	UNI1a	CYC1	UNI1b	UNI2a	CYC2	UNI2b	UNI3a	CYC3	UNI3b
1.2	0	0	0	0	0.03	0	0	0.04	0
5.3	0	0	0	0	0.04	0	0	0.04	0
9.4	0	0.02	0	0	0.05	0	0	0.06	0

Small permeameter: test D-W1-T60-R (repeated)

i_{av}	UNI 1a		UNI 1b		UNI 2a		UNI 2b		UNI 3a		UNI 3b		k_{av} (cm/s)
	GR 25	GR 8	GR 25	GR 8	GR 25	GR 8	GR 25	GR 8	GR 25	GR 8	GR 25	GR 8	
1.0	1.3	1.3	1.3	1.4	1.3	1.3	1.3	1.3	1.3	1.4	1.3	1.4	0.005
5.2	1.3	1.3	1.3	1.2	1.2	1.2	1.2	1.2	1.2	1.2	1.2	1.3	0.004
9.7	1.2	1.3	1.2	1.2	1.2	1.3	1.2	1.3	1.3	1.3	1.3	1.3	0.006

Remarks: MASS LOSS (chapter 4) was observed in all CYC stages, and associated with volume change.

Small permeameter: test D-W1-T60-R (repeated): change in specimen height (mm)

i_{av}	UNI1a	CYC1	UNI1b	UNI2a	CYC2	UNI2b	UNI3a	CYC3	UNI3b
1.0	0	0.02	0	0	0.03	0	0	0.05	0
5.2	0	0.04	0	0	0.04	0	0	0.05	0
9.7	0	0.03	0	0	0.06	0	0	0.09	0

Small permeameter: test D-W1-T120

i_{av}	UNI 1a		UNI 1b		UNI 2a		UNI 2b		UNI 3a		UNI 3b		k_{av} (cm/s)
	GR 25	GR 8	GR 25	GR 8	GR 25	GR 8	GR 25	GR 8	GR 25	GR 8	GR 25	GR 8	
1	1.1	1.1	1.0	1.0	1.0	1.1	1.0	1.1	1.0	1.1	1.0	1.0	0.005
5	1.0	1.0	1.0	1.1	1.0	1.1	1.0	1.1	1.0	1.1	1.0	1.1	0.005
9	1.0	1.1	1.0	1.1	0.9	1.1	1.0	1.0	1.0	1.0	1.0	1.1	0.004

Remarks: MASS LOSS (chapter 4) was observed in some CYC stages, and associated with volume change.

Small permeameter: test D-W1-T120: change in specimen height (mm)

i_{av}	UNI1a	CYC1	UNI1b	UNI2a	CYC2	UNI2b	UNI3a	CYC3	UNI3b
1	0	0	0	0	0	0	0	0	0
5	0	0	0	0	0	0	0	0.03	0
9	0	0.02	0	0	0.02	0	0	0.03	0

Small permeameter: test D-W2-T6

i_{av}	UNI 1a		UNI 1b		UNI 2a		UNI 2b		UNI 3a		UNI 3b		k_{av} (cm/s)
	GR 25	GR 8	GR 25	GR 8	GR 25	GR 8	GR 25	GR 8	GR 25	GR 8	GR 25	GR 8	
1.3	1.1	1.2	1.1	1.0	1.1	1.0	1.0	0.9	1.0	0.9	0.9	0.9	0.004
5.4	0.9	0.8	0.9	0.8	0.9	0.8	-	-	-	-	-	-	0.005

Remarks: MASS LOSS (chapter 4) was observed in all CYC stages, and associated with volume change. Test stopped at the end of stage CYC2 at i_{av} of 5.4.

Small permeameter: test D-W2-T6: change in specimen height (mm)

i_{av}	UNI1a	CYC1	UNI1b	UNI2a	CYC2	UNI2b	UNI3a	CYC3	UNI3b
1.3	0	0.73	0	0	0.96	0	0	1.22	0
5.4	0	1.73	0	0	1.50	-	-	-	-

Large permeameter: test C-W1-T6 (as W1-T6(L) in chapter 3)

i_{av}	UNI 1a		UNI 1b		UNI 2a		UNI 2b		UNI 3a		UNI 3b		k_{av} (cm/s)
	GR 25	GR 8	GR 25	GR 8	GR 25	GR 8	GR 25	GR 8	GR 25	GR 8	GR 25	GR 8	
1.3	1.2	1.0	1.1	1.0	1.1	1.0	1.1	1.0	1.1	1.0	1.1	1.0	0.008
4.8	1.1	1.0	1.1	0.9	1.1	0.9	1.1	0.9	1.1	0.9	1.1	0.9	0.007
8.9	1.0	0.9	1.0	0.9	1.0	0.9	1.0	0.9	1.0	0.9	1.0	0.9	0.007

Remarks: (a) NO MASS LOSS was observed in all UNI and CYC stages.
(b) ZERO volume change.

Large permeameter: test C-W2-T6 (as W2-T6(L) in chapter 3)

i_{av}	UNI 1a		UNI 1b		UNI 2a		UNI 2b		UNI 3a		UNI 3b		k_{av} (cm/s)
	GR 25	GR 8	GR 25	GR 8	GR 25	GR 8	GR 25	GR 8	GR 25	GR 8	GR 25	GR 8	
1.3	0.9	0.9	0.9	0.9	0.9	0.9	0.9	0.8	0.9	0.8	0.9	0.8	0.007
4.9	0.9	0.9	0.9	0.9	0.9	0.8	0.9	0.8	0.8	0.8	0.8	0.8	0.009
8.8	0.9	0.8	0.8	0.8	0.8	0.8	0.8	0.7	0.8	0.7	0.8	0.7	0.010

Remarks: (a) MASS LOSS was observed in all CYC stages (visual observations): total loss = 5487 g/m^2.
(b) Total volume change = 3.1%.

Large permeameter: test C-W2-T60 (as W2-T60(L) in chapter 3)

i_{av}	UNI 1a		UNI 1b		UNI 2a		UNI 2b		UNI 3a		UNI 3b		k_{av} (cm/s)
	GR 25	GR 8	GR 25	GR 8	GR 25	GR 8	GR 25	GR 8	GR 25	GR 8	GR 25	GR 8	
1.4	0.9	1.3	0.9	1.3	0.9	1.2	0.9	1.2	0.9	1.2	0.9	1.2	0.006
4.7	0.9	1.2	0.9	1.0	0.9	1.0	0.9	1.0	0.9	1.1	0.9	0.9	0.007
9.0	0.9	1.0	0.8	1.0	0.8	1.0	0.8	1.0	0.8	1.0	0.9	1.0	0.006

Remarks: (a) NO MASS LOSS was observed in some CYC stages (visual observations): total loss = 959 g/m^2.
(b) Total volume change = 0.47%.

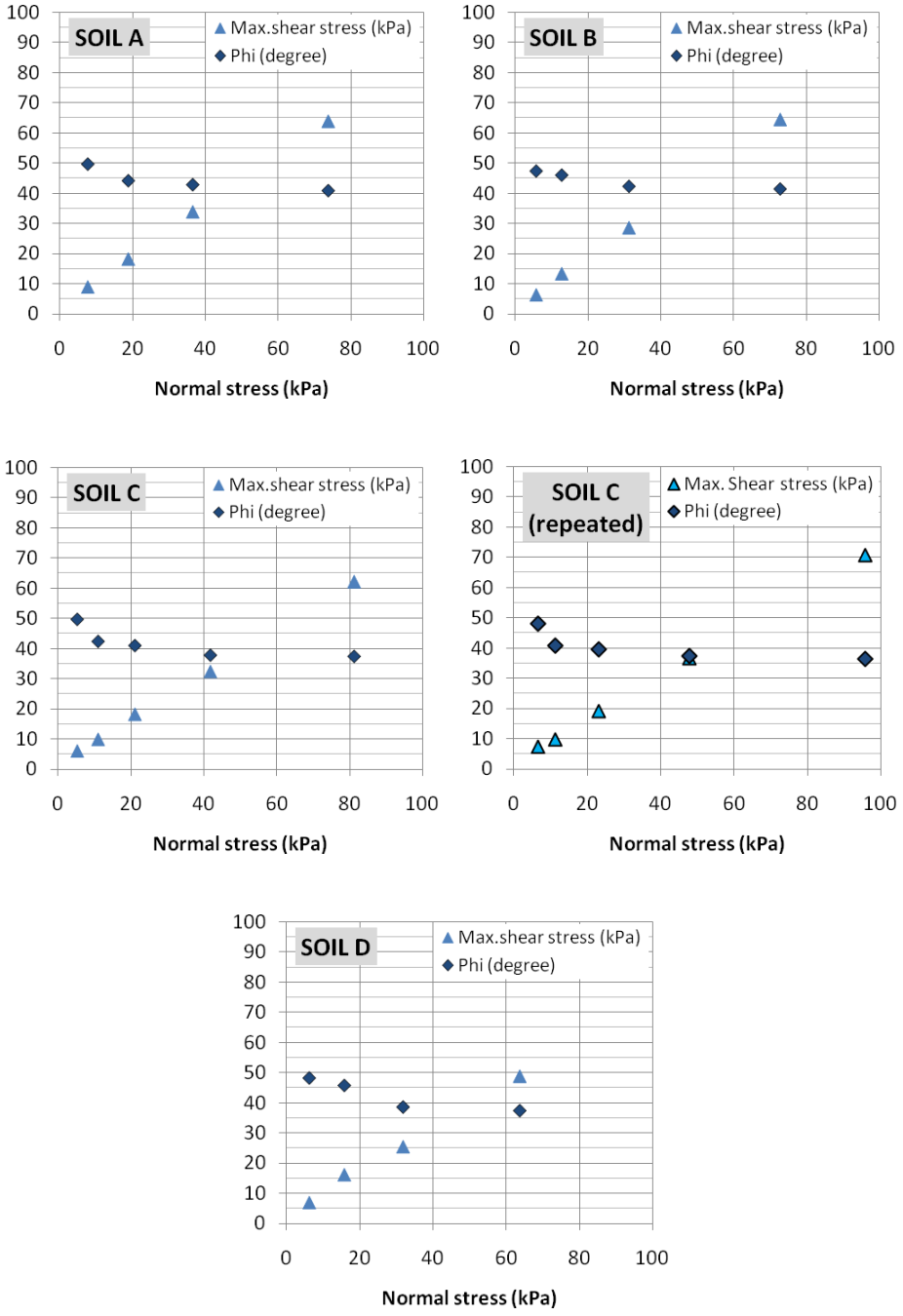

Figure C1 Direct shear test results

Appendix D Select photographs: small permeameter

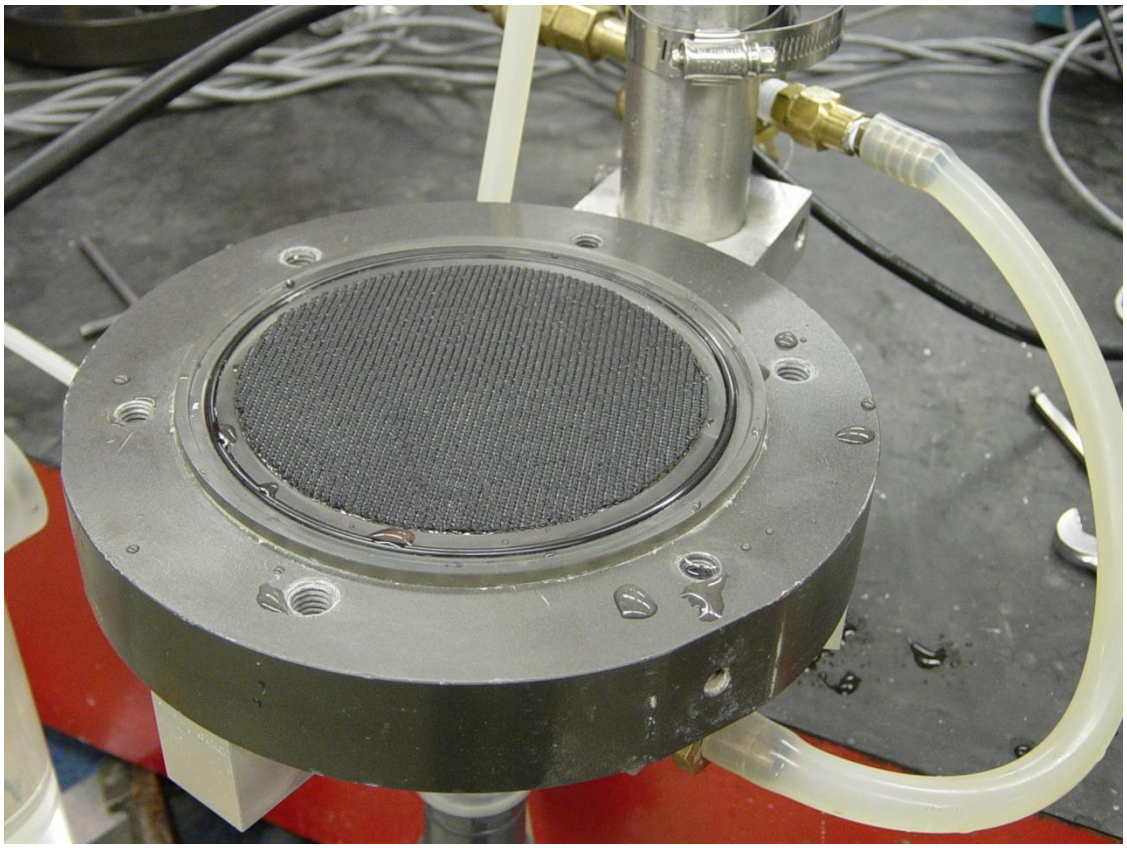

Figure D1 Placement of geotextile W2 sample on permeameter base

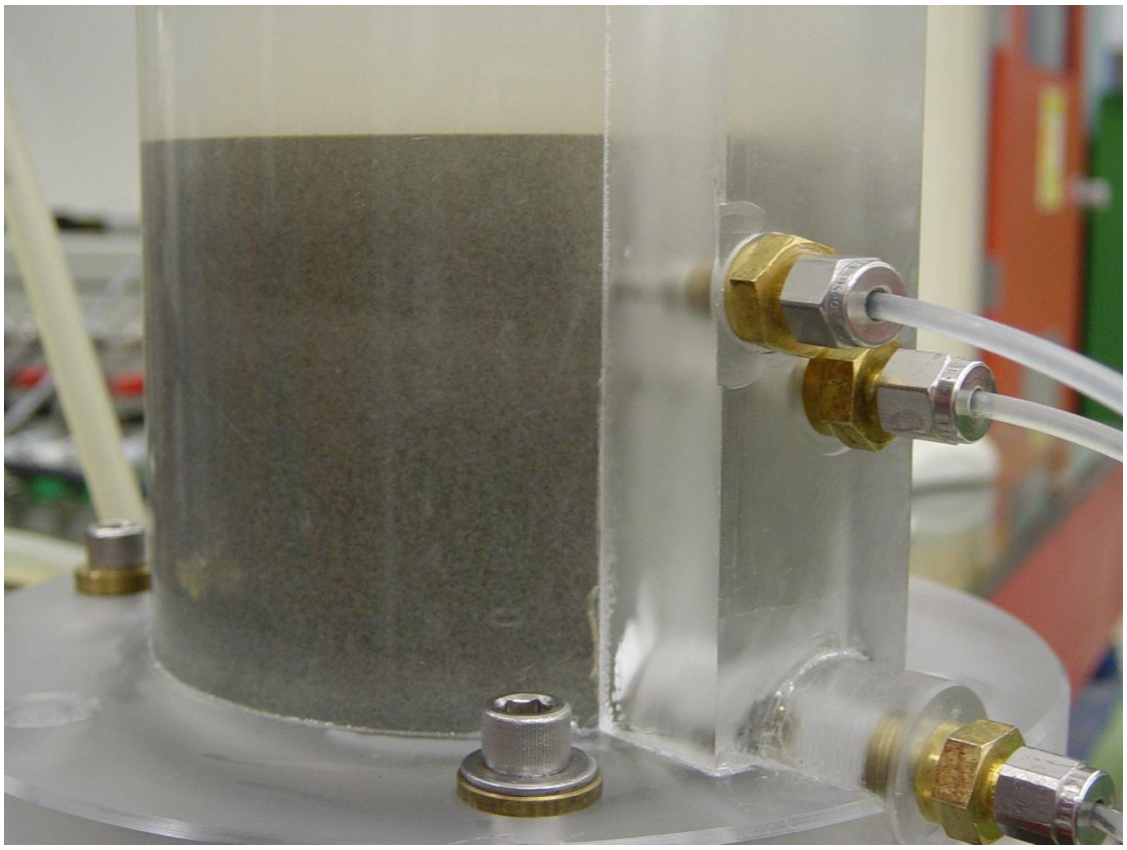

Figure D2 Reconstituted test specimen (soil C)

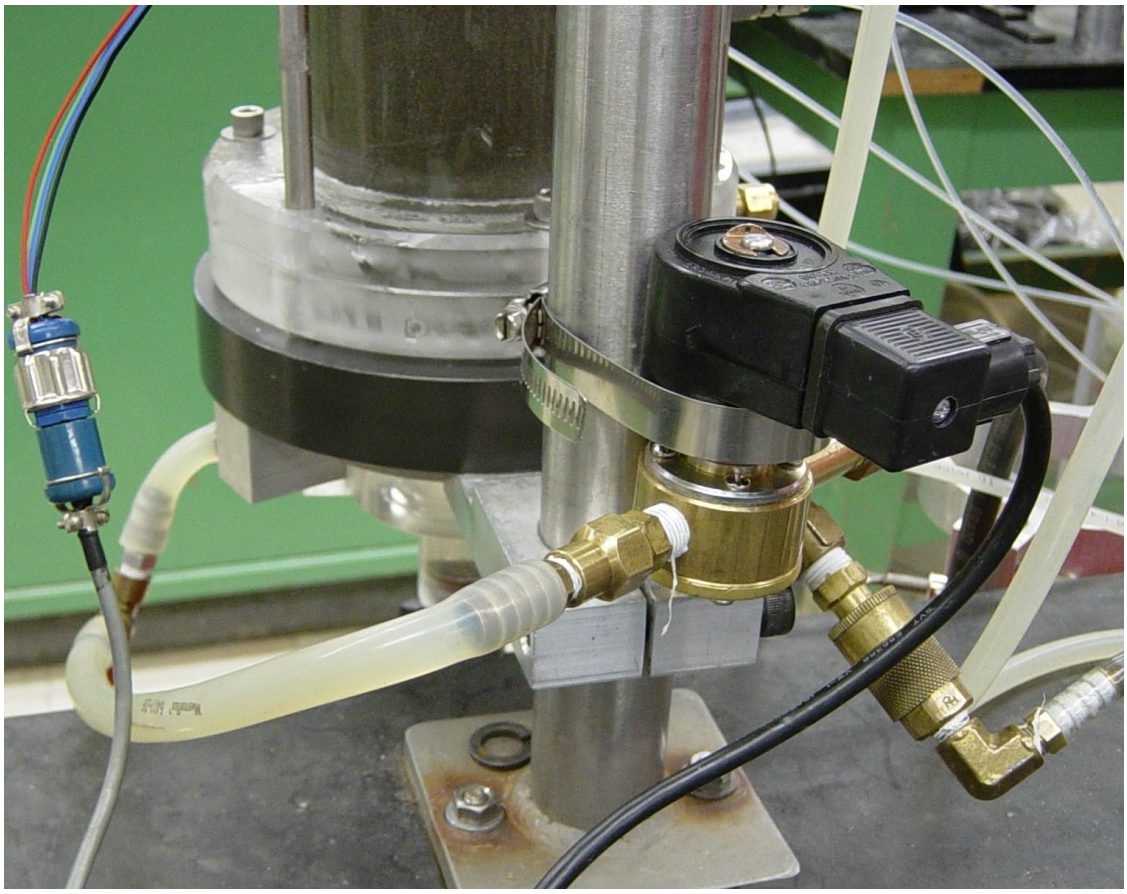

Figure D3 Head-controlled in cyclic flow: 3-way solenoid valve

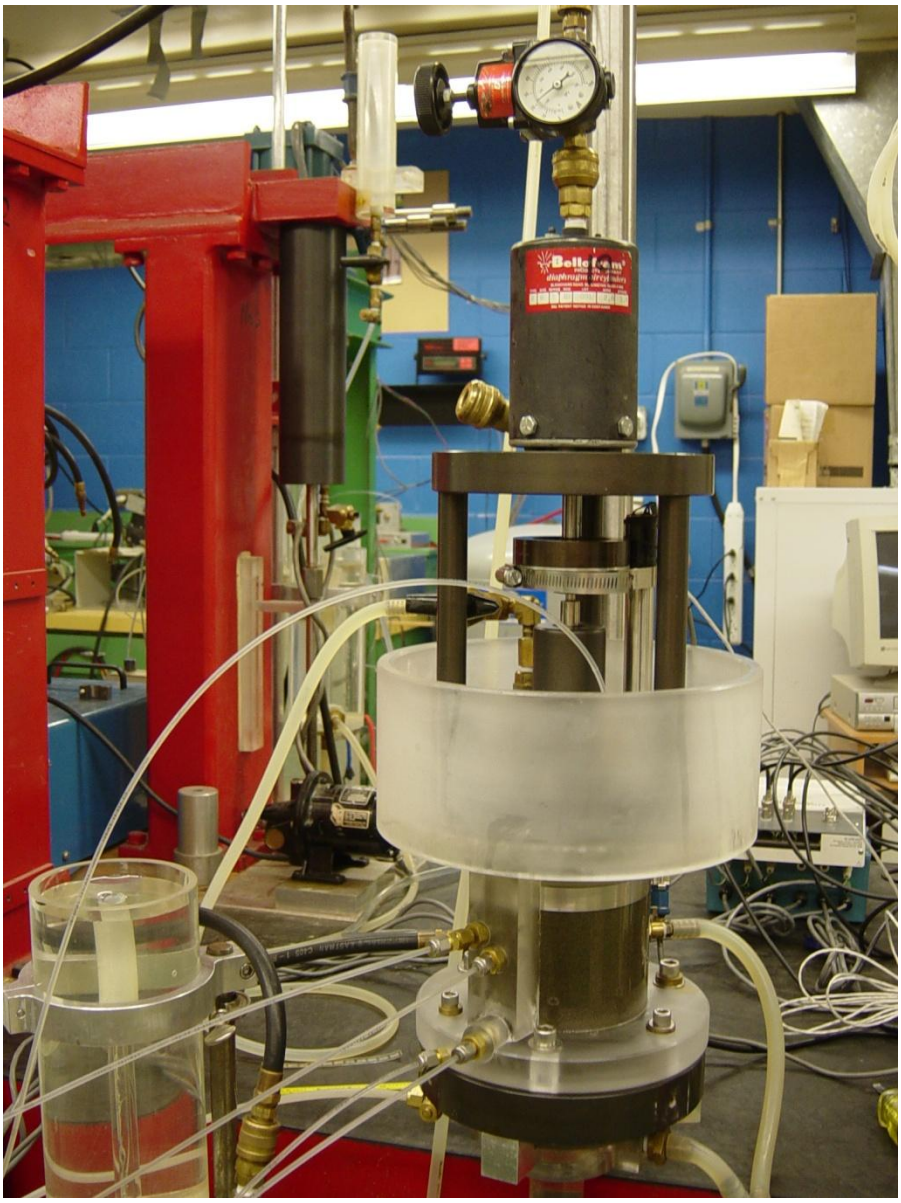

Figure D4 Assembly of the small permeameter: axial loading device

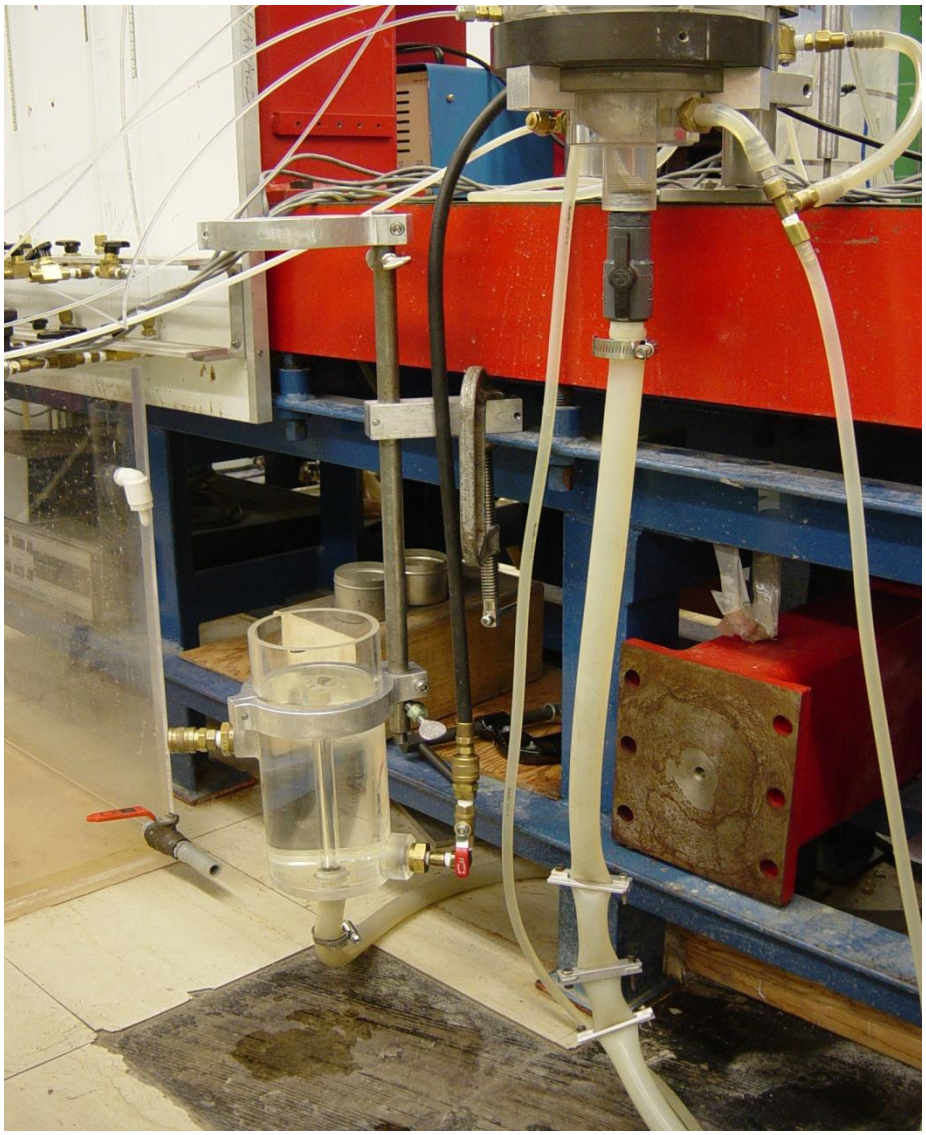

Figure D5 Flexible hose discrete sampling of mass loss through the geotextile

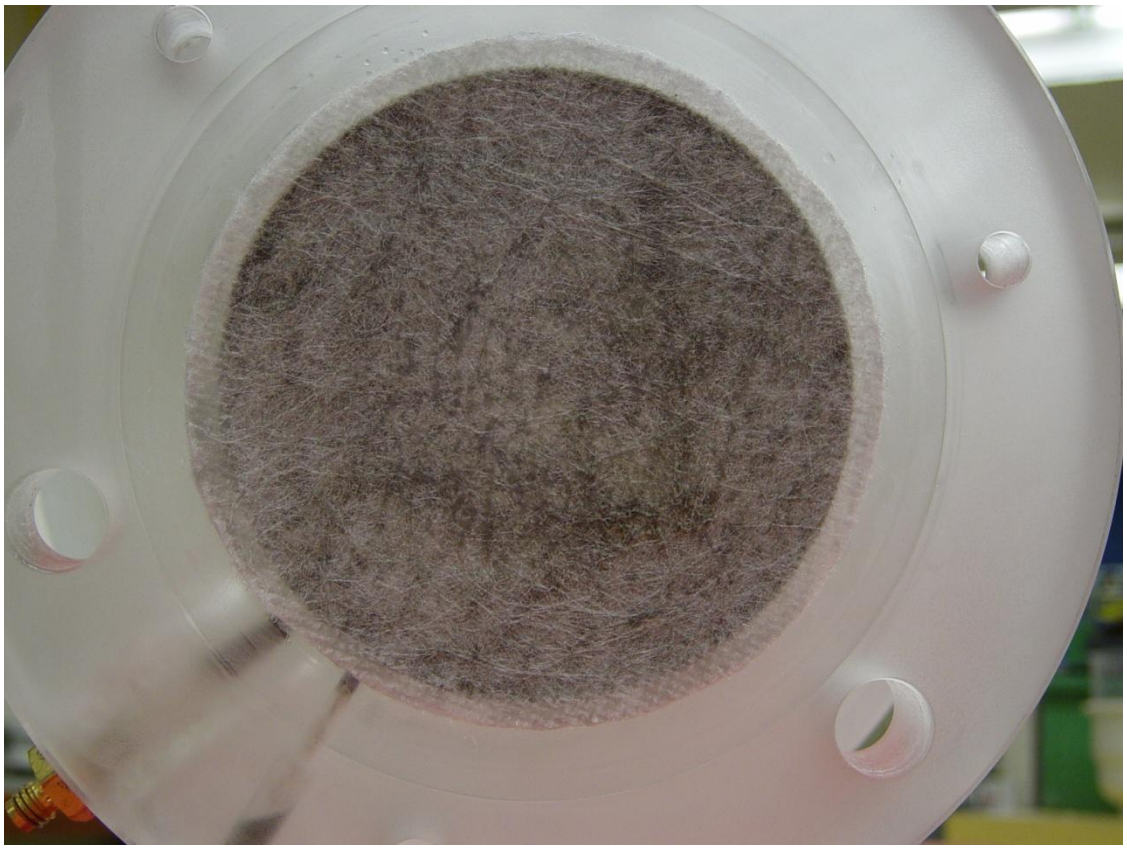

Figure D6 Geotextile NW4 after test D-NW4-T6 ($AOS/D_{85} \approx 2.3$)

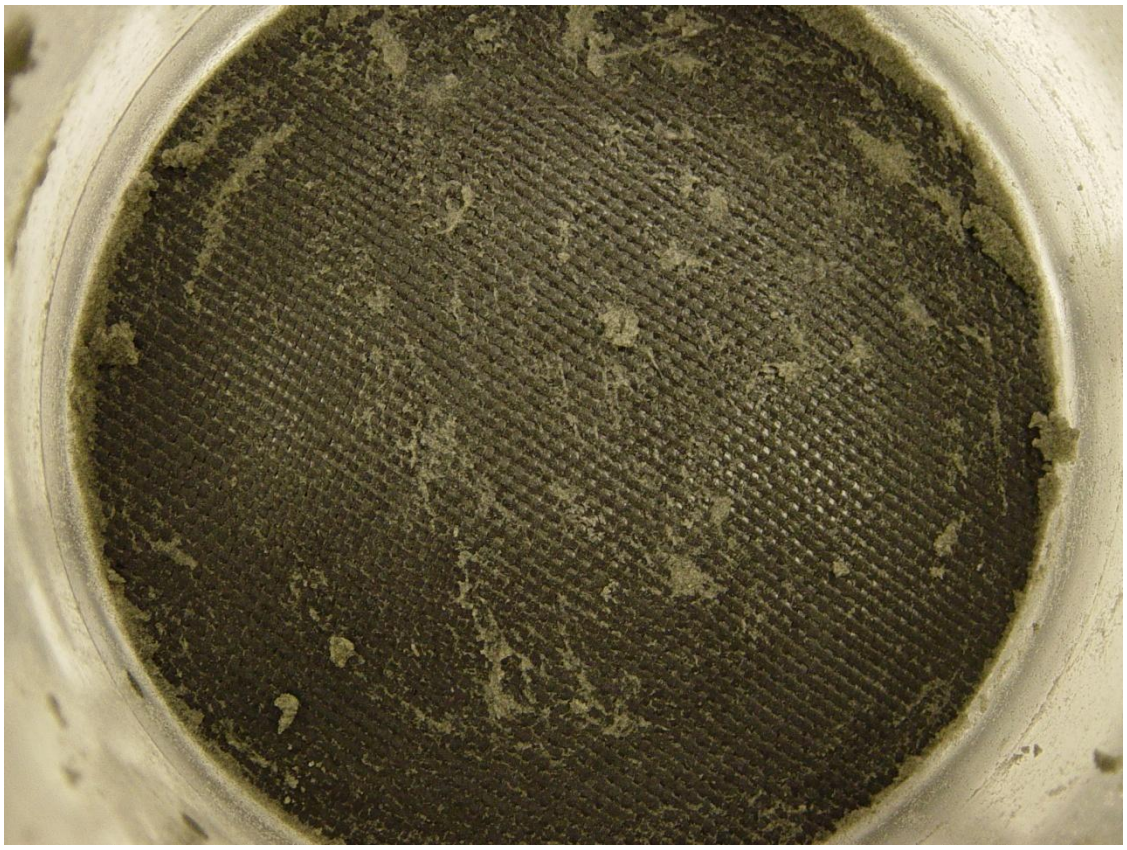

Figure D7 Geotextile W2 after test D-W2-T6 ($AOS/D_{85} \approx 3.7$)

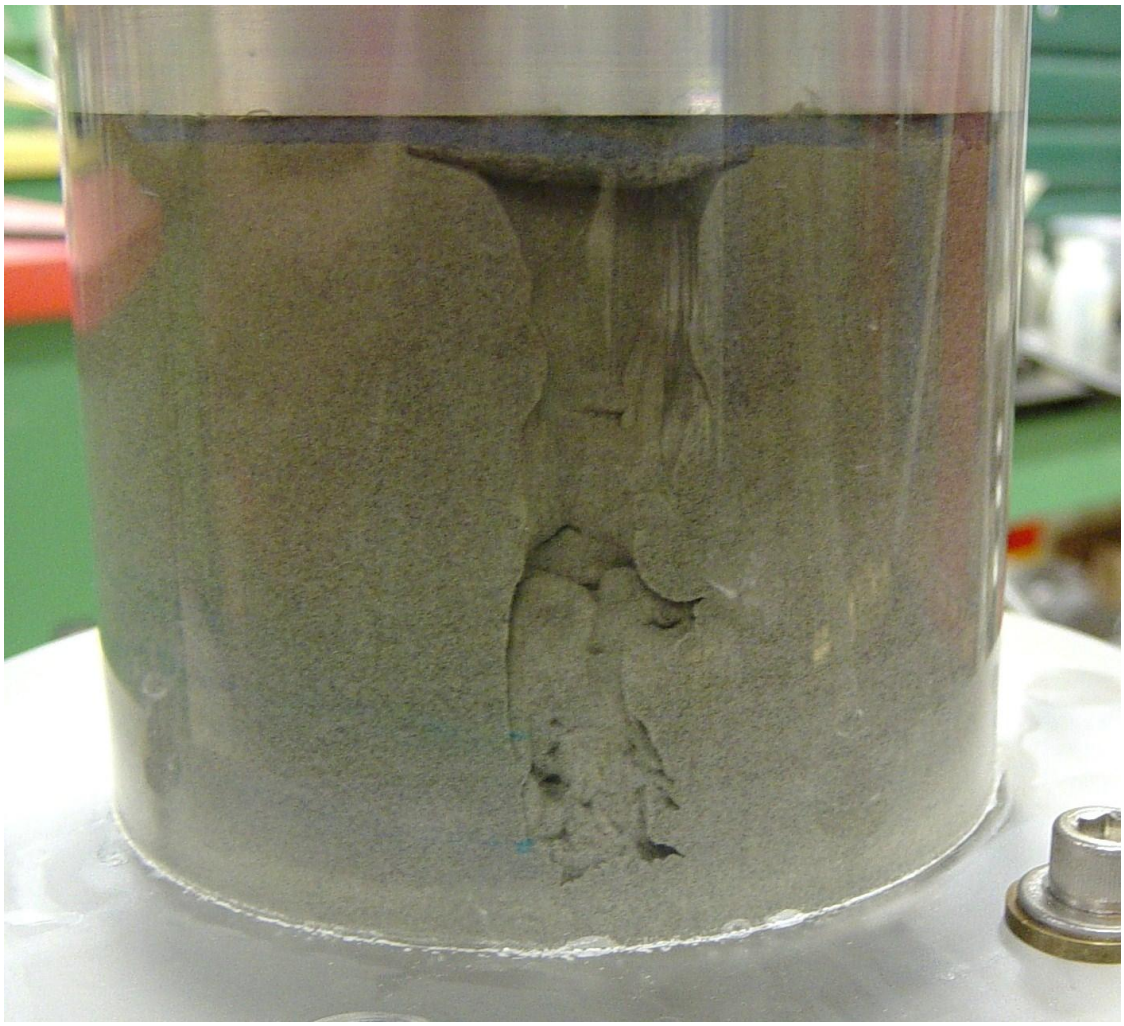

Figure D8 Soil specimen after test D-W2-T6 ($AOS/D_{85} \approx 3.7$)

Appendix E Select photographs: large permeameter

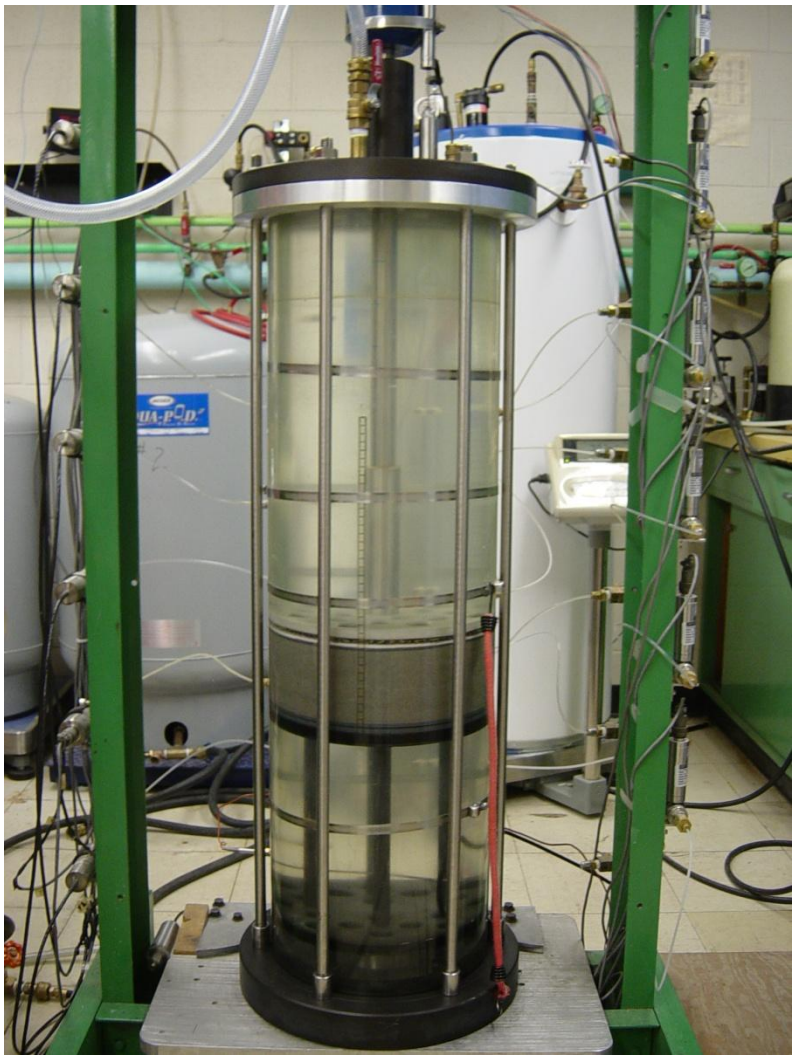

Figure E1 Assembly of the large permeameter

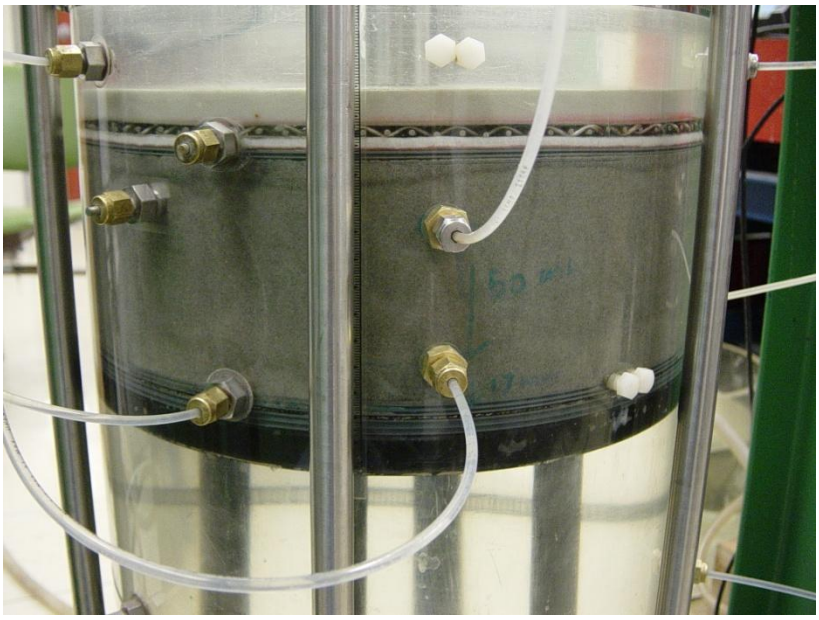

(a)

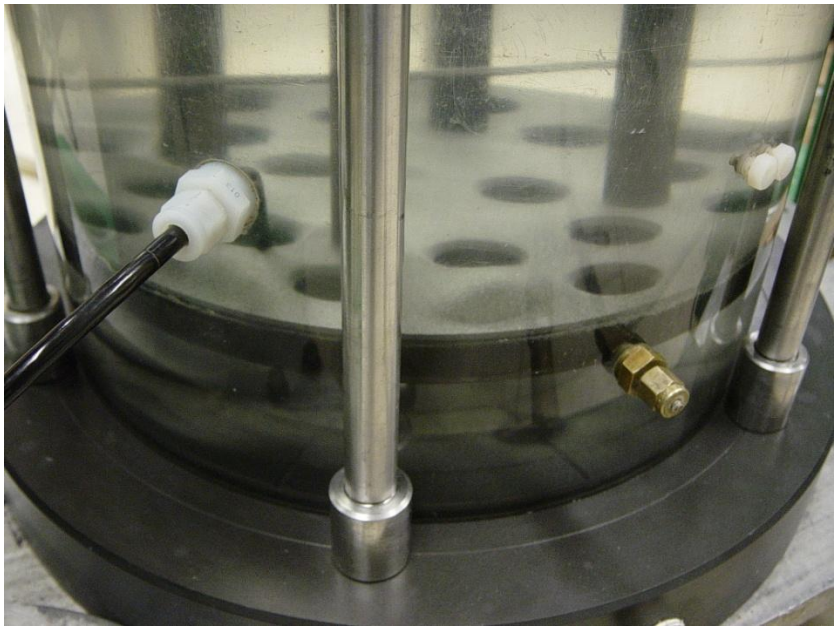

(b)

Figure E2 Test C-W2-T = 6 s (AOS/D85 = 2.8): a) post-test specimen; b) deposition of soil loss through the geotextile

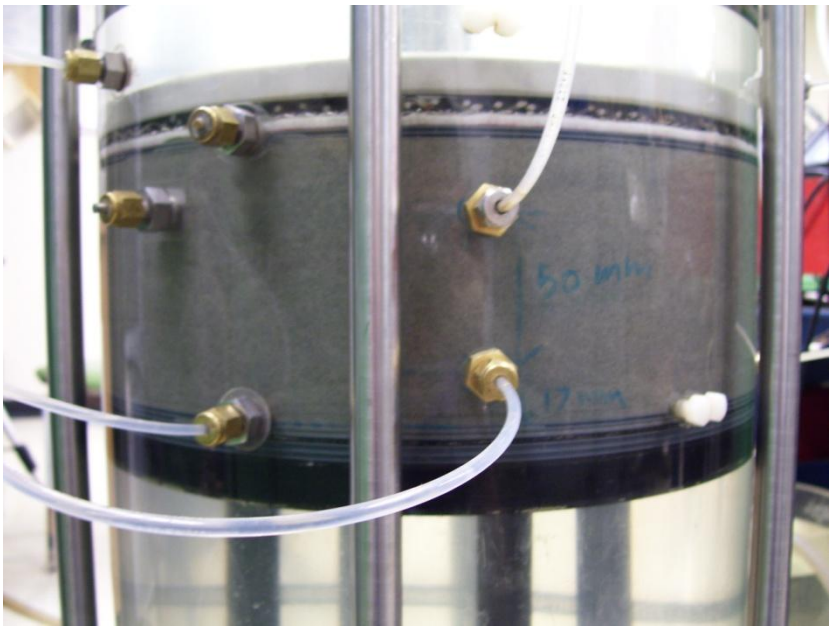

(a)

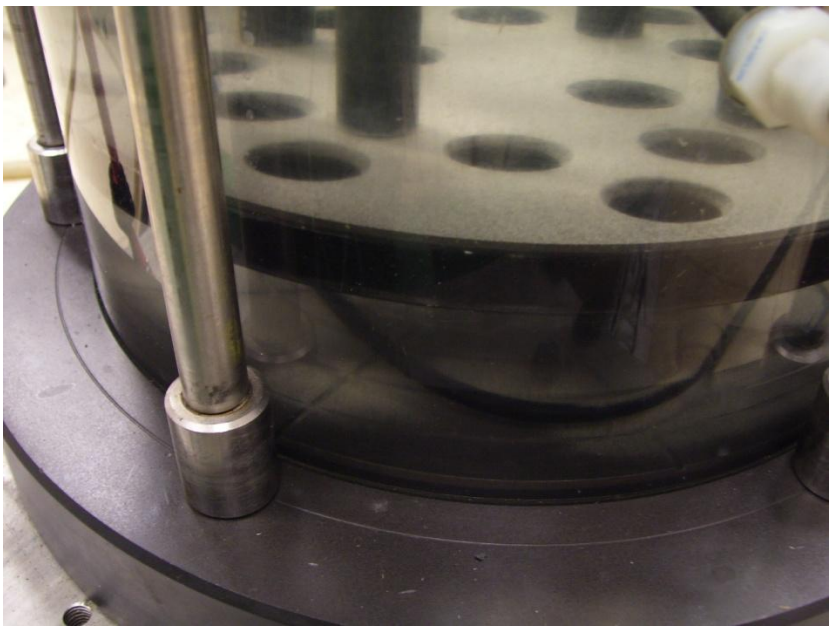

(b)

Figure E3 Test C-W2-T = 60 s (AOS/D85 = 2.8): a) post-test specimen; b) deposition of soil loss through the geotextile